Run-up and Nonlinear Propagation of Oceanic Internal Waves and Their Interactions

Thesis by

Duo-min Lin

In Partial Fulfillment of the Requirements

for the Degree of

Doctor of Philosophy

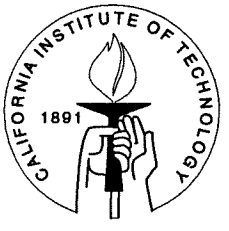

California Institute of Technology

Pasadena, California

June 1996

(Submitted May 2, 1996)

Acknowledgements

I wish to express my sincere gratitude to my advisor, Professor Theodore Yao-tsu Wu, for his deep insight and intellectual encouragement throughout my graduate student career. His constant guidance and help were also essential for carrying out these studies. His friendship and wisdom are highly respected.

I also would like to thank the past and present "family" members of the Engineering Science group for any helpful discussions and collaboration, especially to Wooyoung Choi, Holly Domingo, Gary Guthart, John Kao, Sunao Murashige, Susan Nakashima, Ken Takagi, Michelle Teng, George Yates and Jin Zhang. Their friendship made the graduate study at Caltech colorful and meaningful.

My special thanks are due to my parents and brothers for all they did for me that is necessary in any academic endeavour.

I gratefully acknowledge financial support from the National Science Foundation, the Office of Naval Research, the Li Ming's Scholarship, the Powell Foundation Graduate Fellowship and the California Institute of Technology.

I dedicate this thesis to my wife, Lilly, for her love and support.

Abstract

A weakly nonlinear and weakly dispersive oceanic internal long wave (ILW) model, in analogy with the generalized Boussinesq's (gB) model, is developed to investigate generation and propagation of internal waves (IWs) in a system of two-layer fluids. The ILW model can be further derived to give a bidirectional ILW model for facilitating calculations of head-on collisions of nonlinear internal solitary waves (ISWs). The important nonlinear features, such as phase shift of ISWs resulting from nonlinear collision encounters, are presented. The nonlinear processes of reflection and transmission of waves in channels with a slowly varying bottom are studied.

The terminal effects of IWs running up submerged sloping seabed are studied by the ILW model in considerable detail. Explicit solution of the nonlinear equations are obtained for several classes of wave forms, which are taken as the inner solutions and matched, when necessary for achieving uniformly valid results, with the outer solution based on linear theory for the outer region with waves in deep water. Based on the nonlinear analytic solution, two kinds of initial run-up problems can be solved analytically, and the breaking criteria and run-up law for IWs are obtained. The run-up of ISWs along the uniform beach is simulated by numerial computations using a moving boundary technique. The numerical results based on the ILW model are found in good agreement with the run-up law of ISWs when the amplitudes of the ISWs are small.

The ILW model differs from the corresponding KdV model in admitting bidirectional waves simultaneously and conserving mass. This model is applied to analyze the so-called critical depth problem of ISWs propagating across a critical station at which the depths of the two fluid layers are about equal so as to give rise to a critical point of the KdV equation. As the critical point is passed, the KdV model may predict a new upward facing ISW relative to a local mean interface is about to emerge from the effects of disintegrating original downward ISW. This phenomenon has never been observed in our laboratory. Numerical results are presented based on the present ILW model for ISWs climbing up a curved shelf and a sloping plane seabed. It is shown that in the transcritical region, the behaviour of the ISWs predicted by the ILW model depends on the relative importance of two dimensionless parameters, s_w, the order of ISW wave slope, and s, the beach

slope. For $s >> s_w$, the wave profile of ISWs exhibits a smooth transition across the transcritical region; for $s << s_w$, ISWs emerge with an oscillatory tail after passing across the critical point. Numerical simulations based on the ILW model are found in good agreement with laboratary observations.

Finally, conclusions are drawn from the results obtained in the present study based on the ILW model.

Contents

List of Figures

List of Tables

Chapter 1

Introduction

The physical and geophysical processes taking place in coastal waters generally involve ocean waves, internal waves, currents, vortical eddies, turbulent diffusion of material and momentum, in varying degree under effects of bottom topography. These various related phenomena are of fundamental interest to science, engineering and environmental development. The natural forces that generate internal gravity waves (IW) propagating along pycnoclines in the ocean seems ubiquitous globally in different parts of the oceans (Ostrovsky and Stepanyants 1989). The internal waves (IWs), a huge but little known subsurface disturbance, could affect oil exploration and production in the coastal ocean. Various possible mechanisms underlying generation of internal wave have been proposed to include tidal forcing, atmospheric pressure and wind stress fluctuations and various types of hydrodynamic instability of vortical oceanic motions. Since the advent of the space technology of synthetic aperture radar (SAR), the presence of internal waves underneath the well-mixed ocean top layer can be detected from their superficial signature (Fu and Holt 1982). In scale, IWs span a range from the giant scale of generation, with wave length of order $O(10km)$, cascading down through a mesoscale band to small scale of order $O(10m)$ and finally evanescing

at the turbulent dissipation scale of order $O(cm)$ range (Muller, D'Ascaro and Holloway 1991). Giant internal solitary waves (ISW) have been observed from space satellites to occur in groups of five to over ten waves, with their height measuring up to $200m$, wavelength reaching about $10km$, and with their crests spanning straight laterally to $150km$. These near-surface internal waves of various scales are thought to be generated mainly through the interaction of tidal currents and abrupt changes in topographic features (Fu and Holt 1982). However, many important questions remain to be answered.

Two-layer fluid systems with a discontinuity in density is the simplest model to provide a qualitative description of the behaviour of IWs in typical thermocline. The potential water-wave theory is widely used to introduce many kinds of mathematical models for IWs. The usual approach for describing long IW evolution in coastal regions has employed Korteweg-de Vries (KdV) theory. The existence of a class of nonlinear waves of permanent form for a two-fluid system has been investigated by Long (1956) for a two-fluid system, by Benjamin (1966) for a shallow-water system, by Benjamin (1967) and Ono (1975) for deep water, and by Kubota, Ko & Dobbs (1978) in stratified fluids of finite depth. Joseph (1977) found the exact stationary wave solution to the Whitham equation (1967) in a two-layer fluid of finite depth. Segur and Hammack (1982) examined the KdV-type theories (Joseph 1977, and Kubota, Ko & Dobbs 1978) experimentally by comparing measured and predicted soliton shapes. Koop & Butler (1981) found that the quantitative differences between the rigid-lid and free-surface boundary analyses of weakly nonlinear IWs is not large for conditions typical of their experimental configuration, in which the ratio of typical wave length and the upper-layer depth is about 10. Zhu (1986) found that the forced KdV equation he devel-

oped for modeling two-layer flows predicts the existence of upstream-advancing waves produced under forcing near resonance, with resulting wave characteristics in broad agreement with experiment. In two-layer systems, according to the KdV-type model equation, the ISW is a wave of elevation (or depression) according as $\rho_1 h_1^2/\rho_2 h_2^2 > 1$ (or < 1), where h_1 and h_2 are the depths of the upper and lower layers with densities ρ_1 and ρ_2, respectively. As the incident wave of depression propagates from a region of deeper lower layer up a slope to a body of water of increasingly shallower depths, it will encounter a critical point (or station) where $\rho_1 h_1^2 = \rho_2 h_2^2$, past which it enters a region where a wave of elevation is a natural result if locally generated. Kaup and Newell (1978) suggested that the ISW of depression could reverse its polarity on passing through the critical point. Knickerbocker and Newell (1980) have shown numerically that such a reversal is possible based on a KdV-type model equation with variable coefficient representing the depth change. Helfrich, Melville & Miles (1984) have shown that after crossing a critical point the incident wave scatters into a packet of oscillatory waves from which one or more ISWs of elevation emerge according to their numerical solutions of an extended KdV equation which is generalized to admit variable depths with only one higher-order term to account for this critical-point geometry. In laboratory experiments, Kao, Pan and Renouard (1985) studied the propagation of ISWs in a two-layer system over a sloping shelf topography. The upper layer is everywhere shallower than the lower layer so that solitary waves of depression can supposedly exist throughout the whole region. They found that as an ISW moves up the slope, its rear face steepens without change in polarity. In contrast to Kao et al. (1985), Helfrich and Melville (1986) presented the experimental and theoretical study of propagation and stability of ISWs over a sloping

shelf topography where a critical point exists. They found that the KdV-type model equation, including terms representing the effects of nonlinearity, dissipation and varying bottom topography, gave a very good agreement between theory and experiment.

One successful mathematical model is the generalized Boussinesq model (gB) established by Wu (1981) to evaluate oceanographical generation and evolution of weakly nonlinear and weakly dispersive long waves on coastal waters. Its validity has been first verified experimentally by Lee, Yates & Wu (1989). Teng (1990) developed a generalized channel Boussinesq model (gcB) to investigate generation and propagation of nonlinear long waves in water channels with arbitrary cross section and with moving disturbances as external forcings. Zhu (1986) extended the gB model to derive a two-layer model of the Boussinesq type to evaluate internal solitons generated by moving disturbances. Wang, Wu & Yates (1992) predicted the scattering and propagation of three-dimensional long waves in shallow water by using the generalized Boussinesq (gB) two-equation model. Wu (1994) obtained a bidirectional long-wave model using a multiple scale method and found solutions describing detailed transient evolution of head-on collisions of solitary waves, leaving permanent phase shifts of waves as the only mark of having endured the nonlinear encounter. The phase shifts are known to never arise in linear systems. This interesting feature may indeed hold the key to exposing the basic mechanism underlying such remarkable phenomena of nonlinear wave interaction as the periodic recurrence of initial states that has been discovered by Zabusky and Kruskal (1965) for the KdV-class of solitary waves. Recent numerical and experimental studies on nonlinear water waves in coastal waters have been made based on the gB model (Lee 1985, Zhu 1986, Teng 1990, Wang 1992, Wu 1994).

The problem of run-up of oceanic water waves has been studied by several authors (Dressler 1958, Carrier & Greenspan 1958, Tuck & Hwang 1972, Spielvogel 1975, Zelt 1986, Zelt & Raichlen 1991). Carrier and Greenspan (1958) obtained the classic solutions to the (coupled) nonlinear shallow-water equations for wave run-up on plane beach by adopting the method of hodograph transformations. Tuck and Hwang (1972) used another interesting transformation to render the nonlinear equations linear. Spielvogel (1975) reexplored the same result after Tuck and Hwang (1972). Zelt (1986) and Zelt & Raichlen (1991) investigated the run-up of nonbreaking and breaking solitary waves on plane impermeable beaches with a Lagrangian finite-element Boussinesq wave model. However, the run-up of IWs has been little known. The terminal effects of internal waves on coastal waters, with such possible hazards as the so-called *undersea tsunamis* (Wu & Lin 1994), are known to have inflicted upon the Chesapeake Bay in early 1960's to yield an abrupt anoxic condition coupled with a marked decline in marine production from its previous rich level. It took the five-year three-state U.S. Congress Chesapeake Bay Program (1983) to ascertain the strong activities of the incident internal waves to be primarily responsible for causing a strong impact on physical mixing of nutrients in, and biochemical degradation of, the bay water.

The primary interest of the present study carried out in this thesis is to investigate the following problems with the objectives of (A) establishing a theoretical model, called the "Internal Long Wave model" (ILW), for evaluating nonlinear IWs, in analogy with the gB model for oceanic water waves in coastal regions; (B) examining typical terminal effects of nonlinear internal waves running up submerged sloping seabed; and (C) predicting the nonlinear propagation and evolution of ISWs across a critical point existing in a typical coastal area.

In this study, we formulate the generation and propagation of oceanic nonlinear internal long waves (IWs) in a two-layer system consisting of two mutually immiscible fluids having different specific gravities with a rigid-lid assumption, based on the gB and the generalized channel Boussinesq (gcB) models introduced by Wu (1981) and Teng & Wu (1990). The ILW model will be further developed here to give a bidirectional model for facilitating calculations of head-on interactions of nonlinear internal solitary waves (ISWs). The important nonlinear features, such as phase shifts of ISWs resulting from nonlinear collision encounters, are presented in Chapter 2. In Chapter 3, we apply the model equations to the case of two-dimensional oceanic internal waves on a submerged seabed of uniform slope, a case for which accurate solutions are amenable to the nonlinear model equations. The nonlinear geophysical phenomenon of run-up of IWs is thereby studied in considerable detail. Explicit solutions of the nonlinear equations are obtained for several classes of wave forms, which are taken as the inner solutions and matched, when necessary for achieving uniformly valid results, with the outer solution based on linear theory for the outer region with waves in deep water. Based on the nonlinear analytic solution, two kinds of initial run-up problems can be solved analytically, and the breaking criteria and run-up law for IWs are obtained. The run-up of ISWs along the uniform beach is simulated by numerial computations using a moving boundary technique. In Chapter 4, we apply the ILW model to numerically simulate the evolution of an internal solitary wave initially downward polarized into a deeper lower layer as it passes across a critical point from a subcritical layer to a supercritical layer. A predictor-corrector two-step numerical procedure with the moving boundary conditions at the interfacial waterline is developed to solve the ILW model for nonlinear evolution of waves in

coastal zone. The computational results from the ILW model are also compared with the lab observation performed by Helfrich & Melville (1986). In Chapter 5, conclusions are drawn from the results obtained in the present study based on the ILW model.

Chapter 2

Theory of Generation and Propagation of Oceanic Internal Long Waves

To describe generation and propagation of oceanic internal waves (IWs) in the coastal ocean, weakly nonlinear long internal waves in channels of varying depths are first considered, and an internal long wave model (ILW) for a two-layer fluid system is derived from the Euler equations. This model is further developed to give a bidirectional internal long wave model for evaluating waves propagating in both directions in a channel of rectangular cross-section, which is applied to study the nonlinear processes of reflection and transmission of waves in the channel.

2.1 The Internal Long Wave Model

To facilitate evaluation of the general properties of internal waves propagating in coastal waters and their interaction with each other and with a fixed sloping sea floor, we introduce the following model for describing typical baroclinic wave modes. We consider the motion of three-dimensional internal waves in a channel of gradually varying cross-sectional shape in two horizontal dimensions x, y with the vertical dimension z (see Fig. 2.1). The density stratification of the sea water

is represented by a piecewise homogeneous two-layer distribution, of density ρ_1 in the top layer of depth $h_1 = const.$ and density ρ_2 in the lower layer of depth $h_2(x, y)$, with variations in $|\nabla h_2|/h_2$ taken to be small. The fluid is assumed inviscid and incompressible, with $d\rho_1/dt = 0$ and $d\rho_2/dt = 0$, where d/dt signifies the material differentiation. To simplify the analysis involved, the top water surface is assumed to have negligible elevations for the internal wave (IW) mode so that the top free surface may be regarded as remaining undisturbed or being replaced by a "rigid lid" at which the vertical fluid velocity vanishes. Thus for this IW model, the only free boundary is the interface between the two layers of fluid, with its vertical displacement denoted by $z = \zeta(x, y, t)$, taken positive above the unperturbed interface at $z = 0$. For simplicity, the channel is taken to be symmetric about the mid-channel $x - z$ plane. The interface extends to the channel banks at $y = \pm b(x, t)$. The rigid lid assumption has been found quite accurate for modeling the IW-mode provided the top layer is sufficiently thick compared with typical wave amplitude; it has been shown by Koop & Butler (1981) and Zhu (1986) to remain valid with a high degree of accuracy in comparison with laboratory experiment. For numerical modeling, the fast barotropic modes may appear as a "computational noise" which has to be filtered out by employing a "rigid-lid" condition at the top surface (Glazman 1995).

For an inviscid and incompressible flow, the velocity vector $\mathbf{U}_i (= (u_i, v_i, w_i))$ and the pressure field p_i in the top ($i = 1$) and lower ($i = 2$) layers satisfy the Euler equation and the continuity equation, respectively, for each layer,

$$\nabla \cdot \mathbf{U}_i = 0, \qquad (i = 1, 2) \tag{2.1a}$$

$$\frac{\partial \mathbf{U}_i}{\partial t} + \mathbf{U}_i \cdot \nabla \mathbf{U}_i = -\frac{1}{\rho_i} \nabla p_{ei}, \qquad (i = 1, 2) \tag{2.1b}$$

where the excess pressures $p_{ei} = p_i + \rho_i g z$, g being the gravitational acceleration constant. The boundary conditions, with the surface tension effects neglected, are (i) the kinematic boundary condition at the interface invoking that the fluid particles, once situation on the interface, will remain on it:

$$w_i = \frac{d\zeta}{dt} = \zeta_t + u_i\zeta_x + v_i\zeta_y, \quad z = \zeta(x,y,t), \quad |y| < b(x,t), \quad (i = 1,2); \tag{2.2}$$

(ii) the dynamic boundary condition at the interface:

$$p_1 = p_2, \quad z = \zeta(x,y,t), \quad |y| < b(x,t); \tag{2.3}$$

(iii) the rigid-lid boundary condition at the top surface:

$$w_1 = 0, \qquad z = h_1; \tag{2.4}$$

(iv) the kinematic condition at the bottom:

$$w_2 = -\frac{dh_2}{dt} = -(u_2 h_{2x} + v_2 h_{2y}), \quad z = -h_2(x,y); \quad \text{and} \tag{2.5}$$

(v) the kinematic condition at the side walls:

$$v_i = \pm(b_t + u_i b_x), \qquad y = \pm b(x,t), \quad (i = 1,2). \tag{2.6}$$

Irrotational motion is assumed so that the velocity vector $\mathbf{U}_i = \nabla\phi_i (i = 1,2)$, where the velocity potential ϕ_i satisfies the Laplace and the Bernoulli equations

$$\nabla^2\phi_i = 0, \qquad (i = 1,2), \tag{2.7a}$$

$$\phi_{it} + \frac{1}{2}(\nabla\phi_i)^2 + \frac{p_i}{\rho_i} + gz = \frac{p_{i\infty}}{\rho_i}, \qquad (i = 1,2), \tag{2.7b}$$

where $p_{i\infty}(i = 1, 2)$ are the constant reference pressures. We define a section-mean quantity as

$$\overline{f_i}(x,t) = \frac{1}{A_i}\int\int_{A_i} f_i(x,y,z,t)dydz, \quad (i = 1,2), \tag{2.8}$$

where $A_i(i = 1, 2)$ is the wetted cross-sectional area in the top and lower layers, respectively. To evaluate the section mean value of the material rate of change of any flow quantity $f_i = f_i(x, y, z, t)(i = 1, 2)$, the transport theorem (Wu 1981, Teng 1990) is used; that is

$$A_i\overline{\frac{df_i}{dt}} = \frac{\partial}{\partial t}(A_i\overline{f_i}) + \frac{\partial}{\partial x}(A_i\overline{uf_i}), \quad (i = 1,2). \tag{2.9}$$

By taking $f_i = 1$, we obtain the following continuity equations for channel section as

$$\frac{\partial}{\partial t}A_i + \frac{\partial}{\partial x}(A_i\overline{u_i}) = 0, \quad (i = 1,2), \tag{2.10}$$

where $A_1(x,t) = A_{o1} - A_\zeta(x,t)$ and $A_2(x,t) = A_{o2}(x) + A_\zeta(x,t)$, A_{oi} is the unperturbed wetted area in the top $(i = 1)$ and lower $(i = 2)$ layers, respectively, and A_ζ is the area variation due to wave elevation at the interface. In terms of the sectional interface mean of ζ, we have

$$\tilde{\zeta} = \frac{A_\zeta}{2b} = \frac{1}{2b}\int_{-b}^{b}\zeta(x,y,t)dy. \tag{2.11}$$

Therefore, equation (2.10) becomes

$$-(2b\tilde{\zeta})_t + [(A_{o1} - 2b\tilde{\zeta})\overline{u_1}]_x = 0, \tag{2.12}$$

$$(2b\tilde{\zeta})_t + [(A_{o2} + 2b\tilde{\zeta})\overline{u_2}]_x = 0. \tag{2.13}$$

Equations (2.12) and (2.13) are exact equations which represent the mass conservation in two different non-mixing layers, respectively. In regard to the derivations

of the Bousinesq-class equations, there are several versions. If the section-mean velocities in Eqs. (2.12) and (2.13) are replaced by the axial velocity at the bottom (see Goring 1979) or at the interface (see Whitham 1976) or at an arbitray depth (see Madsen & Sorensen 1991), Eqs. (2.12) and (2.13) will include appropriate dispersive terms (of third order in x-derivative of the velocity) on the right sides so that the mass conservation law appears in different forms of expansions.

For systematically describing irrotational long waves, we introduce the following nondimensional variables

$$x^* = \frac{x}{\lambda}; \quad (y^*, z^*, \zeta^*, h_i^*; b^*) = \frac{(y, z, \tilde{\zeta}, h_i, b)}{h_o}; \quad A_i^* = \frac{A_i}{A_o}; \quad t^* = \frac{c_o t}{\lambda};$$

$$(u^*, v^*, w^*) = \frac{(u, v, w)}{c_o}; \quad \phi^* = \frac{\phi}{c_o \lambda}; \quad (p_i^*, p_a^*) = \frac{(p_i, p_a)}{\rho_i g h_o}, \tag{2.14}$$

where $*$ indicates a dimensionless variable, λ is a characteristic wavelength at the interface, h_o is a constant representative total depth, and $c_o = \sqrt{g h_o}$ a typical wave speed. Long waves are characterized by two important parameters:

$$\alpha = \frac{a}{h_o}, \quad \epsilon = \frac{h_o}{\lambda}, \tag{2.15}$$

where a is a representative internal wave amplitude. We are interested in weakly nonlinear, weakly dispersive wave motions. For the Boussinesq family of wave motion, the Ursell number, i.e., $Ur = \alpha/\epsilon^2$, is the order $O(1)$, i.e., $\alpha = O(\epsilon^2)$. Immediately omitting $*$, we obtain from Eq. (2.7) the following dimensionless equations:

$$\phi_{ixx} + \frac{1}{\epsilon^2}\phi_{iyy} + \frac{1}{\epsilon^2}\phi_{izz} = 0, \quad (i = 1, 2), \tag{2.16}$$

$$p_i + \phi_{it} + \frac{1}{2}({\phi_{ix}}^2 + \frac{1}{\epsilon^2}{\phi_{iy}}^2 + \frac{1}{\epsilon^2}{\phi_{iz}}^2) + z = 0, \quad (i = 1, 2), \tag{2.17}$$

and the boundary conditions from Eqs. (2.2)–(2.6) become

$$\rho_1 p_1 = \rho_2 p_2, \quad \text{at} \quad z = \zeta(x, y, t), \tag{2.18}$$

$$\phi_{1z} = 0, \quad \text{at} \quad z = h_1, \tag{2.19}$$

$$\phi_{1z} = -\epsilon^2[\phi_{2x} h_{2x} + \phi_{2y} h_{2y}], \quad \text{at} \quad z = -h_2, \tag{2.20}$$

$$\phi_{iy} = \pm\epsilon^2(b_t + \phi_{ix} b_x), \quad \text{at} \quad y = \pm b(x, t), \quad (i = 1, 2), \tag{2.21}$$

$$\phi_{iz} = \epsilon^2[\zeta_t + \phi_{ix}\zeta_x + \phi_{iy}\zeta_y], \quad \text{at} \quad z = \zeta, \quad (i = 1, 2). \tag{2.22}$$

We assume that $A_{io}(x) = O(1), b_t = O(\alpha)$, and $h_{2x}, b_x = O(1)$, then $u_i = O(\alpha)$, v_i, $w_i = O(\alpha\epsilon)$. Hence, $\phi_{ix} = O(\alpha)$, $\phi_{iy}, \phi_{iz} = O(\alpha\epsilon^2)$. According to the above equations and boundary conditions, we obtain perturbation expansions in the form

$$\phi_i = \alpha[f_i(x, t) + \epsilon^2 \Phi_i^{(2)}(x, y, z, t) + O(\epsilon^4)], \quad (i = 1, 2), \tag{2.23}$$

$$\zeta = \alpha[\zeta_o(x, t) + \epsilon^2 \zeta_1(x, y, t) + O(\epsilon^4)]. \tag{2.24}$$

Upon substituting Eq. (2.23) in Eq. (2.16), we have, to the order $O(\epsilon^2)$,

$$\Phi_{iyy}^{(2)} + \Phi_{izz}^{(2)} = -f_{ixx}, \quad (i = 1, 2), \tag{2.25}$$

and from Eqs. (2.19)–(2.22) the boundary conditions

$$\Phi_{1z}^{(2)} = 0, \quad \text{at} \quad z = h_1, \tag{2.26}$$

$$\Phi_{2z}^{(2)} = -f_{2x} h_{2x}, \quad \text{at} \quad z = -h_2, \tag{2.27}$$

$$\Phi_{1y}^{(2)} = \pm(b_t + f_{1x} b_x), \quad \text{at} \quad y = \pm b(x, t), \tag{2.28}$$

$$\Phi_{2y}^{(2)} = \pm(b_t + f_{2x} b_x), \quad \text{at} \quad y = \pm b(x, t). \tag{2.29}$$

In order to determine $\Phi_2(x,y,z,t)$, we need to solve a Neumann problem with a unique solution since the solvability condition is fulfilled when the condition on the normal derivative $\partial\phi/\partial n$ along the boundary is altogether considered (Teng & Wu 1992). Along this approach, we may first solve the problem for a rectangular channel with a slowly varying cross-sectional shape. For other geometrical shapes, the model equations may be treated later by adopting a shape factor similarity technique just as Teng and Wu did (1992). For the first case of varying rectangular channel, we assume

$$\Phi_i^{(2)} = -\frac{1}{2}z^2 f_{ixx} + K_i(x,t)(y^2 - z^2) + G_i(x,t)z + F_i(x,t), \quad (i = 1,2), \quad (2.30)$$

where $K_i(x,t)$, $G_i(x,t)$ and $F_i(x,t)$ are arbitrary functions of x and t, which can be determined from Eqs. (2.26)–(2.29), yielding

$$G_1(x,t) = 2h_1 K_1(x,t) + h_1 f_{1xx}, \quad (2.31)$$

$$K_1(x,t) = \frac{1}{2b}(b_t + f_{1x}b_x), \quad (2.32)$$

$$G_2(x,t) = -(2h_2 K_2 + f_{2x}h_{2x} + h_2 f_{2xx}), \quad (2.33)$$

$$K_2(x,t) = \frac{1}{2b}(b_t + f_{2x}b_x). \quad (2.34)$$

Similarly, upon applying the recursion relation, which simply follows from Eq. (2.16) to the expansion (2.23), we can obtain higher-order terms in the expansion of ϕ_i in Eq. (2.23), all of which can be expressed in terms of the two unknown functions $f_1(x,t)$ and $f_2(x,t)$, for each layer respectively.

In the following, in consistency with Eqs. (2.12) and (2.13), we apply the section-mean operation to the Bernoulli equations (2.17). To the order $O(\alpha\epsilon^4)$, we find the following differences between the correponding quantities,

$$\overline{\phi_{1t}} - (\overline{\phi_1})_t = \alpha\epsilon^2[\frac{1}{6}f_{1xxt}h_1^2 - \frac{1}{3}K_1(b^2)_t + \frac{1}{3}K_{1t}h_1^2 - \frac{1}{2}G_{1t}h_1] + O(\alpha\epsilon^4), \quad (2.35)$$

$$\overline{\phi_{2t}}-(\overline{\phi_2})_t=\alpha\epsilon^2[\frac{1}{6}(f_{2xx}h_2^2)_t-\frac{1}{3}K_2(b^2)_t+\frac{1}{3}(K_2h_2^2)_t+\frac{1}{2}(G_2h_2)_t]+O(\alpha\epsilon^4), \quad (2.36)$$

$$\overline{(\nabla\phi_i)^2}-(\nabla\overline{\phi_i})^2=O(\alpha\epsilon^4), \quad (i=1,2). \quad (2.37)$$

After substituting the section-mean value of Eq. (2.17) into Eq. (2.18), in physical coordinates, we get

$$\frac{\partial}{\partial t}(\tilde{\rho}\overline{\phi_1}-\overline{\phi_2})+\frac{1}{2}[\tilde{\rho}(\nabla\overline{\phi_1})^2-(\nabla\overline{\phi_2})^2]+(\tilde{\rho}-1)\tilde{\zeta}=$$

$$\alpha\epsilon^2\tilde{\rho}[-\frac{1}{6}f_{1xxt}h_1^2+\frac{1}{3}K_1(b^2)_t-\frac{1}{3}K_{1t}h_1^2+\frac{1}{2}G_{1t}h_1]+$$

$$\alpha\epsilon^2[\frac{1}{6}(f_{2xx}h_2^2)_t-\frac{1}{3}K_2(b^2)_t+\frac{1}{3}(K_2h_2^2)_t+\frac{1}{2}(G_2h_2)_t]+O(\alpha\epsilon^4), \quad (2.38)$$

where $\tilde{\rho}=\rho_1/\rho_2$. For uniform rectangular channels, $b=const$ and all quantities are independent of y, then Eq. (2.38) reduces to

$$\frac{\partial}{\partial t}(\tilde{\rho}\overline{\phi_1}-\overline{\phi_2})+\frac{1}{2}[\tilde{\rho}(\nabla\overline{\phi_1})^2-(\nabla\overline{\phi_2})^2]+(\tilde{\rho}-1)\tilde{\zeta}=$$

$$[\frac{1}{3}h_1^2\tilde{\rho}\overline{\phi_{1xxt}}-\frac{1}{3}(h_2^2\overline{\phi_{2xx}})_t-\frac{1}{2}(h_{2x}\overline{\phi_{2x}}h_2)_t]+O(\alpha\epsilon^4). \quad (2.39)$$

Finally, for the case of rectangular channels with $b_x, h_{2x}=O(\alpha)$, and $b_t=0$, the ILW model for slowing varying channels may be written as (omitting the overbars)

$$[b(h_1-\zeta)]_t+[b(h_1-\zeta)\phi_{1x}]_x=0, \quad (2.40)$$

$$[b(h_2+\zeta)]_t+[b(h_2+\zeta)\phi_{2x}]_x=0, \quad (2.41)$$

$$\tilde{\rho}\phi_{1t}-\phi_{2t}+\frac{1}{2}(\tilde{\rho}\phi_{1x}^2-\phi_{2x}^2)+(\tilde{\rho}-1)\zeta=\frac{1}{3}\kappa_1h_1^2\tilde{\rho}\phi_{1xxt}-\frac{1}{3}\kappa_2h_2^2\phi_{2xxt}, \quad (2.42)$$

where κ_1,κ_2 are the channel-shape factors determined solely by the geometrical shape of channel section, with $\kappa_i(i=1,2)=1$ for rectangular channels as a standard reference. For other channel shapes, the value of κ_2 can be determined

in a manner similar to the single layer calculation by Teng & Wu (1992). In general, we may take $\kappa_1 = 1$. Different from the gcB model (Teng & Wu 1992), we do not yet have general transformation (Wu 1994) to transform the model equations (2.40)-(2.42) for waves on a two-layer fluid in a uniform channel of arbitrary shape into the basic case of rectangular channels.

2.2 The Bidirectional Channel Model – for nonlinear IWs in two-layer fluids

2.2.1 Derivation

In this section, we shall first investigate the special case of a rectangular channel of uniform width and slowly varying depth of the lower layer of water, in which $\kappa_i = 1 (i = 1, 2)$ is taken. Letting $h_1 = c_1^2$, $h_2(x) = C_2^2$, $r = \tilde{\rho} - 1$, and eliminating ζ between Eqs. (2.40)-(2.42) by substituting Eq. (2.42) for ζ into Eqs. (2.40) and (2.41), and neglecting the terms of order higher than the two leading orders, we have two coupled equations for ϕ_1 and ϕ_2 as follows:

$$\tilde{\rho}\phi_{1tt} - \phi_{2tt} + rc_1^2\phi_{1xx} = -rc_1^2\phi_{1x}(\log bc_1)_x + [\frac{1}{3}h_1^2\tilde{\rho}\phi_{1xxtt} - \frac{1}{3}h_2^2\phi_{2xxtt} +$$
$$\frac{1}{2}(\phi_{2x}^2)_t - \tilde{\rho}(\phi_{1x}^2)_t + \phi_{1x}\phi_{2xt} + \phi_{1xx}\phi_{2t} - \tilde{\rho}\phi_{1xx}\phi_{1t}] + h.r.t., \qquad (2.43a)$$

$$\phi_{2tt} - \tilde{\rho}\phi_{1tt} + rC_2(C_2\phi_{2x})_x = -rC_2^2\phi_{2x}(\log bC_2)_x + \frac{1}{3}h_2^2\phi_{2xxtt} - \frac{1}{3}h_1^2\tilde{\rho}\phi_{1xxtt} +$$
$$\frac{1}{2}\tilde{\rho}(\phi_{1x}^2)_t - (\phi_{2x}^2)_t + \tilde{\rho}\phi_{2x}\phi_{1xt} + \tilde{\rho}\phi_{1t}\phi_{2xx} - \phi_{2xx}\phi_{2t} + h.r.t. \qquad (2.43b)$$

In order to derive the bidirectional model, we adopt the multiple scale expansion in terms of the new variables,

$$\eta_\pm = \alpha^{1/2}[t \mp \int \frac{dx}{C(x)}], \qquad \tau = \alpha^{3/2}t, \qquad (2.44a)$$

with corresponding expansions

$$\phi_i = \alpha^{1/2}[\phi_i^{(o)}(\eta_+, \eta_-; \tau) + \alpha\phi_i^{(1)}(\eta_+, \eta_-; \tau) + \cdots], \tag{2.44b}$$

$$\zeta = \alpha(\zeta_o + \alpha\zeta_1 + \cdots), \tag{2.44c}$$

$$b(x) = b_o + \alpha b_1 + \cdots, \tag{2.44d}$$

$$C_2(x) = c_2 + \alpha c_{21}(x) + \cdots, \tag{2.44e}$$

$$C(x) = c + \alpha c_{o1}(x) + \cdots, \tag{2.44f}$$

where c is the phase speed of the baroclinic slow-mode IWs motion satisfying the equation

$$\tilde{\rho}(\frac{c}{c_1})^2 + (\frac{c}{c_2})^2 + r = 0, \qquad r = \tilde{\rho} - 1. \tag{2.44g}$$

The corresponding differential operators are

$$\partial_t = \alpha^{1/2}[(\partial_+ + \partial_-) + \alpha\partial_\tau], \qquad c\partial_x = \alpha^{1/2}(\partial_- - \partial_+), \tag{2.45a}$$

$$\partial_+ = \frac{\partial}{\partial\eta_+}, \qquad \partial_- = \frac{\partial}{\partial\eta_-}, \qquad \partial_\tau = \frac{\partial}{\partial\tau}. \tag{2.45b}$$

Hence, to the first order, Eqs. (2.43a,b) and (2.42) yield the following equations:

$$O(\alpha^{3/2}): \quad (\partial_+ + \partial_-)^2(\tilde{\rho}\phi_1^{(o)} - \phi_2^{(o)}) + r(\frac{c_1}{c})^2(\partial_- - \partial_+)^2\phi_o^{(1)} = 0, \tag{2.46a}$$

$$O(\alpha^{3/2}): \quad (\partial_+ + \partial_-)^2(\phi_2^{(o)} - \tilde{\rho}\phi_1^{(o)}) + r(\frac{c_2}{c})^2(\partial_- - \partial_+)^2\phi_o^{(2)} = 0, \tag{2.46b}$$

$$O(\alpha): \quad (\partial_+ + \partial_-)(\tilde{\rho}\phi_1^{(o)} - \phi_2^{(o)}) + r\zeta_o = 0. \tag{2.46c}$$

Combining Eqs. (2.46a,b,c), we find for ζ_o the equation

$$\partial_+\partial_-\zeta_o = 0, \tag{2.47a}$$

and the general solution of the form

$$\zeta_o = \zeta_+(\eta_+;\tau) + \zeta_-(\eta_-;\tau), \tag{2.47b}$$

which composes a right-going and a left-going wave independently. Their interaction can be sought by solving the next order equations. To the second order, Eqs. (2.43a,b)(2.42) give

$$O(\alpha^{5/2}): \quad (\partial_+ + \partial_-)^2(\tilde{\rho}\phi_1^{(1)} - \phi_2^{(1)}) + r(\frac{c_1}{c})^2(\partial_- - \partial_+)^2\phi_1^{(1)} =$$

$$-r(\frac{c_1}{c})^2[(\partial_- - \partial_+)\phi_1^{(o)}](\partial_- - \partial_+)(\log bc_1) + \frac{1}{3c^2}(\partial_-^2 - \partial_+^2)^2(\tilde{\rho}h_1^2\phi_1^{(o)} - h_2^2\phi_2^{(o)}) +$$

$$\frac{1}{2c^2}(\partial_+ + \partial_-)[(\partial_- - \partial_+)\phi_2^{(o)}]^2 - \frac{\tilde{\rho}}{c^2}(\partial_+ + \partial_-)[(\partial_- - \partial_+)\phi_1^{(o)}]^2 +$$

$$\frac{1}{c^2}[(\partial_- - \partial_+)\phi_1^{(o)}][(\partial_-^2 - \partial_+^2)\phi_2^{(o)}] + \frac{1}{c^2}[(\partial_- - \partial_+)^2\phi_1^{(o)}][(\partial_+ + \partial_-)\phi_2^{(o)}] -$$

$$\frac{\tilde{\rho}}{c^2}[(\partial_- - \partial_+)^2\phi_1^{(o)}][(\partial_- + \partial_+)\phi_1^{(o)}] - 2(\partial_+ + \partial_-)\partial_\tau(\tilde{\rho}\phi_1^{(o)} - \phi_2^{(o)}), \tag{2.48a}$$

$$O(\alpha^{5/2}): \quad (\partial_+ + \partial_-)^2(\phi_2^{(1)} - \tilde{\rho}\phi_1^{(1)}) + r(\frac{c_2}{c})^2(\partial_- - \partial_+)^2\phi_2^{(1)} =$$

$$-r(\frac{c_2}{c})^2[(\partial_- - \partial_+)\phi_2^{(o)}](\partial_- - \partial_+)(\log bc_2) + \frac{1}{3c^2}(\partial_-^2 - \partial_+^2)^2(h_2^2\phi_2^{(o)} - \tilde{\rho}h_1^2\phi_1^{(o)}) +$$

$$\frac{\tilde{\rho}}{2c^2}(\partial_+ + \partial_-)[(\partial_- - \partial_+)\phi_1^{(o)}]^2 - \frac{1}{c^2}(\partial_+ + \partial_-)[(\partial_- - \partial_+)\phi_2^{(o)}]^2 +$$

$$\frac{\tilde{\rho}}{c^2}[(\partial_- - \partial_+)\phi_2^{(o)}][(\partial_-^2 - \partial_+^2)\phi_1^{(o)}] + \frac{\tilde{\rho}}{c^2}[(\partial_- - \partial_+)^2\phi_2^{(o)}][(\partial_+ + \partial_-)\phi_1^{(o)}] -$$

$$\frac{1}{c^2}[(\partial_- - \partial_+)^2\phi_2^{(o)}][(\partial_- + \partial_+)\phi_2^{(o)}] - 2(\partial_+ + \partial_-)\partial_\tau(\phi_2^{(o)} - \sigma\phi_1^{(o)}), \tag{2.48b}$$

$$O(\alpha^2): \quad (\partial_+ + \partial_-)(\tilde{\rho}\phi_1^{(1)} - \phi_2^{(1)}) + r\zeta_1 = -\partial_\tau(\tilde{\rho}\phi_1^{(o)} - \phi_2^{(o)}) - \frac{\tilde{\rho}}{2c^2}[(\partial_- - \partial_+)\phi_1^{(o)}]^2 +$$

$$\frac{1}{2c^2}[(\partial_- - \partial_+)\phi_2^{(o)}]^2 + \frac{1}{3c^2}(\partial_+ + \partial_-)(\partial_- - \partial_+)^2(\tilde{\rho}h_1^2\phi_1^{(o)} - h_2^2\phi_2^{(o)}). \qquad (2.48c)$$

Assuming the flow at $x = \pm\infty$ to be regular, i.e.,

$$\overline{u}, \overline{u_x}, \overline{u_{xx}}, \zeta, \zeta_x \to 0, \quad \text{sufficiently fast as} \quad |x| \to \infty, \qquad (2.49)$$

and using Eq. (2.47b), we obtain from Eqs. (2.46a,b) the following relations:

$$(\partial_+ + \partial_-)(\tilde{\rho}\phi_1^{(o)} - \phi_2^{(o)}) = -r(\zeta_- + \zeta_+), \qquad (2.50a)$$

$$(\partial_- - \partial_+)\phi_1^{(o)} = (\frac{c}{c_1})^2(\zeta_- - \zeta_+), \qquad (2.50b)$$

$$(\partial_- - \partial_+)\phi_2^{(o)} = -(\frac{c}{c_2})^2(\zeta_- - \zeta_+), \qquad (2.50c)$$

$$(\partial_+ + \partial_-)\phi_1^{(o)} = (\frac{c}{c_1})^2(\zeta_+ + \zeta_-), \qquad (2.50d)$$

$$(\partial_+ + \partial_-)\phi_2^{(o)} = -(\frac{c}{c_2})^2(\zeta_+ + \zeta_-). \qquad (2.50e)$$

By taking $(\frac{c}{c_1})^2\tilde{\rho} \times (2.47a) - (\frac{c}{c_2})^2 \times (2.47b)$, we obtain for $(\tilde{\rho}\phi_1^{(1)} - \phi_2^{(1)})$ the equation

$$-4\partial_+\partial_-(\tilde{\rho}\phi_1^{(1)} - \phi_2^{(1)}) = -2r\partial_\tau(\zeta_- + \zeta_+) + r(\zeta_- - \zeta_+)(\partial_- - \partial_+)\log bc -$$

$$\frac{1}{3}D(\partial_-^3\zeta_- + \partial_+^3\zeta_+) + \frac{A}{2}\partial_+(\zeta_+^2) + \frac{A}{2}\partial_-(\zeta_-^2) + B(\partial_-\zeta_+\zeta_- + \partial_+\zeta_+\zeta_-), \qquad (2.51a)$$

where

$$A = 3c^2(\frac{\tilde{\rho}}{c_1^4} - \frac{1}{c_2^4}), \quad B = -\frac{1}{3}A, \quad D = (\tilde{\rho}c_1^2 + c_2^2). \qquad (2.51b)$$

The solvability condition that prevents $(\tilde{\rho}\phi_1^{(1)} - \phi_2^{(1)})$ from growing linearly with ζ_+ or ζ_- requires that the secular terms on the right-hand side of (2.51a) must vanish separately with respect to ζ_+ and ζ_-. In other words, the solvability condition must obey the conservation laws and be consistant with uni-directional

KdV equation when a right-going or a left-going wave is the only traveling wave. Following the general principles enunciated by Wu (1994), we obtain a set of equations as follows:

$$-2r\partial_\tau\zeta_+ - r(\zeta_+ - \zeta_-)(\partial_- - \partial_+)\log bc - \frac{1}{3}D\partial_+^3\zeta_+ + \frac{A}{2}\partial_+(\zeta_+^2) = 0, \qquad (2.52a)$$

$$-2r\partial_\tau\zeta_- - r(\zeta_+ - \zeta_-)(\partial_- - \partial_+)\log bc - \frac{1}{3}D\partial_-^3\zeta_- + \frac{A}{2}\partial_-(\zeta_-^2) = 0, \qquad (2.52b)$$

$$-4\partial_+\partial_-(\tilde{\rho}\phi_1^{(1)} - \phi_2^{(1)}) = -r(\zeta_- - \zeta_+)(\partial_- - \partial_+)\log bc + B(\partial_-\zeta_+\zeta_- + \partial_+\zeta_+\zeta_-). \qquad (2.52c)$$

Under the same principle as that established for the case of single layer of fluid (Wu 1994), the separation (2.52a,b,c) is unique. Therefore, Eq. (2.47c) provides for ζ_1 the equation

$$r\zeta_1 = -(\partial_- + \partial_+)(\tilde{\rho}\phi_1^{(1)} - \phi_1^{(2)}) - \partial_\tau(\tilde{\rho}\phi_o^{(1)} - \phi_o^{(2)}) - \frac{A}{6}(\zeta_- - \zeta_+)^2 + \frac{1}{3}D(\partial_-^2\zeta_- + \partial_+^2\zeta_+). \qquad (2.53)$$

From Eq. (2.50), we find for $\zeta_\pm$ the relation

$$\zeta_\pm = -\partial_\pm\psi_\pm, \qquad (2.54a)$$

where $r(\psi_+ + \psi_-) = \tilde{\rho}\phi_1^{(o)} - \phi_2^{(o)}$, and we assume that for varying channels with negligible convexity of the channel admittance (bc) (Wu 1994), namely

$$(bc)_{xx} << (bc)_x, \qquad \psi_\pm(\log bc)_\pm|_{+\infty}^{-\infty} = 0. \qquad (2.54b)$$

Eqs. (2.52a,b,c) yield the relation

$$-2r\partial_\tau\psi_\pm = -2r\zeta_\mp\int(\log bc)_x dx - \frac{1}{3}D\partial_\pm^2\zeta_\pm + \frac{A}{2}\zeta_\pm^2, \qquad (2.55a,b)$$

$$(\tilde{\rho}\phi_1^{(1)} - \phi_2^{(1)}) = \frac{B}{4}(\psi_+\zeta_- + \zeta_+\psi_-) + \frac{1}{2}r(\psi_- + \psi_+)\int(\log bc)_x dx + \Phi_+(\zeta_+) + \Phi_-(\zeta_-). \tag{2.55c}$$

In general, we may choose the integration constant function $\Phi_\pm$ as

$$\partial_\pm \Phi_\pm = \frac{1}{6}D\partial_\pm^2\zeta_\pm + \frac{1}{12}A\zeta_\pm^2, \tag{2.56}$$

then Eq. (2.53) reduces to the form of

$$\zeta_1 = -\frac{B}{2r}\zeta_-\zeta_+ - \frac{B}{4r}(\psi_+\partial_x\zeta_- - \psi_-\partial_x\zeta_+) - \frac{1}{2}(\zeta_- + \zeta_+)\int(\log bc)_x dx. \tag{2.57c}$$

In the physical coordinates, the Eqs. (2.52a,b) for $\zeta_\pm$ are

$$(\pm\frac{1}{c}\partial_t + \partial_x)\zeta_\pm \pm \frac{1}{2}(\zeta_+ - \zeta_-)(\log bc)_x - \frac{1}{6r}Dc^2\partial_x^3\zeta_\pm + \frac{1}{4r}A\partial_x(\zeta_\pm^2) = 0. \tag{2.57a,b}$$

In the case of uniform channel admittance, $bc = const$, Eqs. (2.57a,b) coincide with that of Mei's (1987). If $\tilde{\rho} = 0$, the result is the same as Wu's (1994). Therefore, the modelling equations in the physical coordinates ($\epsilon = 1$) are

$$\zeta = \zeta_+ + \zeta_- + \zeta_1$$

$$= [\zeta_+(x + \frac{B}{4r}\psi_-, t) + \zeta_-(x - \frac{B}{4r}\psi_+, t)][1 - \frac{1}{2}\int(\log bc)_x dx] - \frac{B}{2r}\zeta_-\zeta_+, \tag{2.58}$$

which says that a head-on collision between a right-going ISW and a left-going ISW results in a phase shift in x by $B\psi_-/4r$ for ζ_+ and $B\psi_+/4r$ for ζ_-. The phase shifts of two waves are both backward in space, i.e., both retarded in time (as shown in Figure 2.2). These phase shifts are noted to never arise in the linear theory. The final shifts vary with the wave amplitudes. The terminal phase shifts appear to play an important role in processes of nonlinear wave interaction and

evolution. For the uniform channels with flat bottoms, the phase shifts of head-on collisions of two ISWs can be expressed in terms of the time (for fixed x) as

$$\delta_{\pm} = \Delta t_{\pm} = \frac{B}{4r}[\psi_{\mp}(x \pm \frac{B}{4r} = 0, t = \infty) - \psi_{\mp}(x \pm \frac{B}{4r} = 0, t = -\infty)]$$
$$= \frac{B}{4r} a_{\mp} \Delta_{\mp} > 0, \tag{2.59}$$

where $a_{\pm}$ are nondimensional amplitudes of right-going and left-going waves, respectively, and $\Delta_{\pm} = \sqrt{8c^2 D/A a_{\pm}}$. When $\tilde{\rho} = 0, h_1 = h_2 = 1$, we have

$$\delta_{\pm} = \sqrt{\frac{a_{\mp}}{3}}, \tag{2.60}$$

which is the same as that of Wu's theory (1995). The relations between phase shifts and the depth ratio for head-on collision of two ISWs in the density ratio are shown in Figure 2.3(a,b). For the head-on collision of two ISWs of elevation, the phase shift increases as the depth ratio increases with a fixed density ratio; for the head-on collision of two ISWs of depression, the phase shift has a maximum value at a given depth ratio.

2.2.2 Validation and Discussion

The model equations (2.57a,b,c) are found to ensure invariance of excess mass to second order; that is

$$\dot{m_e} = \frac{d}{dt} m_e = \frac{d}{dt} \int_{-\infty}^{+\infty} b(x)\zeta(x,t)dx = \int b(x)(\zeta_- + \zeta_+)_t dx$$
$$= \int [bc(\zeta_- - \zeta_+ - \frac{Dc^2}{6r}(\partial_x^2 \zeta_- - \partial_x^2 \zeta_+) + \frac{A}{4r}(\zeta_-^2 - \zeta_+^2)]_x dx + O(\alpha^3), \tag{2.61a}$$

which vanishes, leaving an error of $O(\alpha^3)$. In addtion, we have for the energy conservation the relation

$$\dot{E} = \frac{d}{dt} \int b(x)(\zeta_-^2 + \zeta_+^2)dx$$

$$= 2\int [bc(\zeta_-^2 - \zeta_+^2 + \frac{A}{12r}(\zeta_-^3 - \zeta_+^3) + \frac{1}{12r}Dc^2(\zeta_{-x}^2 - \zeta_{+x}^2)]_x dx + O(\alpha^3), \quad (2.61b)$$

which also vanishes with an error of $O(\alpha^3)$. For the momentum variation $\Delta\mathcal{L}$ when $b = const$, which is equal to the sum of the products of the excess mass of the ISW ($m_\pm = \lambda_\pm \alpha_\pm \quad for \quad \zeta_\pm$) with their respective phase shift in x (for fixed t) which is $\Delta x_\pm = \mp\Delta t_\pm = \pm(B/2r)\lambda_\mp \alpha_\mp$, we have

$$\Delta\mathcal{L} = m_+\Delta x_+ + m_-\Delta x_- = 0, \quad (2.62)$$

where $\lambda_\pm = \frac{4}{3}(D/\alpha_\pm B)$, and α_+ and α_- are the amplitudes for the right-going '+' and left-going '−' waves, respectively.

The ultimate definitive measure of accuracy of the bidirectional wave model (2.57a,b,c) can be made by comparison with the numerical results based on the ILW model (2.40)-(2.42). The agreement between the two models for constant channel width, as shown in Figure 2.4, appears very good in terms of wave profiles and phase shifts throughout the head-on collision. The head-on collision of two ISWs of depression are solved numerically with the predictor-corrector two-step procedure which will be discussed in Chapter 4. The depths of two layers are $h_1 = 1.0$ and $h_2 = 2.0$. The density ratio $\tilde{\rho} = 0.9$.

In the model equations (2.57a,b), the linear terms $\pm\frac{1}{2}(\zeta_+ - \zeta_-)(logbc)_x$ may represent the forcing term to generate reflected waves in (2.57b) (or (2.57a)) when there exists only right-going (or left-going) waves as incident waves. This model tells us that there exist reflected waves as long as $c_x \neq 0$. Besides, we found that this kind of splitting form is unique under the conservation laws, and that Eqs. (2.40)-(2.42) are equivalent to the model equations exactly in the linear system. If we take ζ_+ and ζ_- as new variables, namely

$$\zeta = \zeta_+ + \zeta_-, \quad (2.63a)$$

$$M = \tilde{\rho}\phi_{1x} - \phi_{2x} = \frac{\tilde{\rho} - 1}{c}(\zeta_+ - \zeta_-), \tag{2.63b}$$

the linear system of Eqs. (2.40)-(2.42) without dispersion is found to agree with the linearized model equations (2.57a,b) directly. These two kinds of linear systems provide the same numerical solution, shown in Figure 2.5, for a specific initial wave climbing a cosine-shape shelf, which is shown in Figure 4.1. The reflected wave, which is about 1% of the transmitted wave, is exactly predicted by Eq. (2.57b). The numerical computations are done by the Lax-Wendroff scheme. The computational parameters for the results shown in Figure 4.1 are taken with $h_1 = 1.0, h_2 = 1.5, a = -0.1, X_o = 150, X_1 = 200, L = 20, d = 1.2, \tilde{\rho} = 0.85$.

Figures for Chaper 2

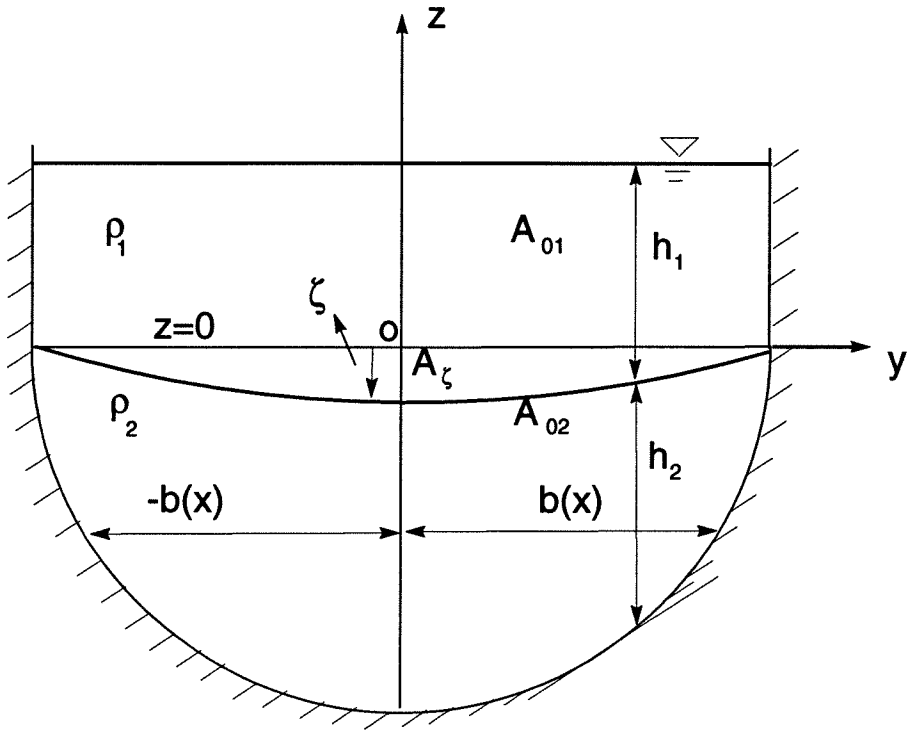

(a) main view

Figure 2.1(a,b,c) The coordinate system of a channel with an arbitrary cross section. The x coordinate varies along the channel. The undisturbed interface is $z = 0$. The sides of the channel are specified by $y = b(x)$. The depths of two layers are h_1 and h_2 with densities ρ_1 and ρ_2, respectively. A_{o1} and A_{o2} are unperturbed wetted areas in the top and lower regions, respectively. A_ζ is the area variation due to wave motion at the interface.

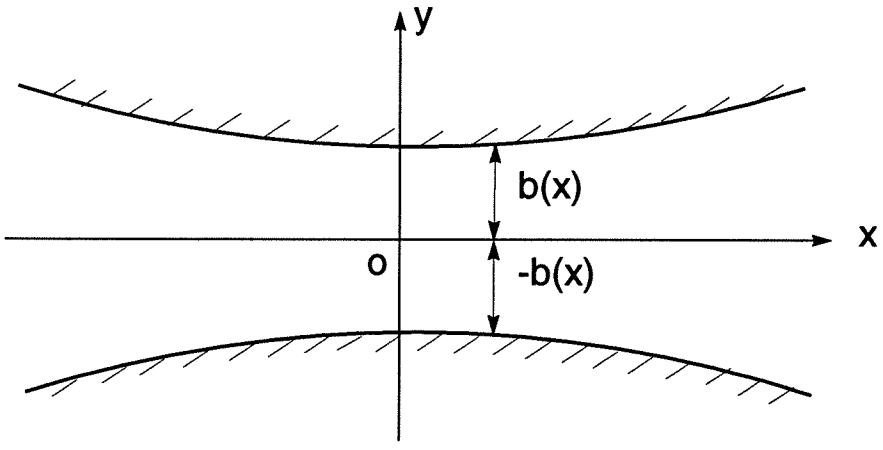

(b) top view

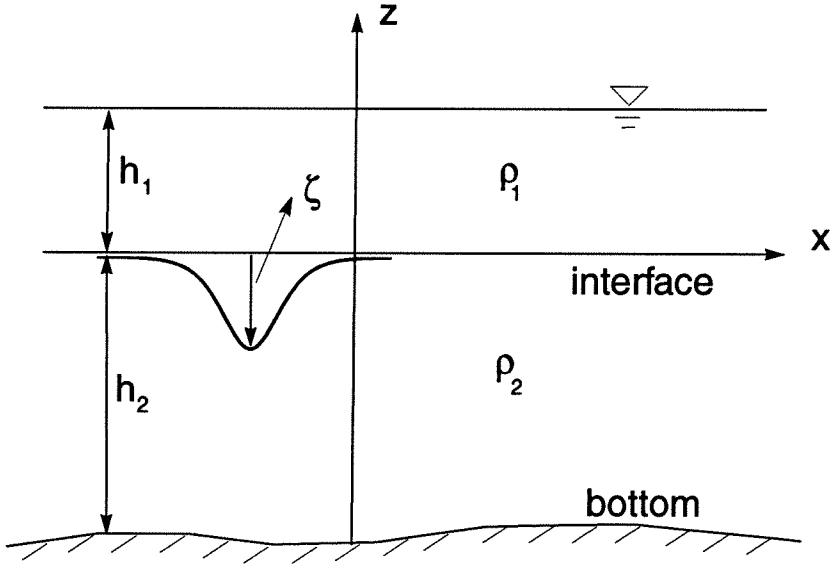

(c) side view

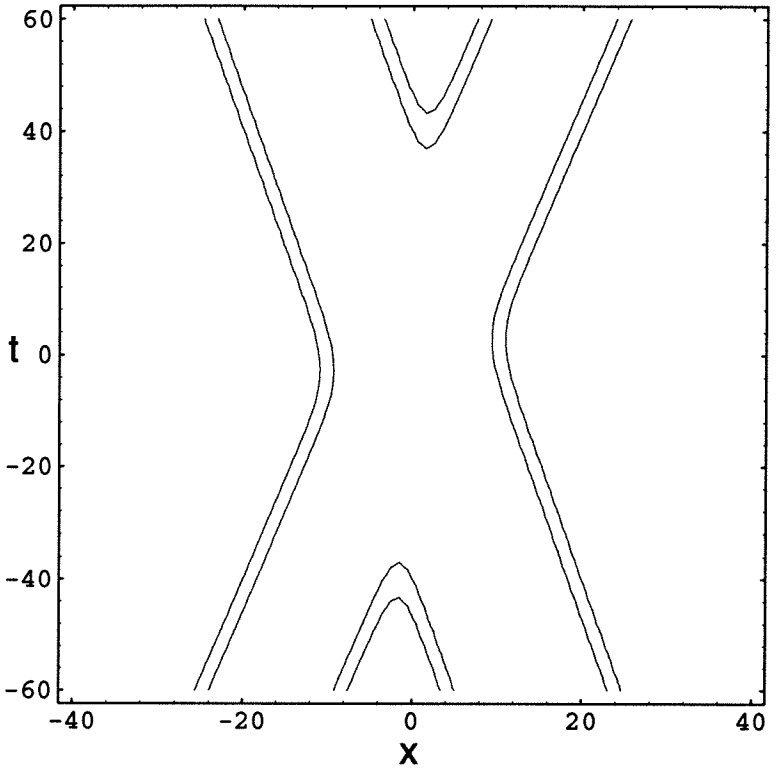

Figure 2.2 The space-time contour plot shows two ISWs of depression experience backward phase shifts in space after their head-on collision. The parameters are taken with $h_1 = 1.0, h_2 = 2.0, a_1 = -0.2, a_2 = -0.5, \tilde{\rho} = 0.9$.

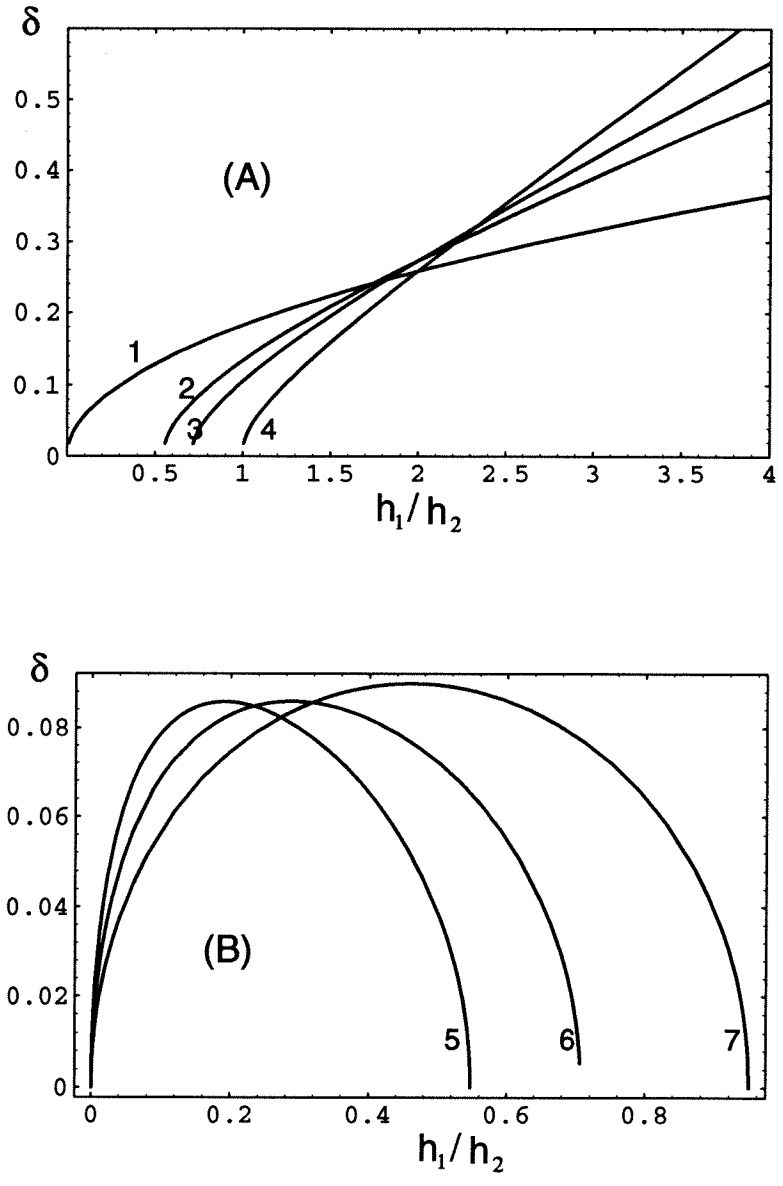

Figure 2.3 The relation between phase shifts δ and depth ratio (h_1/h_2) for head-on collisions of: (A) two ISWs of elevation ($a = 0.1$); (B) two ISWs of depression ($a = -0.1$). The density ratios for each line are: *0 in line 1; 0.3 in line 2; 0.5 in line 3; 0.99 in line 4; 0.5 in line 6; 0.9 in line 7.*

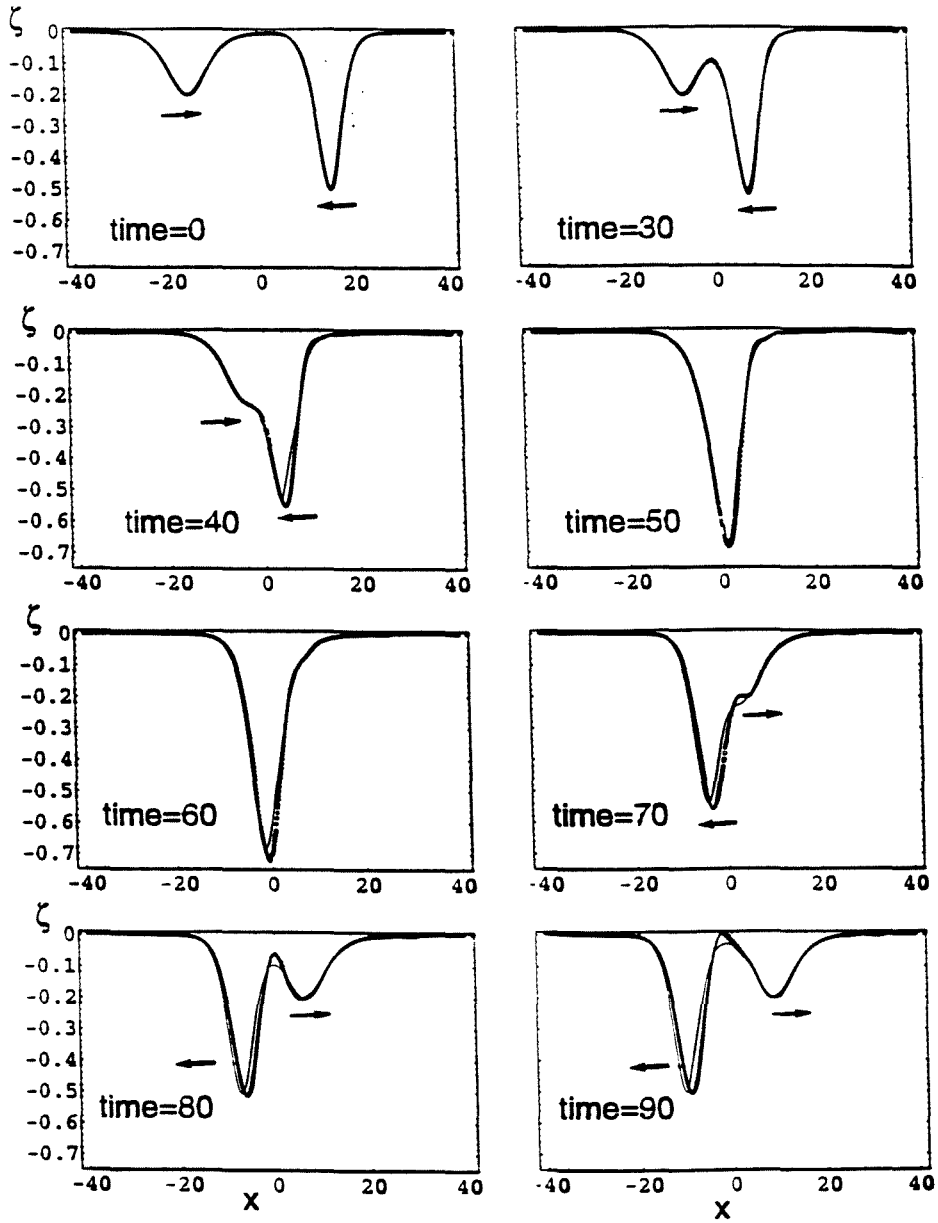

Figure 2.4 The comparison between Eq. (2.58) and the numerical result from the ILW model for head-on collision of two ISWs of depression. The parameters are taken with $h_1 = 1.0, h_2 = 2.0, a_1 = -0.2, a_2 = -0.5, \tilde{\rho} = 0.9$. The phase shifts are shown in Fig. 2.3. —— from Eq. (2.58); ···· from the ILW model.

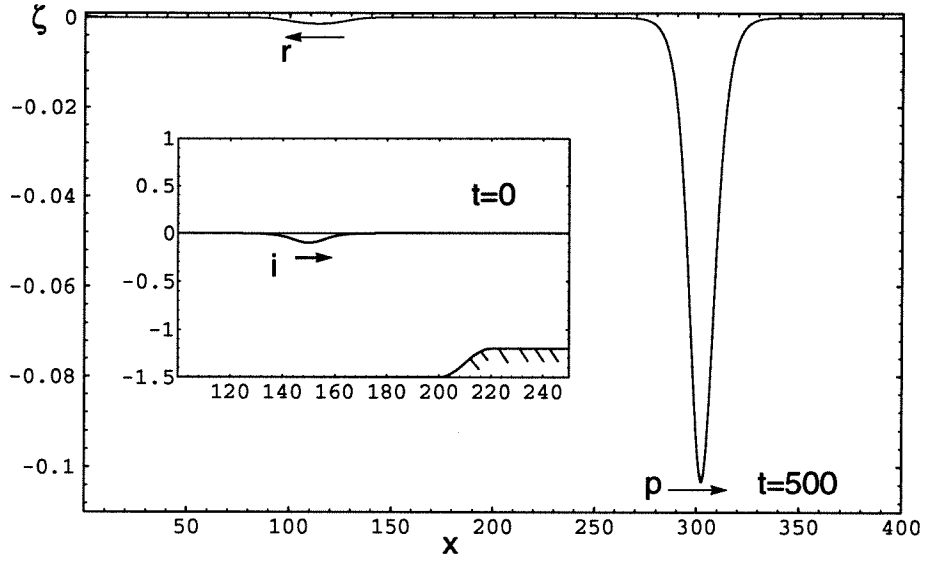

Figure 2.5 The numerical solutions of two linear systems from Eqs. (2.40)–(2.42) with dispersive terms neglected and Eqs. (2.57a,b) provide same transmitted and reflected ISWs when an incident ISW of depression propagates on a cosine-shaped bottom topography. The parameters shown in Fig. 4.1 are taken with $a_1 = -0.1, h_1 = 1.0, h_2 = 1.5, d = 1.2, x_o = 150, x_1 = 200, L = 20, \tilde{\rho} = 0.85$. i: incident wave; r: reflected wave; p: transmitted wave.

Chapter 3

The Run-up of Oceanic Internal Waves on the Sloping Seabeds

In this chapter, devoted in particular to the 2D case, we apply the ILW model to study the nonlinear geophysical phenomenon of run-up of two-dimensional oceanic internal waves on a submerged seabed of uniform slope. An internal-wave run-up model is developed for nonlinear and nondispersive long waves propagating along the interface of a two-layered inviscid fluid and incident upon the sloping seabed.

3.1 The Theoretical Model

In the 2D case, the ILW model with the dispersive terms neglected may be written as

$$(h_1 - \zeta)_t + [(h_1 - \zeta)u_1]_x = 0, \tag{3.1}$$

$$(h_2 + \zeta)_t + [(h_2 + \zeta)u_2]_x = 0, \tag{3.2}$$

$$u_{2t} + u_2 u_{2x} + g_e \zeta_x = \tilde{\rho}(u_{1t} + u_1 u_{1x}), \tag{3.3}$$

where the subscripts x and t denote partial differentiation with respect to the seaward x-axis and the time t, $\tilde{\rho} = \rho_1/\rho_2$, $g_e = (1-\tilde{\rho})g$, g being the gravitational

acceleration, $u_1 = \bar{u_1}(x,t)$ and $u_2 = \bar{u_2}(x,t)$ are the depth-mean values of the horizontal fluid velocities $u_1(x,y,t)$ and $u_2(x,y,t)$ in the upper and lower layers, here with the overhead bar omitted. For the general case of two-dimensional non-uniform sloping seabed (with slope varying with x), the above set of nonlinear equations for the unknowns u_1, u_2, ζ is very difficult to solve by analytical means, even with the rigid-lid approximation. To help make resolution of this nonlinear system more amenable, we shall assume the seabed to have a uniform slope,

$$h_2 = sx, \quad h_1 = \text{const}, \quad (0 < \mathrm{x} < \infty) \tag{3.4a}$$

$$h_2 = sx, \quad h_1 = \text{const} + \mathrm{sx}, \quad (-\mathrm{h_1/s} < \mathrm{x} < 0), \tag{3.4b}$$

where s is the slope of the seabed which intersects the undisturbed interface at the origin and the upper (fixed) ocean surface at $(-h_1/s, h_1)$ (see Figure 3.1). In addition, we assume that the motion vanishes at infinity,

$$u_1, u_2, \zeta \to 0 \quad \text{as} \quad \mathrm{x} \to +\infty. \tag{3.5}$$

3.2 Linear Theory

The system of equations (3.1)–(3.3) can be linearized by retaining only the first order terms to give the following equations:

$$\zeta_t - (h_1 u_1)_x = 0, \tag{3.6a}$$

$$\zeta_t + (h_2 u_2)_x = 0, \tag{3.7a}$$

$$u_{2t} + g_e \zeta_x = \tilde{\rho} u_{1t}. \tag{3.8a}$$

Under condition (3.5), Eqs. (3.6a) and (3.7a) can be integrated on x to give

$$h_1 u_1 + h_2 u_2 = 0, \qquad u_1 = -\frac{h_2}{h_1} u_2. \tag{3.9}$$

Substituting (3.9) into (3.8a), we have

$$(1 + \tilde{\rho}\frac{h_2}{h_1}) u_{2t} + g_e \zeta_x = 0. \tag{3.10}$$

Eliminating u_2 between Eqs. (3.7a) and (3.10), we get for ζ the equation

$$\zeta_{tt} + [(\frac{g_e h_2}{1 + \frac{\tilde{\rho} h_2}{h_1}})\zeta_x]_x = 0, \tag{3.11}$$

which is the basic equation for the outer region of nonlinear equations (3.1)-(3.3) for waves in deep water and also for the inner region of linear waves. The amplitude of waves is assumed to be finite at $x = 0$. A periodic internal wave on a gradually varying slope will have the form of

$$\zeta = A J_o(2K_e\sqrt{x}) \sin \omega t, \tag{3.12}$$

where A is a constant, $K_e = \omega/\sqrt{g_e s}$, J_o is the first kind Bessel function of order zero, and ω represents frequency. In the asymptotic limit of $2K_e\sqrt{x} >> 1$, Eq. (3.12) becomes

$$\zeta \approx A_i \sin(\omega t + 2K_e\sqrt{x} - \frac{\pi}{4}) + A_r \sin(\omega t - 2K_e\sqrt{x} + \frac{\pi}{4}), \tag{3.13}$$

where

$$A_i = A_r = \frac{A}{2}(\frac{1}{\pi K_e})^{1/2} x^{-1/4}. \tag{3.14}$$

We find that reflected wave has the same amplitude as the incident wave but differs in phase.

In the following, the linear WKB theory is applied to solve the linear equations (3.6a)–(3.8a) for the outer region of linear equations (3.6a)–(3.8a). First, we introduce for very small s the slow coordinates

$$\overline{x} = sx, \quad \overline{t} = st, \tag{3.15}$$

then Eqs. (3.6a)–(3.8a) are changed to the form of

$$\zeta_{\overline{t}} - (h_1 u_1)_{\overline{x}} = 0, \tag{3.6b}$$

$$\zeta_{\overline{t}} + (h_2 u_2)_{\overline{x}} = 0, \tag{3.7b}$$

$$u_{2\overline{t}} + g_e \zeta_{\overline{x}} = \tilde{\rho} u_{1\overline{t}}. \tag{3.8b}$$

After eliminating u_1 and u_2, we obtain for ζ the equation

$$\gamma_1(\overline{x})\zeta_{\overline{t}\overline{t}\overline{x}} - \beta_1(\overline{x})\zeta_{\overline{x}\overline{x}\overline{x}} - 2\gamma_2(\overline{x})\zeta_{\overline{x}\overline{x}} + 2\beta_2(\overline{x})\zeta_{\overline{t}\overline{t}} = 0, \tag{3.16}$$

where

$$\gamma_1(\overline{x}) = 1 + \frac{\tilde{\rho} h_2}{h_1}, \quad \beta_1(\overline{x}) = g_e \overline{x}, \quad \gamma_2(\overline{x}) = \frac{\tilde{\rho}}{h_1}, \quad \beta_2(\overline{x}) = g_e. \tag{3.17}$$

The required form of expansion is assumed to take for small s the form

$$\zeta = e^{i\Theta/s} \sum_{n=0}^{\infty} s^n A_n(\overline{x}, \overline{t}), \tag{3.18}$$

where wave number $k = \Theta_{\overline{x}}$, and wave frequency $\omega = -\Theta_{\overline{t}}$, which provide

$$k_{\overline{t}} + \omega_{\overline{x}} = 0. \tag{3.19}$$

For the waves are steady, i.e., $\partial/\partial t = 0$, Eq. (3.19) implies that $\omega = constant$ in both time and space. Substituting (3.18) into (3.16) by straightforward differentiation, we obtain the equations by successive orders. The first order equation gives the dispersion relation between ω and k, namely

$$\gamma_1 \omega^2 = \beta_1 k^2. \tag{3.20}$$

The second order equation gives for A_o the equation

$$(\omega A_o^2)_{\bar{t}} + (\omega A_o^2 \frac{\omega}{k})_{\bar{x}} = 0. \tag{3.21}$$

It is easy to find that the relevant solution of (3.20) and (3.21) is

$$A_o = A_\infty (\frac{1}{K_e})^{1/2} x^{-1/4}, \tag{3.22a}$$

along the characteristic line

$$\frac{dx}{dt} = C_g, \tag{3.22b}$$

where A_∞ is a constant, the group velocity $C_g = \partial\omega/\partial k$, which is same as the phase velocity from Eq. (3.20). This is the outer limit of the solution based on the linear equations. Hence, we may match the inner solution (3.13) with the outer solution (3.22a); we find the phase shift

$$\delta_1 = -\frac{\pi}{4}, \quad A_\infty = \frac{A}{2\sqrt{\pi}}. \tag{3.23}$$

The phase shift may be observed in the experiment, which will be discussed in Chapter 4.

3.3 Nonlinear Theory

3.3.1 Analysis

For fixed seabed, the sum of Eq. (3.1) and Eq. (3.2) can be integrated on x to give

$$(h_1 - \zeta)u_1 + (h_2 + \zeta)u_2 = 0, \tag{3.24a}$$

in which an additive integration constant function of t is set to zero according to the condition (3.5). While the internal waves need not be small compared to the depth $h_2(x)$ of the lower layer, especially near the interfacial waterline at which $\zeta(x,t) + h_2(x) = 0$, we shall however assume that the wave amplitude is small compared to the depth h_1 of the upper layer,

$$|\zeta| \ll h_1 \ , \tag{3.24b}$$

implying that the upper layer is sufficiently deep as supposed. Under this condition, Eq. (3.24a) reduces to

$$u_1 = -(h_2 + \zeta)u_2/h_1 = -(c_2/c_1)^2 u_2, \tag{3.25a}$$

where

$$c_2^2 = g_e(h_2 + \zeta), \qquad c_1^2 = g_e h_1, \tag{3.25b}$$

c_2 and c_1 being two critical wave velocities for this nonlinear system. In terms of u_2 and c_2 as two unknowns, Eq. (3.2) and Eq. (3.3) can be converted to read:

$$2c_{2t} + 2u_2 c_{2x} + c_2 u_{2x} = 0, \tag{3.26a}$$

$$a_1 u_{2t} + a_2 u_2 u_{2x} + 2a_3 c_2 c_{2x} = g_e h_{2x} = g_e s \equiv m, \tag{3.26b}$$

where

$$a_1 = 1 + \tilde{\rho}\gamma^2, \quad a_2 = 1 - \tilde{\rho}\gamma^2(1+\gamma^2), \quad a_3 = 1 - \tilde{\rho}\mu^2(1+\gamma^2), \tag{3.26c}$$

$$\gamma^2 = (h_2 + \zeta)/h_1 = (c_2/c_1)^2, \quad \mu = u_2/c_1, \tag{3.26d}$$

in which $m = g_e s$ is a constant. The above equations (3.26a,b) are our basic system for analysis and calculation of internal waves interacting with sloping seabed.

The effects of change in depth of the seabed are reflected through a specific variation in the variable c_2 and in combination with the effect of stratification to yield variable coefficients a_1, a_2, and a_3 in Eqs. (3.26b) as slowly varying functions of position and flow states. In the absence of the top layer, i.e., with $\tilde{\rho} = 0$, this system reduces to the case of single layer of a homogeneous fluid considered by Stoker (1948), Carrier & Greenspan (1958), Tuck & Hwang (1972) and others. We shall, however, consider the case of practical interest with $(1 - \tilde{\rho}) \simeq 0.02 - 0.03$ as for typical thermoclines in the ocean.

By conventional methods of considering the linear combination of Eqs. (3.26a, b), adding Eq. (3.26a) and $l_{\pm}$Eq. (3.26b), respectively, we find that (3.26a,b) have two mathematical characteristics, $C_{\pm}$, along which

$$\frac{dx}{dt} = \eta_+(u_2, c_2) \quad \text{on} \quad C_+, \quad (1 + \tilde{\rho}\gamma^2)\frac{\mathrm{du_2}}{\mathrm{dt}} + 2\mathrm{l}_+\frac{\mathrm{dc_2}}{\mathrm{dt}} = \mathrm{m}, \tag{3.27a}$$

$$\frac{dx}{dt} = \eta_-(u_2, c_2) \quad \text{on} \quad C_-, \quad (1 + \tilde{\rho}\gamma^2)\frac{\mathrm{du_2}}{\mathrm{dt}} + 2\mathrm{l}_-\frac{\mathrm{dc_2}}{\mathrm{dt}} = \mathrm{m}, \tag{3.27b}$$

where

$$l_{\pm} = \tilde{\rho}\gamma\mu \pm [1 + \frac{1}{2}\tilde{\rho}(\gamma^2 - \mu^2)], \tag{3.27c}$$

and $\eta_{\pm}$ are the roots of

$$a_1\eta^2 - (a_1 + a_2)^2 u_2\eta + (a_2u_2^2 - a_3c_2^2) = 0,$$

or

$$\eta_{\pm} = \frac{1}{a_1}\{\frac{a_1 + a_2}{2}u_2 \pm [a_1a_3c_2^2 + (\frac{a_1 - a_2}{2})^2u_2^2]^{\frac{1}{2}}\}. \tag{3.27d}$$

If we set $\tilde{\rho} = 0$, we have $\eta_{\pm} = u_2 \pm c_2$, which is the known result (Stoker 1948) for the single layer case. For the two-layer case, $\eta_{\pm}$ is real, inferring that Eqs. (3.26a,b) are hyperbolic in type provided

$$a_1a_3c_2^2 + \frac{1}{4}(a_1 - a_2)^2u_2^2 > 0, \tag{3.28}$$

which is generally satisfied in cases of practical interest.

However, a critical point of considerable importance is to observe that (i) the coefficient a_2 of the nonlinear term $u_2 u_{2x}$ in Eq. (3.26b) has a zero at the critical point where the depths of the two layers are approximately equal (called the critical depth), and (ii) the coefficient a_3 of the nonlinear term $c_2 c_{2x}$ in Eq. (3.26b) vanishes at another critical point which is motion dependent (on u_2). Here, the first turning point is seen to be at $a_2 = 0$, with

$$\gamma^2 \simeq h_2/h_1 \simeq (\sqrt{5}-1)/2 \simeq 0.62, \qquad \text{with} \qquad 0 < (1-\tilde{\rho}) \ll 1, \tag{3.29}$$

and the second critical point being further out since u_2/c_1 is, in general, small. These singular properties are peculiar to stratified fluids, for they do not arise for the simple case of one-layer flows. The critical point at the critical depth has been noted also to exist in the KdV equation modeling uni-directional internal waves propagating on the thermocline of a two-layered fluid. Its effects on the transmission of an incoming solitary wave (facing down in the outer ocean with a deeper lower layer) has been investigated by Knickerbocker & Newell (1980), and Helfrich, Melville & Miles (1984). The critical point problem will be studied based on our ILW model in the next chapter; here we will focus on the nonlinear analysis for applications to an inner region of $\gamma^2 = (h_2 + \zeta)/h_1$ with

$$0 \leq \tilde{\rho}\gamma^2 \ll 1, \tag{3.30}$$

so that the terms comparable with or higher in order than $O(\tilde{\rho}\gamma^4, \tilde{\rho}\mu^2\gamma^2)$ may be neglected compared with unity. This parametric range is nevertheless very useful since it will afford solutions in closed form to provide detailed simulations and predictions of the inner flow field over a moderate fetch containing the moving

waterline of the interface intersecting the seabed. The extreme to-and-fro reaches of the interfacial waterline then gives the range of the run-up of the internal wave.

With the approximation (3.30), the characteristic equations are still Eqs. (3.27a,b), but with

$$\eta_{\pm} = (1 - \hat{\rho}c_2^2)u_2 \pm [1 - \frac{1}{2}\hat{\rho}(c_2^2 + u_2^2)]c_2, \tag{3.31a}$$

where

$$\hat{\rho} = \tilde{\rho}/c_1^2 = \rho_1/(\rho c_1^2). \tag{3.31b}$$

With the same degree of approximation, the original system (3.26a,b) is found, after Eqs. (3.27a,b) are integrated by some straightforward algebra, to possess the Riemann invariants:

$$R_+ = \text{const} = \alpha_+ \quad \text{on} \quad \mathcal{C}_+ : \quad \mathrm{x}_{\alpha_-} = \eta_+(\mathrm{u}_2, \mathrm{c}_2)\mathrm{t}_{\alpha_-}, \tag{3.32a}$$

$$R_- = \text{const} = \alpha_- \quad \text{on} \quad \mathcal{C}_- : \quad \mathrm{x}_{\alpha_+} = \eta_-(\mathrm{u}_2, \mathrm{c}_2)\mathrm{t}_{\alpha_+}, \tag{3.32b}$$

where

$$R_{\pm} = u_2[1 + \hat{\rho}(c_2^2 + \frac{1}{6}u_2^2)] \pm 2c_2(1 + \frac{1}{6}\hat{\rho}c_2^2) - m(t + t_c), \tag{3.32c}$$

$$t_c = \frac{1}{2}\hat{\rho}\int_0^t u_2^2(x(t'), t')dt', \tag{3.32d}$$

in which $x(t')$ assumes the value of x along the characteristics $\mathcal{C}_{\pm}$, as specified by (3.27a,b) and (3.31), respectively, both passing through (x, t) as understood. (α_+, α_-) are the characteristic variables.

Since the value of α_+ or α_- are different along $\mathcal{C}_+$ or $\mathcal{C}_-$ characteristics, the x, t plane may be covered with a new set of coordinate curves $\alpha_+ = const$ and

$\alpha_- = const.$ This suggests that the independent coordinates can be transformed from x, t to α_+, α_-. Let us further adopt the new independent variables (τ, σ), similar to Carrier & Greenspan (1958) for the single-layer case, defined by

$$\frac{\tau}{2} = \frac{\alpha_+ + \alpha_-}{2} = u_2[1 + \hat{\rho}(c_2^2 + \frac{1}{6}u_2^2)] - m(t + t_c), \tag{3.33a}$$

$$\frac{\sigma}{4} = \frac{\alpha_+ - \alpha_-}{4} = c_2(1 + \frac{1}{6}\hat{\rho}c_2^2). \tag{3.33b}$$

In terms of the new independent variables (τ, σ), the equations for the characteristic curves, that is $x_{\alpha_\mp} = \eta_\pm(u_2, c_2)t_{\alpha_\mp}$, become

$$x_\tau - (1 - \hat{\rho}c^2)u_2 t_\tau + [1 - \frac{1}{2}\hat{\rho}(c_2^2 + u_2^2)]c_2 t_\sigma = 0, \tag{3.34a}$$

$$x_\sigma - (1 - \hat{\rho}c_2^2)u_2 t_\sigma + [1 - \frac{1}{2}\hat{\rho}(c_2^2 + u_2^2)]c_2 t_\tau = 0. \tag{3.34b}$$

From Eqs. (3.33a,b), the partial derivatives are also related by

$$mt_\tau = (1 + \hat{\rho}c_2^2)u_{2\tau} - \frac{1}{2}(1 - \frac{1}{2}\hat{\rho}u_2^2), \tag{3.35a}$$

$$mt_\sigma = (1 + \hat{\rho}c_2^2)u_{2\sigma} + \frac{1}{2}\hat{\rho}c_2 u_2. \tag{3.35b}$$

Substituting (3.35a,b) into Eqs. (3.34a,b) to eliminate t, we obtain

$$[x - \frac{u_2^2}{2m} - \frac{\sigma^2}{16m}(1 + \frac{\hat{\rho}\sigma^2}{48})^{-1}]_\sigma + [\frac{\sigma u_2}{4m}(1 + \frac{\hat{\rho}}{48}\sigma^2 - \frac{\hat{\rho}}{6}u_2^2)]_\tau = 0, \tag{3.36a}$$

$$[x - \frac{u_2^2}{2m}]_\tau + \frac{1}{\sigma}[\frac{\sigma^2 u_2}{4m}(1 + \frac{\hat{\rho}}{48}\sigma^2 - \frac{\hat{\rho}}{6}u_2^2)]_\sigma = \frac{\hat{\rho}u_2}{48m}(\sigma^2 + 8u_2^2). \tag{3.36b}$$

These two equations are accurate up to the order specified in Eq. (3.30) and its sequel. The divergence form of Eq. (3.36a) prompts the use of the new variable ψ such that

$$x - \frac{u_2^2}{2m} - \frac{\sigma^2}{16m}(1 + \frac{\hat{\rho}\sigma^2}{48})^{-1} = \frac{1}{4}\psi_\tau, \tag{3.37a}$$

$$\frac{\sigma u_2}{m}[1+\frac{1}{48}\hat{\rho}(\frac{\sigma^2}{48}-8u_2^2)]=-\psi_\sigma. \tag{3.37b}$$

Then (3.36b) yields the equation

$$\frac{1}{\sigma}(\sigma\psi_\sigma)_\sigma-\psi_{\tau\tau}=-\frac{\hat{\rho}u_2}{12m}(\sigma^2+8u_2^2). \tag{3.38}$$

In the absence of the top layer, with $\tilde{\rho}=0$, the above equations (3.37) and (3.38) reduce to those of Carrier & Greenspan (1958) for the case of a single homogeneous layer of fluid. For the present two-layer problem, however, these equations are more complicated.

In view of the inhomogeneous term on the right-hand side of (3.38) being of higher order relative to the terms on the left-hand side, an expedient algorithm is to adopt an iterative approach based on taking the following expansion of ψ in ρ_*, which is a small reference quantity of order $O(\hat{\rho}\gamma^3,\ \hat{\rho}\mu^3)$ near the shoreline and independent of σ and τ,

$$\psi(\sigma,\tau;\rho_*)=\psi_o(\sigma,\tau)+\rho_*\psi_1(\sigma,\tau)+\cdots, \tag{3.39a}$$

$$\frac{1}{\sigma}(\sigma\psi_{o_\sigma})_\sigma-\psi_{o_{\tau\tau}}=0, \tag{3.39b}$$

$$\frac{1}{\sigma}(\sigma\psi_{1_\sigma})_\sigma-\psi_{1_{\tau\tau}}=-\frac{\hat{\rho}u_o}{12m\rho_*}(\sigma^2+8u_o^2), \tag{3.39c}$$

where u_o corresponds to ψ_o.

This method will be applied to evaluate the following classes of internal waves running up the submerged seabed. After the solution is obtained for $\psi_o(\sigma,\tau)$, the mean fluid velocity $u_2(\sigma,\tau)$ of the lower ocean layer is then given by (3.37b), the coordinate position $x(\sigma,\tau)$ by (3.37a), the time $t(\sigma,\tau)$ by (3.33a), and the internal wave elevation $\zeta(\sigma,\tau)$ from (3.25b), $c_2^2/g_e=h_2+\zeta=\zeta+sx$, or

$$\zeta=-sx+\frac{\sigma^2}{16g_e}(1+\frac{1}{48}\hat{\rho}\sigma^2)^{-1}. \tag{3.40a}$$

The interfacial waterline, always fixed at $\sigma = 0$ in virtue of (3.25b) and (3.33b) with $h_2 + \zeta = 0$, moves in the physical (x,t)-plane according to

$$x(0,\tau) = \frac{1}{2m}u_2^2(0,\tau) + \frac{1}{4}\psi_\tau(0,\tau), \tag{3.40b}$$

$$t(0,\tau) = -\frac{1}{2m}\tau + \frac{1}{m}u_2(0,\tau)[1 + \frac{\hat{\rho}}{6}u^2(0,\tau)] - t_c(0,\tau), \tag{3.40c}$$

$$t_c(0,\tau) = \frac{1}{2}\hat{\rho}\int_o^\tau u_2^2(0,\tau')t_\tau(0,\tau')\,d\tau'. \tag{3.40d}$$

The corrected solution of Eq. (3.38) is presented in Appendix A. The difference between Eq. (3.40) and Eq. (A.14) is very small.

Numerical results have been obtained for several specific cases which will be given below. In these numerical results, we shall set, without loss of generality,

$$h_1 = 1, \qquad \text{and} \qquad g = 1 \tag{3.41}$$

for the scale of length and time.

3.3.2 Run-up of Internal Standing Waves

We shall first consider the problem of a train of incoming internal waves, of sufficiently small amplitude compared with the depth h_1 of the top layer, running up on a submerged flat seabed which is sufficiently inclined so that the waves are not breaking but totally reflected. For this problem a particular simple solution of Eq. (3.39) is for standing waves given by

$$\psi(\sigma,\tau) = \frac{8g_e}{m}AJ_o(\xi)\cos\vartheta, \qquad \xi = \frac{\omega\sigma}{2m}, \qquad \vartheta = \frac{\omega\tau}{2m}, \tag{3.42a}$$

where J_o is the Bassel function of the first kind and for x large, $\tau \sim -2mt$ so that $\cos\vartheta = \cos\omega t$. This solution is expected to hold valid in an inner region as

specified by (3.30) so that it can be matched to another solution that will behave appropriately in an outer region and they can be combined by matching to provide a uniformly valid solution.

The solution of this nonlinear flow problem can now be given parametrically as

$$u_2(\sigma,\tau) = \frac{2\omega}{s}A\frac{J_1(\xi)}{\xi}\cos\vartheta[1 - \frac{\hat{\rho}\sigma^2}{48} + \frac{\hat{\rho}}{6}(\frac{2\omega A}{s})^2\frac{J_1^2(\xi)}{\xi^2}\cos^2\vartheta], \tag{3.42b}$$

$$\zeta(\sigma,\tau) = AJ_o(\xi)\sin\vartheta - \frac{1}{2g_e}u_2^2, \tag{3.42c}$$

$$x(\sigma,\tau) = -\frac{1}{s}AJ_o(\xi)\sin\vartheta + \frac{u_2^2}{2m} + \frac{\sigma^2}{16m}(1 + \frac{\hat{\rho}\sigma^2}{48})^{-1}, \tag{3.42d}$$

$$t(\sigma,\tau) = -\frac{\tau}{2m} + \frac{1}{m}[1 + \hat{\rho}(\frac{\sigma^2}{16} + \frac{1}{6}u_2^2)]u_2 - t_c(\sigma,\tau), \tag{3.42e}$$

where J_1 is the first kind Bessel function of order 1. Here, u_2 is deduced from (3.37b), ζ from $c_2^2 = g_e(h_2+\zeta) = g_e(\zeta + sx)$ and using x of (3.37b) which comes from (3.37a), t is derived by using (3.33a) and $t_c(\sigma,\tau)$ is calculated numerically. At the interfacial waterline, $u_2 = u_2(0,\tau), \zeta = \zeta(0,\tau), x = x(0,\tau)$ and $t(0,\tau)$ are obtained by setting $\sigma = 0$ in the above equations.

The maximum run-up of the interfacial waterline ($\sigma = 0$) occurs when the depth-mean velocity comes to a stop, i.e., at $\vartheta = \pi/2$, giving, by (3.42c,d),

$$\zeta_{r.u.} = A, \qquad \text{at} \qquad \mathrm{x_{r.u.}} = -\mathrm{A/s}. \tag{3.43}$$

The above results are based on the assumption that the waves do not break.

3.3.3 Wave Breaking Criterion

The standing wave solution (3.42a), which is clearly single-valued in (σ,τ), will also be single-valued in (x,t) provided the Jacobian

$$J = \frac{\partial(x,t)}{\partial(\sigma,\tau)} = x_\sigma t_\tau - x_\tau t_\sigma \neq 0. \tag{3.44}$$

Substituting x_σ and x_τ from Eqs. (3.34a,b) into this equation gives

$$J = [1 - \frac{1}{2}\hat{\rho}(c_2^2 + u_2^2)]c_2(t_\sigma^2 - t_\tau^2). \tag{3.45}$$

By making use of (3.35a,b) and (3.42b), we find, after some algebra, that near the interfacial waterline, for $0 < \hat{\rho}\sigma^2 \ll 1$, J will not vanish if

$$4g_e A(\frac{\omega}{2m})^2 < 1, \tag{3.46a}$$

$$A < g_e s^2/\omega^2 = (2\pi)^{-2} g_e T^2 s^2, \tag{3.46b}$$

where T is the wave period. This upper bound for wave amplitude, which is supposedly serving only as a guiding estimate, assumes the same form as for the single-layer case (Mei 1983) except with its g replaced by g_e in (3.46). In physical context, the smallness of g_e/g is well offset by larger values of period T for internal waves than those of surface long waves.

Some typical numerical results of the instantaneous interface profile predicted by the present nonlinear theory are shown in Figure 3.2. Since the theory is limited in offshore range, by the presence of the critical-depth singularity, to small values of $\hat{\rho}c_2^2 \simeq \tilde{\rho}h_2/h_1$ according to (3.30), these results will be used as the inner solution which is to be matched with a linear standing wave solution in the outer region with a deeper lower layer of the ocean.

3.3.4 Matching With the Outer Solution

As the nonlinear effects are expected to become negligible for sufficiently large σ, we shall assume the corresponding linear model to be applicable to this outer region which will include the section where $\tilde{\rho}h_2/h_1$ is no longer so small as assumed (see Eq. (3.30)) to maintain the validity of the approximations introduced for the

inner solutions of the nonlinear theory for the inner region spanning across the interfacial waterline. The solution of the linearized equation (3.11) will be used as the outer solution to be matched with the inner solution of the nonlinear theory.

To match the linear theory for the outer region with the nonlinear theory for the inner region, the latter of which has time-dependent terms with $\sin\vartheta, \cos\vartheta$, and their products to the third power, we take the solution of (3.11) in the form of Fourier series in t,

$$\zeta = \sum_{n=0}^{\infty} \eta_n \sin(\omega_n t + \delta_n), \quad (x > x_m) \tag{3.47}$$

where ω_n are constants to be determined by matching and the phase angle δ_n are taken as slowly-varying functions of t, so varied as to accommodate minor departures of τ from the physical time t. Substituting Eq. (3.47) in Eq. (3.11) yields for $\eta_n(x)$ the equation

$$\eta_n'' + p(x)\eta_n' + q(x)\eta_n = 0, \tag{3.48a}$$

$$p(x) = x^{-1}(1 - \frac{x}{x_o})^{-1}, \quad q(x) = \frac{\omega_n^2}{m}(1 - \frac{x}{x_o})x^{-1}, \quad (x_o = -h_1/(\tilde{\rho}s)). \tag{3.48b}$$

The only singularities of this equation, for x finite, are two regular singularities at $x = 0$, which is the undisturbed interfacial waterline, and at $x = x_o$ which is very close to the shoreline of the top free surface (for $0 < 1 - \tilde{\rho} \ll 1$), and is beyond the reach of the internal wave run-up. Both singularities are thus outside the range in which the solution is sought on the linear theory. It is to be noted that the turning point singularity arising in Eq. (3.26b) is entirely owing its presence to the nonlinear effects, for it disappears with the nonlinear terms neglected.

Let $x = x_k$ denote the position where the inner and outer solutions are to be matched. A choice of x_k is, in general, based on numerical tests. However, there

is not much difference in the structures of the matched solution as long as x_k is less than x_c, which is the position of the critical depth. Thus, the turning-point singularity is avoided for the inner solution while Eq. (3.48) to be solved for the outer solution has no singularity in the range of interest with $x > x_k$. At any point x_1 within this range, the required solution of (3.48) can be expressed in a Taylor series

$$\eta(x) = \sum_{k=0}^{\infty} b_k (x - x_1)^k, \tag{3.49}$$

where the subindex of η_n is omitted as understood. By substituting this expansion and those for $p(x)$ and $q(x)$ about $x = x_1$ in Eq. (3.48) and setting the coefficients of various order to zero, we obtain a set of recursion formulas relating all the b_k ($k \geq 2$) to b_o and b_1, which can be determined for each fixed time t by matching this solution with the known inner solution under two conditions that both ζ and ζ_x be continuous at x_1. This process can be repeated over the time period during which the circular frequency ω_n and the slowly-varying phase function δ_n will have been determined for all the relevant Fourier modes. And the outer solution can be extended analytically from the starting position $x = x_k$ seaward to a new x_1 position for repeating the process as may be dictated by the desired accuracy. The result of such a sequence of matching calculations is shown in Figure 3.2 together with the inner solution for the case with $A = 0.1, \tilde{\rho} = 0.8, h_1 = 1, g = 1, \omega = 2m$, and the seabed slope $s = 1$.

3.3.5 Run-ups of an Initial Hump and an Initial Elevation

Initial value problems with a prescribed internal wave shape $\zeta(x, 0)$ released with $u_2(x, 0) = 0$ everywhere can be solved by integral transform techniques when the necessary boundary conditions are also specified. The general solution

bounded at $\sigma = 0$ and $\sigma = \infty$ may assume the Hankel integral form

$$\psi = \int_0^\infty H(k) k^{-1} J_o(k\sigma) \sin k\tau dk, \tag{3.50}$$

where $H(k)$ is an unknown function of k (e.g., see Carrier & Greenspan (1958)). The solution (3.50) can be conveniently used to treat initial-value problems. A typical example is to let $\psi(\sigma, 0) = 0$ at $\tau = 0$ and $\psi_\tau(\sigma, 0)$ be prescribed for $\sigma > 0$. These initial conditions imply that the initial velocity $u_2(x, 0)$ is zero everywhere and the initial amplitude of the wave $\zeta(x, 0)$ at $t = 0$ satisfies

$$\zeta(x, 0) + sx = \frac{\sigma^2}{16 g_e}(1 + \frac{1}{48}\hat{\rho}\sigma^2)^{-1}, \tag{3.51}$$

which follows from $c_2^2 = g_e(\zeta + h_2)$, here with $x(\sigma, \tau = 0)$ given parametrically by Eq. (3.37a).

For $\tau = 0, u_2 = 0$, we have, by Eq. (3.33) $t = 0, t_c = 0$, and

$$u_{2\tau} = \frac{1}{2}(1 - \frac{1}{16}\hat{\rho}\sigma^2) - \frac{4m}{\sigma}(1 - \frac{1}{48}\hat{\rho}\sigma^2)x_\sigma = f_1(\sigma). \tag{3.52}$$

And from Eq. (3.34b),

$$t_\tau = -\frac{4}{\sigma}(1 + \frac{1}{24}\hat{\rho}\sigma^2)x_\sigma, \tag{3.53}$$

where x_σ can be obtained from Eq. (3.51). Alternatively, from Eq. (3.37b), we find that at $\tau = 0$,

$$u_{2\tau} = f_2(\sigma)\psi_{\tau\sigma}, \tag{3.54a}$$

where

$$f_2(\sigma) = -\frac{m}{\sigma}(1 - \frac{1}{48}\hat{\rho}\sigma^2). \tag{3.54b}$$

Hence, from Eq. (3.52) and Eq. (3.54),we have at $\tau = 0$,

$$\psi_{\tau\sigma}(\sigma, 0) = \frac{f_1(\sigma)}{f_2(\sigma)} = F(\sigma), \tag{3.55}$$

which gives, with Eq. (3.50), the relation

$$F(\sigma) = \int_0^\infty H(k) k J_1(k\sigma) dk. \tag{3.56}$$

From the Hankel transform of order 1 of F, the inverse transform gives

$$H(k) = -\int_0^\infty \sigma J_1(k\sigma) F(\sigma) d\sigma, \tag{3.57}$$

and therefore

$$\psi = -\int_0^\infty k^{-1} J_o(k\sigma) \sin k\tau dk \int_0^\infty \sigma J_1(k\sigma) F(\sigma) d\sigma, \tag{3.58}$$

which satisties Eq. (3.39b) and the specified boundary conditions and initial conditons.

CASE I: Now we consider the motion of an initial hump of water released at the interface at $t = 0$, which is similar to that considered by Carrier & Greenspan (1958), and given by

$$\zeta = a\sigma^4 e^{-b\sigma^2}, \tag{3.59a}$$

$$x = -\frac{a\sigma^4 e^{-b\sigma^2}}{s} + \frac{\sigma^2}{16m}(1 + \frac{1}{48}\hat{\rho}\sigma^2)^{-1}, \tag{3.59b}$$

where a and b are constants. This initial wave is shown in Figure 3.3 for specified a and b. With this initial profile, (3.52) and (3.55) give

$$f_1(\sigma) = \frac{4m}{\sigma}[\frac{a\sigma^4 e^{-b\sigma^2}}{s}]_\sigma (1 - \frac{1}{48}\hat{\rho}\sigma^2), \tag{3.60}$$

$$F(\sigma) = -\frac{4a}{s}(4\sigma^3 e^{-b\sigma^2} - 2b\sigma^5 e^{-b\sigma^2}). \tag{3.61}$$

Substituting Eq. (3.61) in Eq. (3.58) yields

$$\psi = \frac{4a}{s}\int_o^\infty Z(k,b) e^{-\frac{k^2}{4b}} J_o(k\sigma) \sin k\tau dk, \tag{3.62a}$$

where

$$Z(k,b) = -\frac{1}{b^3} + \frac{k^2}{2b^4} - \frac{k^4}{32b^5}. \tag{3.62b}$$

From this solution of ψ we readily deduce from Eq. (3.37b) that

$$u_2 = \frac{4ag_e}{\sigma}(1 + \frac{1}{48}\hat{\rho}\sigma^2)^{-1} \int_o^\infty Z(k,b) k e^{-\frac{k^2}{4b}} J_1(k\sigma) \sin k\tau dk$$

$$+\frac{1}{6}\hat{\rho}(1 + \frac{1}{16}\hat{\rho}\sigma^2)^{-1}[\frac{4ag_e}{\sigma} \int_o^\infty Z(k,b) k e^{-\frac{k^2}{4b}} J_1(k\sigma) \sin k\tau dk]^3, \tag{3.63}$$

and from the relation $\zeta = c_2^2/g_e - sx$ and Eq. (3.37a), we have

$$\zeta = -a \int_o^\infty Z(k,b) k e^{-\frac{k^2}{4b}} J_o(k\sigma) \cos k\tau dk - \frac{u_2^2}{2g_e}, \tag{3.64a}$$

$$x = \frac{a}{s} \int_o^\infty Z(k,b) k e^{-\frac{k^2}{4b}} J_o(k\sigma) \cos k\tau dk$$

$$+\frac{u_2^2}{2m} + \frac{\sigma^2}{16m}(1 + \frac{1}{48}\hat{\rho}\sigma^2)^{-1}. \tag{3.64b}$$

From Eq. (3.33), t and τ are related by

$$t(0,\tau) = -\frac{\tau}{2m} + \frac{U}{m}(1 + \frac{1}{6}\hat{\rho}U^2) - t_c(0,\tau), \tag{3.64c}$$

$$t_c(0,\tau) = \frac{1}{2}\hat{\rho} \int_o^\tau u(0,\tau') x_\tau(0,\tau') d\tau', \tag{3.64d}$$

where $U(\tau) = u(0,\tau)$. The solution of run-up of the internal hump is shown in Fig. 3.3 and Fig. 3.4. For small σ and a, the Jacobian is not zero if $|a/b| < (8g_e)^{-1}$.

CASE II: Specializing further, we may consider an initial elevation which decays exponentially in σ^2 away from the shore at $t = 0$, which is similar to that considered by Tuck & Hwang (1972), and is given by

$$\zeta = ae^{-b\sigma^2}, \tag{3.65a}$$

$$x = -\frac{ae^{-b\sigma^2}}{s} + \frac{\sigma^2}{16m}(1 + \frac{1}{48}\hat{\rho}\sigma^2)^{-1}, \tag{3.65b}$$

where a is the elevation at the shoreline $\sigma = 0$, and b is a constant. Following the same calculation of Case I, we find

$$u_2 = -\frac{2ag_e}{b\sigma}(1 + \frac{1}{48}\hat{\rho}\sigma^2)^{-1}\int_o^\infty ke^{-\frac{k^2}{4b}}J_1(k\sigma)\sin k\tau dk$$

$$+\frac{1}{6}\hat{\rho}(1 + \frac{1}{16}\hat{\rho}\sigma^2)^{-1}[\frac{2ag_e}{b\sigma}\int_o^\infty ke^{-\frac{k^2}{4b}}J_1(k\sigma)\sin k\tau dk]^3, \tag{3.66a}$$

$$\zeta = \frac{a}{2b}\int_o^\infty ke^{-\frac{k^2}{4b}}J_o(k\sigma)\cos k\tau dk - \frac{u_2^2}{2g_e}, \tag{3.66b}$$

$$x = -\frac{a}{2bs}\int_o^\infty ke^{-\frac{k^2}{4b}}J_o(k\sigma)\cos k\tau dk$$

$$+\frac{u_2^2}{2m} + \frac{\sigma^2}{16m}(1 + \frac{1}{48}\hat{\rho}\sigma^2)^{-1} \tag{3.66c}$$

and the relation of t and τ is the same as Eqs. (3.64c,d). The solution of run-up of the initial elevation is shown in Fig. 3.5 and Fig. 3.6. For small σ and a, the Jacobian is not zero if $|ab| < (16g_e)^{-1}$.

3.4 The Run-up of ISWs

3.4.1 The Run-up Law

Now we consider the run-up of ISWs over the bathymetry consisted of a plane beach of slope s adjacent to a region of constant depth (shown in Figure 3.7), which is similar to that considered by Synolakis (1986). The topography is described as follows:

$$h_1 = h_{1o}, \quad \text{for} \quad x \geq 0, \tag{3.67a}$$

$$h_2 = sx, \quad \text{when} \quad \mathrm{x} < \mathrm{x}_1, \tag{3.67b}$$

$$h_2 = d, \quad \text{when} \quad \mathrm{x} > \mathrm{x}_1. \tag{3.67c}$$

For the run-up of ISWs of elevation (i.e., with $d < h_{1o}$ for this type of polarity, there is no critical point; for the run-up of ISWs of depression (i.e., with $h_{1o} < d$), there is a critical point at a certain station on the beach where $\rho_1 h_1^2 = \rho_2 h_2^2$; however, we may discuss the case without wave breaking and with incident waves of small amplitudes. First, considering the linear theory (3.6a)–(3.8a), we find that in the region of constant depth, i.e., $x > x_1$, this linear system can be reduced to the classical wave equation with a steady state solution, namely

$$\zeta(x,t) = A_i e^{-ik(x+ct)} + A_r e^{ik(x-ct)}, \tag{3.68}$$

where $c^2 = g_e h_o, h_o = h_{1o} d/(h_{1o} + \tilde{\rho} d)$, and A_i is the amplitude of the incident wave of wave number k, A_r the amplitude of the reflected wave, and that in the region of sloping beach, i.e., $0 < x < x_1$, this linear system has a solution, namely

$$\zeta(x,t) = A(k) J_o(2K_e\sqrt{x}) e^{-ikct}, \tag{3.69}$$

where $K_e = kc/\sqrt{g_e s} = k\sqrt{h_o/s}$, and $A(k)$ is the coefficient related to the wave number. A combined solution of equations (3.68)(3.69) can be derived by matching the two solutions at $x = x_1$ under the conditions that the amplitude and its derivative are continuous. The relation between $A(k)$ and A_i is

$$A(k) = \frac{2A_i e^{-kx_1}}{J_o(2K_e\sqrt{x_1}) - i\beta J_1(2K_e\sqrt{x_1})}, \tag{3.70}$$

where $\beta = \sqrt{h_o/d}$. If the incident wave is an ISW, i.e.,

$$\zeta(x_o, t=0) = a_o sech^2 \frac{x - x_o}{\lambda} = \frac{1}{2\pi} \int_{-\infty}^{+\infty} \frac{a_o \lambda^2 k}{2} cosech(\frac{\pi k \lambda}{2}) e^{ikx_o} e^{-ikx} dx, \tag{3.71}$$

where x_o is the initial peak position, and a_o is the initial amplitude of the ISW. By linear superposition of the solution (3.69), the wave transmitted onward over the seabed is given by

$$\zeta(x,t) = 2\int_{-\infty}^{+\infty} \phi(k) \frac{e^{-ik(x_1+ct)}}{J_o(2K_e\sqrt{x_1}) - i\beta J_1(2K_e\sqrt{x_1})} dk, \tag{3.72a}$$

where

$$\phi(k) = \frac{a_o\lambda^2 k}{2} cosech(\frac{\pi k\lambda}{2}) e^{ikx_o} J_o(2K_e\sqrt{x}). \tag{3.72b}$$

Secondly, we consider the nonlinear systems (3.1)-(3.3) for x near the interfacial waterline where the nonlinear solution (3.40) is valid. For large σ, the nonlinear effects may be assumed small, and the nonlinear solution (3.40) may be approximately written with the asympotic representations:

$$\zeta = -\frac{s}{4}\psi_\tau, \quad t(0,\tau) = -\frac{1}{2m}\tau, \quad x = \frac{\sigma^2}{16m}, \tag{3.73}$$

where ψ is considered to be solved from Eq. (3.39b) by the Fourier transformation as

$$\psi(\sigma,\tau) = \frac{1}{2\pi}\int_{-\infty}^{+\infty} F(\tilde{k}) \frac{J_o(\tilde{k}\sigma)}{J_o(\tilde{k}\sigma_o)} e^{i\tilde{k}\tau} d\tilde{k}, \tag{3.74a}$$

where

$$F(\tilde{k}) = \int_{-\infty}^{+\infty} \psi(\sigma_o,\tau) e^{-i\tilde{k}\tau} d\tau, \tag{3.74b}$$

and σ_o is a point related to τ which will be chosen. Matching the two solutions (3.72a) and (3.74a) at $\sigma = \sigma_o$, i.e., at $x = x_2$, we obtain

$$\psi(\sigma,\tau) = \frac{16mi}{sc}\int_{-\infty}^{+\infty} \frac{\phi(k)}{k} \frac{J_o(\tilde{k}\sigma) e^{-ikx_1 + i\frac{kc}{2m}\tau}}{J_o(2K_e\sqrt{x_1}) - i\beta J_1(2K_e\sqrt{x_1})} dk. \tag{3.75}$$

From Eq. (3.73), Eq. (3.75) provides an amplitude at $\sigma = 0$, which is the same as the amplitude given by Eq. (3.72a) at $x = 0$. This result tells us that in this

kind of analysis, the linear theory (3.72a) and the nonlinear theory (3.74a) provide same value for run-up of ISWs of elevation and run-down of ISWs of depression for very small amplitudes of ISWs (Synolakis 1986). Therefore, the amplitude at the interfacial waterline is

$$\zeta(\sigma=0,t)=\int_{-\infty}^{+\infty}\frac{a_o k\lambda^2 cosech\frac{\pi k\lambda}{2}e^{-ik(-x_o+x_1+ct)}}{J_o(2K_e\sqrt{x_1})-i\beta J_1(2K_e\sqrt{x_1})}dk. \tag{3.76}$$

After integration of Eq. (3.76), we obtain the run-up law as

$$(\frac{\zeta}{a_o})_{max}=\frac{5.662}{(1+\beta)}[\frac{(h_{1o}^2-\tilde{\rho}d^2)a_o}{h_{1o}s^2(h_{1o}+\tilde{\rho}d)(d+\tilde{\rho}h_{1o})}]^{1/4}, \tag{3.77}$$

which states that the maximum run-up of ISWs is proportional to the initial amplitude of ISWs with a $\frac{5}{4}$-power law in amplitude a_o, other parameters being equal. The solution (3.77) is valid only if the Jacobian is not zero, i.e.,

$$u_\tau-\frac{1}{2}\neq 0, \tag{3.78}$$

which should impose a limit to the amplitude of incident ISWs so that the waves would progress without breaking. More specially, we have

(i)for the ISWs of elevation,

$$a_o<0.273g_e^{-8/7}(\frac{1+\beta}{\beta})^{2/7}[\frac{(h_{1o}+\tilde{\rho}d)^{2/3}(d+h_{1o}\tilde{\rho})}{h_{1o}^2-\tilde{\rho}d^2}]^{3/7}(\frac{s}{d})^{2/7}; \tag{3.79a}$$

(ii)for the ISWs of depression,

$$(-a_o)<0.65g_e^{-8/7}(\frac{1+\beta}{\beta})^{2/7}[\frac{(h_{1o}+\tilde{\rho}d)^{2/3}(d+h_{1o}\tilde{\rho})}{\tilde{\rho}d^2-h_{1o}^2}]^{3/7}(\frac{s}{d})^{2/7}. \tag{3.79b}$$

When $\tilde{\rho}=0, h_{1o}=1$, the run-up $\frac{5}{4}$-power law (3.77) of ISWs reduces to that of Synolakis' (1986). The numerical solution with the dispersive terms included will

be given in the following section and the run-up law (3.77) will be compared with the numerical results.

3.4.2 Direct Numerical Simulation

Direct numerical simulations are performed to evaluate the run-up of ISWs over the same topography as described in the last section. The predictor-corrector two-step procedure, which will be discussed in the next chapter, is used to solve the nonlinear system of equations (4.2)-(4.4) numerically. The moving boundary satisfying the dynamical, kinematical and geometrical conditions (which will be given in Chapter 4) are incorporated into our investigation of the behaviour of ISWs at the interfacial waterline. In the present numerial calculations, we take the time step $\Delta t = 0.05$ and the space interval $\Delta x = 0.1$. The stability and accuracy of our calculations are checked by comparision with the corresponding numerical result of a free soliton on a flat bottom of which the exact solution is known. The relative change in maximum wave amplitude of the ISW is about -0.5% after the wave has traveled 100 water depth. All computations are done in the Cray Y-MP. Because the topography here has a critical point, the slopes of all computed waves (see definition in Chapter 4) are smaller than the beach slope in order that according to the criterion Eq. (3.79b), waves would be propagating without breaking. Figure 3.8 shows the wave profiles of ISWs of depression near the interfacial waterline evolving with the parameters chosen to be $x_o = 100, \tilde{\rho} = 0.85, x_1 = 200, h_1 = 1.0, h_2 = 1.5, s = 0.01, a_1 = -0.01$. When the toe of the ISWs of depression reaches the interfacial waterline on the beach, this toe starts to move down the beach until its velocity is zero with its maximum run-up. After

this moment, it goes up across the interfacial waterline and arrives at another maximum amplitude, then it comes back to the interfacial waterline. Due to the reflection of the beach, this kind of motion becomes weaker and weaker after each period. Figure 3.9(a,b) shows the history of the run-up position and the lower-layer fluid velocity.

The run-up law (3.77) is compared with the numerical results with different amplitudes of incident ISWs to a beach with a fixed slope. The parameters adopted are $\tilde{\rho} = 0.85, h_1 = 1.0, h_2 = 1.5, s = 0.01, \beta = 0.663$. With a small initial amplitude for the ISWs, the two values from Eq. (3.77) and the numerical results with dispersive terms are quite close. The run-up law (3.77) is expected to give a good estimate for waves of very small amplitudes and non-breaking IWs.

Figures for Chapter 3

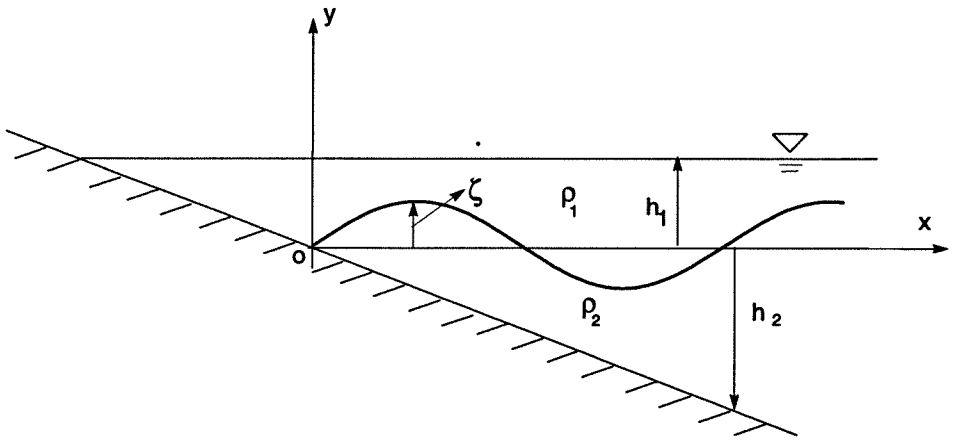

Figure 3.1 A sketch delineating run-up of an internal wave propagating in a two-layered fluid and incident on a sloping seabed, the top free surface being assumed to remain undisturbed.

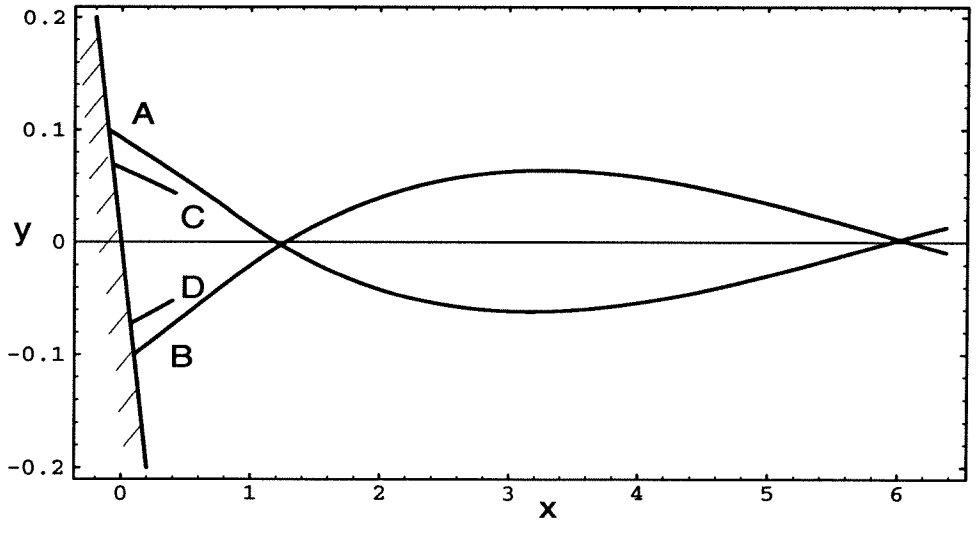

Figure 3.2 A typical internal standing wave profile obtained by matching the nonlinear solution with the linear solution for $A = 0.1, s = 1.0, x_c = 1.0, \tilde{\rho} = 0.8, h_1 = 1, g = 1, \omega = 2m$ matched at $x_m = 0.75$; in which: A, point of maximum run-up, $\vartheta = \pi/2$; B, minimum run-down, $\vartheta = 3\pi/2$; C & D, intermediate phases with $\vartheta = 3\pi/4, 5\pi/4$, respectively.

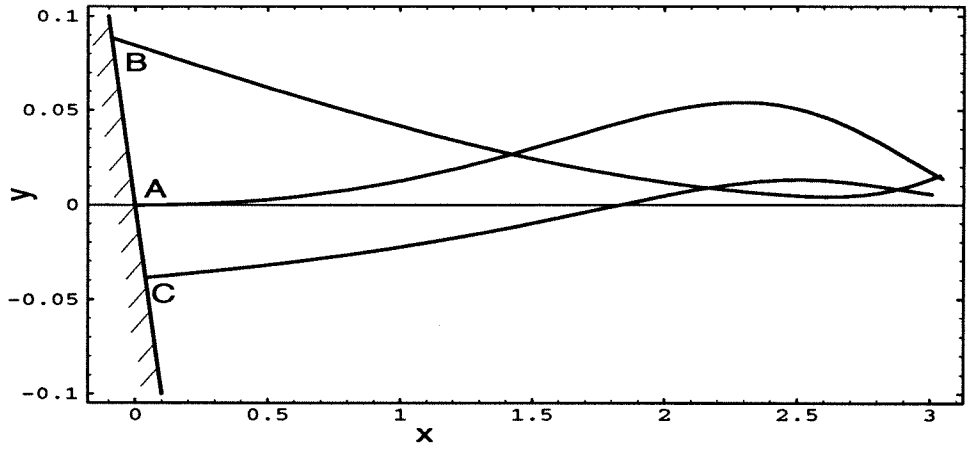

Figure 3.3 Wave profiles of the motion given by (3.63) and (3.64) subsequent to the initial internal water elevation (3.59) for $a = 0.001, b = 0.1, \tilde{\rho} = 0.8, g = 1, s = 1, h_1 = 1$; — A, initial profile at $\tau = 0$; — B, Maximum run-up at $\tau = -3.85$; — C, minimum run-down at $\tau = -7.85$.

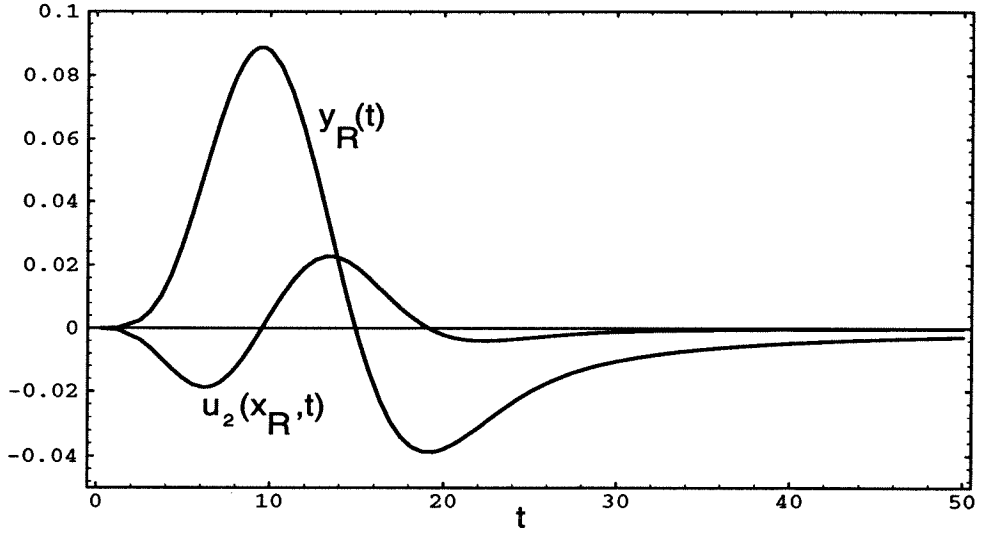

Figure 3.4 A plot of time history of the run-up, $y = y_R(t) = -sx_R(t)$, and fluid velocity, $u_2(x_R, t)$, given by (3.63) and (3.64) for $a = 0.001, b = 0.1, \tilde{\rho} = 0.8, g = 1, s = 1, h_1 = 1$.

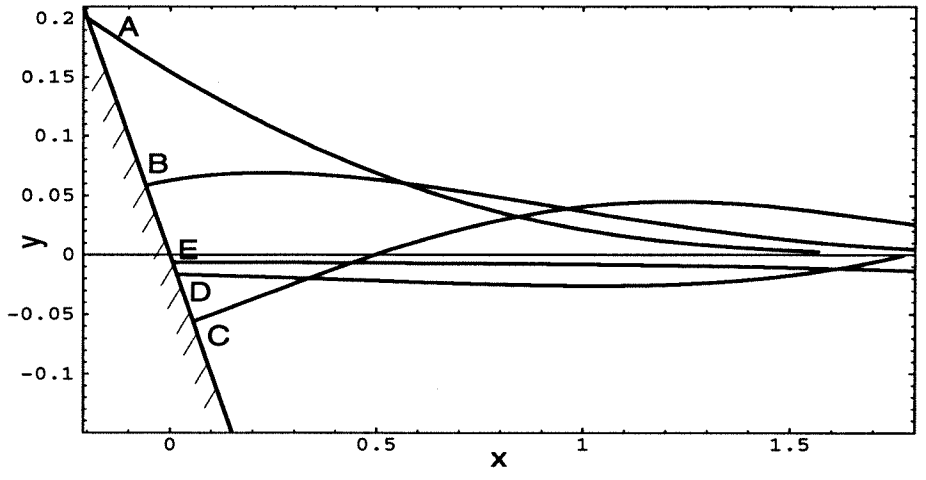

Figure 3.5 Wave profiles of the motion given by (3.66) subsequent to the initial internal water elevation (3.65) for $a = 0.2, b = 0.5, \tilde{\rho} = 0.8, g = 1, s = 1, h_1 = 1$; — A, initial profile at $\tau = 0$; — B, at $\tau = -2.0$; — C, at $\tau = -4.0$; — D, at $\tau = -6.0$; — E, at $\tau = -0.9$.

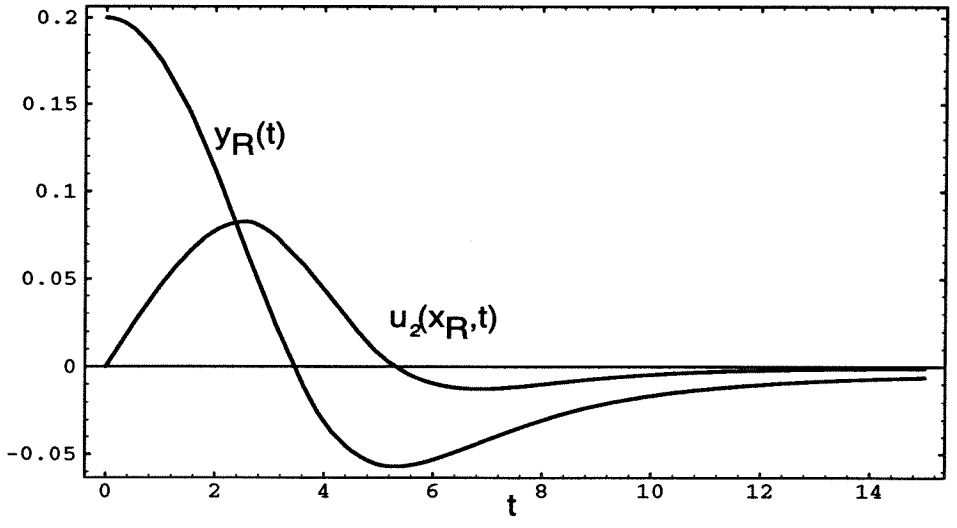

Figure 3.6 A plot of time history of the run-up, $y = y_R(t) = -sx_R(t)$, and fluid velocity, $u_2(x_R, t)$, given by (3.65) and (3.66) for $a = 0.2, b = 0.5, \tilde{\rho} = 0.8, g = 1, s = 1, h_1 = 1$.

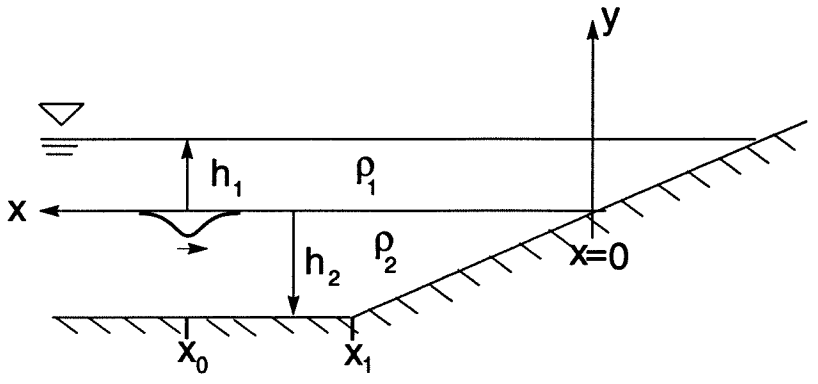

Figure 3.7 Sketch of a slope bottom topography in a two-layer system. x_o is the peak position of an initial incident ISW; x_1 is a slope-start point.

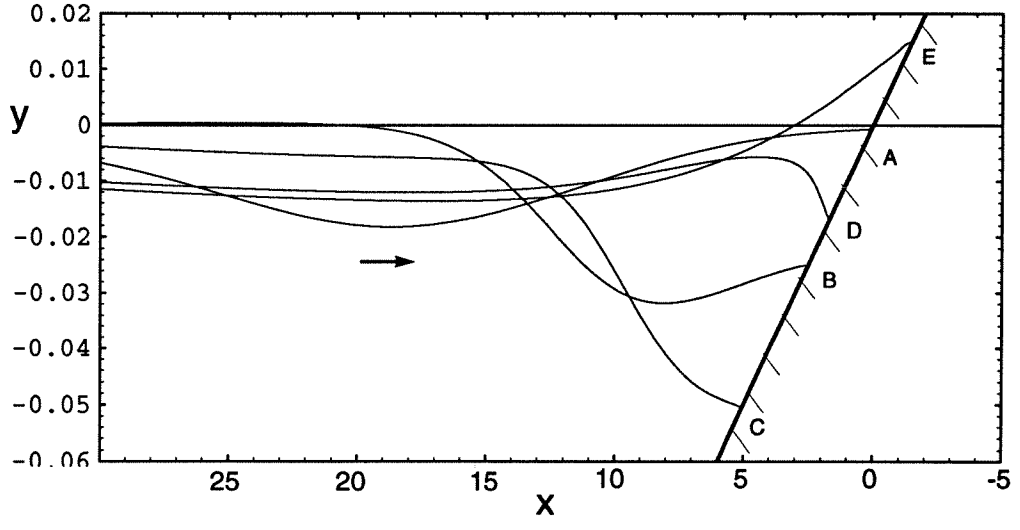

Figure 3.8 Run-up of an ISW near the interfacial waterline with the parameters $x_o = 100, \tilde{\rho} = 0.85, x_1 = 200, h_1 = 1.5, s = 0.01, a_o = -0.01, \Delta x = 0.1, \Delta t = 0.05$. At point A: $t = 900$; at point B: $t = 1150$; at point C: $t = 1300$; at point D: $t = 1400$; at point E: $t = 1425$.

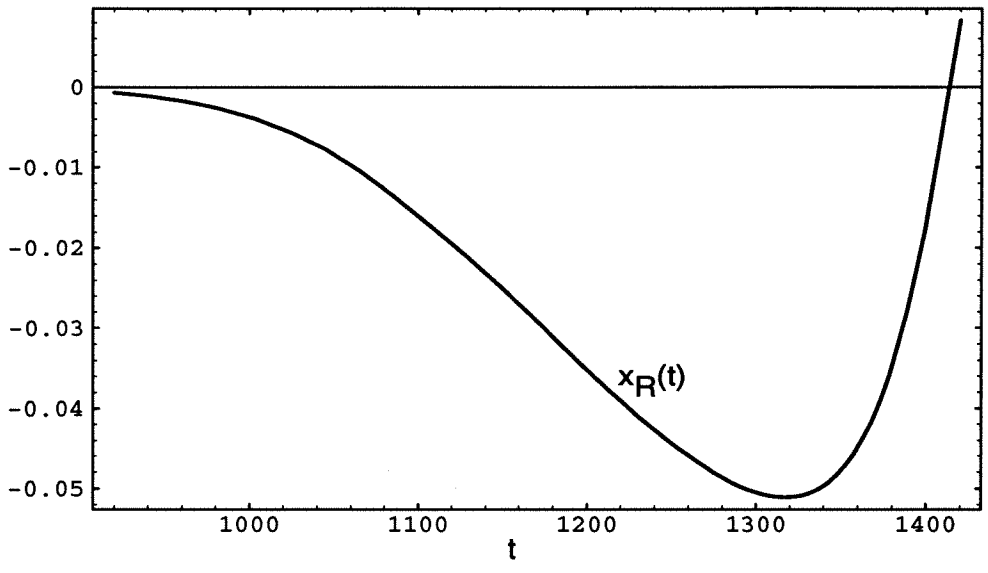

Figure 3.9(a) A plot of time history of the run-up position, $x/s = x_R(t)/s$ in case of Fig. 3.8.

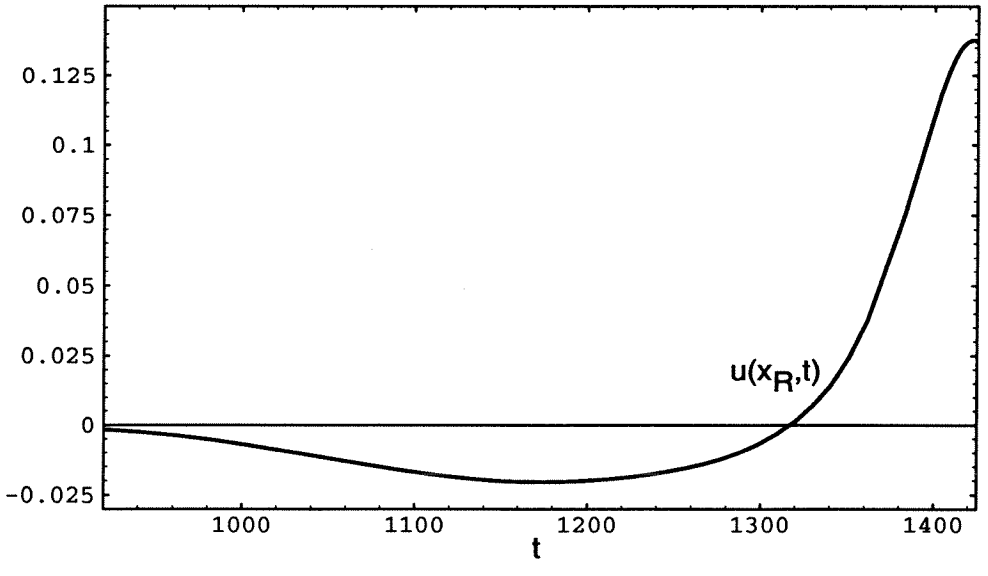

Figure 3.9(b) A plot of time history of the fluid velocity, $u(x_R, t)$, in the case of Fig. 3.8.

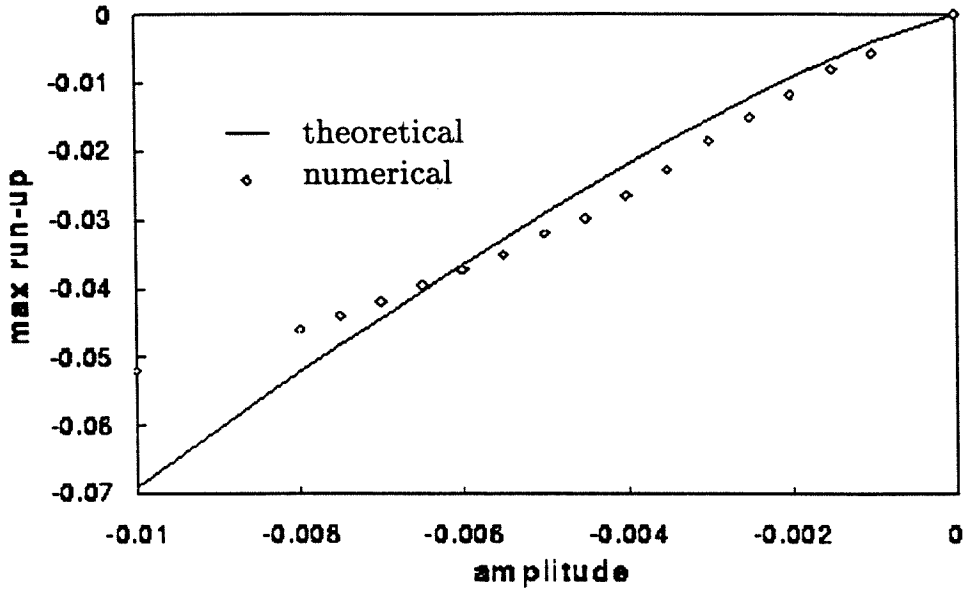

Figure 3.10 The comparison of the theory (3.77) and numerical results based on the ILW model for ISWs incident on the slope seabed with the parameters $\tilde{\rho} = 0.85, h_1 = 1.0, h_2 = 1.5, s = 0.01, \beta = 0.663$.

Chapter 4

Nonlinear Wave Propagation Across Critical Point

In this chapter, the weakly nonlinear and weakly dispersive oceanic internal long wave (ILW) model is applied to study the nonlinear behaviour of internal solitary waves (ISWs) progressing in a system of two-layer fluids with variable depth. It differs from the corresponding KdV-type model in admitting bidirectional waves simultaneously while still observing the laws of mass and energy conservation. This ILW model is applied especially to analyze the so-called critical depth problem of ISWs propagating across a critical station at which the depths of the two fluid layers are about equal so as to give rise to a critical point of the KdV equation. Numerical results are presented based on the present ILW model for ISWs climbing up a curved shelf and a sloping plane seabed. It is shown that in the transcritical region, the behaviour of the ISWs predicted by the ILW model depends on the relative importance of two dimensionless parameters, s_w, the magnitude of ISW wave slope, and s, the beach slope. For $s >> s_w$, the wave profile of ISWs exhibits a smooth transition across the transcritical region; for $s << s_w$, ISWs emerge with an oscillatory tail after passing across the critical point. Numerical simulations are found in good agreement with laboratary observations.

4.1 Theoretical Description

We begin with the weakly nonlinear and weakly dispersive oceanic internal long wave (ILW) model which admits both right- and left-going waves in describing generation, propagation and evolution of long oceanic internal waves in nonuniform medium with possible reflection and transmission of waves by varying boundaries. This model is based on the assumption, i.e.,

$$\alpha = a/h << 1, \qquad \epsilon^2 = (h/\lambda)^2 = O(\alpha), \tag{4.1}$$

for weakly nonlinear and weakly dispersive internal long waves of typical amplitude a and length λ, propagating at the interface between two layers of fluid. The fluid has a piecewise homogeneous two-layer density distribution, of density ρ_1(=const) in the top layer of depth $h_1 = const$, and density ρ_2(=const) in the lower layer of depth $h_2(x,t)$ slowly varying with a specific rate of variation no greater than $O(\alpha^2)$ (see Figure 4.1). The typical height h is equal to $h_1 + h_{2o}$. The fluids are assumed inviscid and incompressible. To simplify the analysis involved, we adopt the "rigid-lid" top surface assumption, which is found to be very satisfactory (see Wu & Lin 1994) provided the top layer is sufficiently thick compared to internal wave amplitude, in the absence of barotropic forcing disturbances. The ILW model may be written as, to order $O(\alpha\epsilon^4)$,

$$\zeta_t - [(h_1 - \zeta)u_1]_x = 0, \tag{4.2}$$

$$\zeta_t + [(h_2 + \zeta)u_2]_x = 0, \tag{4.3}$$

$$\sigma u_{1t} - u_{2t} + (\sigma u_1 u_{1x} - u_2 u_{2x}) + (\sigma - 1)\zeta_x = \frac{1}{3}h_1^2 \sigma u_{1xxt} - \frac{1}{3}h_2^2 u_{2xxt}, \qquad (4.4)$$

where the subscripts x and t denote differentiation, and $u_i(x,t)(i = 1,2)$ is the depth-mean value of the longitudinal flow velocity along the channel axis x for the upper $(i = 1)$ and lower $(i = 2)$ layers respectively. $u_1(x,t)$ is the axial velocity averaged from the interface elevation at $y = \zeta(x,t)$ at time t to the top water surface at $y = h_1$, $u_2(x,t)$ is the axial velocity averaged from the channel bottom at $y = -h_2(x)$ to the interface elevation at $y = \zeta(x,t)$ at time t, and σ is the density ratio ρ_1/ρ_2 of two layers. We assume for u_i and ζ the following expansions:

$$u_i = \alpha[u_i^{(o)}(\eta,\tau) + \alpha u_i^{(1)}(\eta,\tau) + \cdots], \quad (i = 1,2), \qquad (4.5)$$

$$\zeta = \alpha[\zeta_1(\eta,\tau) + \alpha\zeta_2(\eta,\tau) + \cdots], \qquad (4.6)$$

in terms of multiple-scale variables,

$$\eta = \alpha^{3/2}x, \quad \tau = \alpha^{1/2}(\int \frac{dx}{c(x)} - t), \qquad (4.7)$$

where $c(x)$ is the local wave speed. Substituting those relations into Eqs. (4.2)-(4.4), and keeping terms up to $O(\alpha\epsilon^4)$, we may obtain for ζ an equation of KdV type as

$$\zeta_\eta + A_1\zeta\zeta_\tau + A_2\zeta_{\tau\tau\tau} = 0, \qquad (4.8)$$

where

$$A_1 = \frac{3c_o^2}{2(\tilde{\rho}-1)}(\frac{\tilde{\rho}}{h_1^2} - \frac{1}{h_2^2}), \qquad A_2 = \frac{1}{6c_o(1-\tilde{\rho})}(\tilde{\rho}h_1 + h_2), \qquad (4.9a)$$

and c_o is the phase speed of the baroclinic slow-mode IWs motion satisfying

$$c_o^2(\frac{\tilde{\rho}}{h_1} + \frac{1}{h_2}) + (\tilde{\rho} - 1) = 0. \qquad (4.9b)$$

The internal solitary waves (ISWs) can be waves of either elevation or depression depending on the sign of the cofficient A_1 of the nonlinear term in Eq. (4.8). When the upper layer is shallow (or deep) enough, compared to the lower layer, so as to make A_1 positive (or negative), stationary ISWs are found to have a polarity of depression (or elevation). Accordingly, as an incident solitary wave of depression propagates from a subcritical region of deeper lower layer, with $\rho_1 h_2^2 > \rho_2 h_1^2$, up a slope to a supercritical region of shallower lower layer where $\rho_1 h_2^2 < \rho_2 h_1^2$, it will encounter a point where A_1 is zero, i.e., $\rho_1 h_2^2 = \rho_2 h_1^2$, which is called a critical point. The whole region of wave propagation may be divided into subcritical and supercritical parts which hold ISWs of depression and elevation respectively. Oceanic internal solitary waves (ISW) near the critical point has been studied by Knickerbocker & Newell (1980) based on direct numerical calculation of the KdV-type equation for ISWs with variable depth in which the quadratic term of the coefficient A_1 varies linearly over a sloping region (i.e., the L section in Figure 4.1). Their results indicate that after passing the critical point, the original downward facing solitary wave disintegrates to form a new upward facing solitary wave in the supercritical region. Djordjevic & Redekopp (1978) have argued that this reversal is impossible by application of the eigendepth relation (Tappert & Zabusky 1971, Johnson 1972), which predicts that the finite number of solitons is related to a shelf depth, independent of the shape of the shelf formation. Helfrich, Melville & Miles (1984) extend the previous works by direct numerical computation of a modified KdV-type equation which includes a certain new cubic nonlinear term (while leaving out the terms of the same next higher order). Their results based on this new equation show that an incident ISW of depression scatters into a train of oscillatory wave from which one or more ISWs

of elevation emerge asymptotically. It has been known that a KdV-type equation with variable coefficients may be transformed into a nonhomogeneous KdV equation but with constant coefficients. However, both types of equations do not hold the conservation of mass. In another word, the variable-coefficient KdV equation is a unidirectional wave equation, so it does not hold wave propagations in both directions. In this connection, we note that the continuous stratification model in a variable depth developed by Djordjevic & Redekopp (1978) does not have a critical point where the cofficient of the nonlinear term vanishes.

4.2 Numerical Solution of the KdV Equation

For seeking numerical solutions, it is convenient to take the following transformation, i.e.,

$$\zeta' = {A_2}^{1/3}\zeta, \quad \tau' = {A_2}^{-1/3}\tau, \tag{4.10}$$

then Eq. (4.8) becomes (after omitting $'$)

$$\zeta_\eta + B\zeta\zeta_\tau + \zeta_{\tau\tau\tau} = 0, \tag{4.11a}$$

where

$$B = (-a_1 + \frac{a_2}{h_2^2}), \quad a_1 = \frac{9\tilde{\rho}c_o^2}{h_1^2(\tilde{\rho}h_1 + h_2)}, \quad a_2 = \frac{\tilde{\rho}}{a_1 h_1^2}. \tag{4.11b}$$

A finite difference equation that approximates the variable-coefficient KdV equation (4.11a) is

$$\zeta_i^{n+1} = \zeta_i^{n-1} - B_i^n \frac{\Delta\eta}{\Delta\tau}(\zeta_{i+1}^n + \zeta_i^n + \zeta_{i-1}^n)(\zeta_{i+1}^n - \zeta_{i-1}^n) -$$

$$\frac{\Delta\eta}{(\Delta\tau)^3}(\zeta_{i+2}^n - 2\zeta_{i+1}^n + 2\zeta_{i-1}^n - \zeta_{i-2}^n), \tag{4.12}$$

where $\zeta_i^n = \zeta(i\Delta\tau, n\Delta\eta)$ and $\Delta\eta$ and $\Delta\tau$ are the appropriate grid sizes. The Von Neuman stability analysis provides that error associated with the solution of Eq. (4.12) will grow indefinitely unless

$$\frac{\Delta\eta}{\Delta\tau}[\frac{3}{2}B|\zeta_o| + \frac{2}{3}\frac{1}{(\Delta\tau)^2}] \leq 1. \tag{4.13}$$

The truncation error involved in Eq. (4.12) is seen to be proportional to $(\Delta\tau)^3$ and $\Delta\eta(\Delta\tau)^2$. Since the scheme is centered in η and in τ, the initial step in η can be found by using a standard forward-integration procedure. It is also worth noting that the present computational scheme conserves both mass and energy. The initial condition can be provided by Eq. (4.11a) with a specified amplitude a_o. The geometric configuration of water depth variation above the seabed is described in Figure 4.2 to lie within the L section. The stability and accuracy of the numerical scheme are investigated by applying it to compute a free ISW in water of uniform depth ($s = 0$). The relative change in the maximum wave amplitude of the ISW is about 0.1% after the wave has traveled 100 water depth. The grid sizes are taken to be $\Delta\tau = 0.1$ and $\Delta\eta = 0.0001$ in computation, for which the CPU time took about 2 minutes for Cray. The computational result of Eq. (4.12) is shown in Figure 4.2, in which the related coefficients are taken with $a_1 = 1.63, a_2 = 1.26, s = 0.01, h_1 = 0.8, h_{2o} = 1.26, \tilde{\rho} = 0.99$. As the down-facing ISW approaches the critical point ($\eta = 50$), it emerges to have an oscillatory tail. After passing through the critical point, it starts to break up into a dispersive wave train. Because the excess mass is conserved, the local mean level of the interface appears to subside a little lower than the original interfacial zero level. Gradually the leading pulse appears to rise as an upward-facing ISW relative to the local interfacial mean level. The polarity of the ISW of depression has thus

been changed related to the local mean level after it has passed the critical point based on the KdV-type equation.

4.3 Numerical Analysis of the ILW Model

The numerical procedure desribed in this section has been applied to perform computation of head-on collisions in Chapter 2, to investigate the run-up of ISWs on submerged seabeds in Chapter 3 and will be used throughout the rest of this study to solve the ILW model equation for two kinds of bottom topographies. We consider propagation of ISWs of depression from a constant depth, up a mild cosine-shaped transition or a straight beach with a critical point, into a shallower flat region. Two significant dimensionless parameters, i.e., a beach slope s and a represntative IW slope s_w defined by the ratio of a typical wave height to a typical wave length, are considered. Based on the computational results from the ILW model, we find that when s is much greater than s_w, it seems that there is no discernible influence from the presence of critical point. However, when s is much less than s_w, the ISW is seen first to gain its amplitude, to reduce its speed as it passes through the trans-critical region and to develop an oscillatory tail in the neighbourhood of the critical point.

4.3.1 Computational Scheme

Integrating the sum of Eqs. (4.2) and (4.3) under condition (3.5), we find

$$u_1 H_1 + u_2 H_2 = 0, \tag{4.14}$$

where $H_1 = h_1 - \zeta$, $H_2 = h_2 + \zeta$. In order to solve Eqs. (4.2)-(4.4) numerically, new variables are introduced as $M = \sigma u_1 - u_2$ and $u = u_1$. In terms of the new

variables, Eq. (4.14) becomes

$$u - \frac{H_2}{H_1 + \sigma H_2} M = 0, \tag{4.15}$$

$$u_2 = \sigma u - M. \tag{4.16}$$

For evaluating waves of very small amplitude ($|\zeta| << h_1$), keeping the same order of the model equation up to $O(\alpha^3)$ as with Eq. (4.15), we may write Eq. (4.4) as

$$A_1 M_t + A_2 M_{xt} + A_3 M_{xxt} = A_4, \tag{4.17a}$$

where

$$A_1 = 1 - \frac{2}{3}\frac{h_1(\sigma H_{2x})^2(h_2^2 - h_1^2)}{(h_1 + \sigma h_2)^3} - \frac{1}{3}\sigma\frac{(h_1^2 - h_2^2)}{(h_1 + \sigma h_2)^2}(h_1 H_{2xx} - h_2 H_{1xx}), \tag{4.17b}$$

$$A_2 = -\frac{2}{3}\sigma\frac{(h_1^2 - h_2^2)}{(h_1 + \sigma h_2)^2}[h_1 h_{2x} + (h_1 + h_2)\zeta_x], \tag{4.17c}$$

$$A_3 = -\frac{1}{3}h_1 h_2 \frac{\sigma h_1 + h_2}{h_1 + \sigma h_2}, \tag{4.17d}$$

$$A_4 = \frac{1}{3}\sigma(h_1^2 - h_2^2)\frac{(H_1 u)_x}{h_1 + \sigma h_2} M_{xx} + (\sigma - 1)\sigma u u_x + M M_x - \sigma(uM)_x - (\sigma - 1)\zeta_x, \tag{4.17e}$$

where $(\cdot)_x = \partial(\cdot)/\partial x$, $(\cdot)_{xx} = \partial^2(\cdot)/\partial x^2$. Thus, the model equations for computations are Eqs. (4.2) and (4.17).

Besides the model equations, appropriate boundary conditions are required. For computing run-up of ISWs, the moving boundary condition is adopted from the physical and geometrical conditions at the interfacial waterline at which $H_2 = h_2 + \zeta = 0$. At the interfacial waterline, where Eq. (4.14) remains valid, it follows that $u_1 = 0$ and $\partial u_1/\partial t = 0$, hence by Eq. (4.16), $u_2 = -M$, and Eq. (4.4) gives

$$u_{2t} + u_2 u_{2x} - (\sigma - 1)\zeta_x = \frac{1}{3}H_2^2 u_{2xxt} + O(\alpha\epsilon^4). \tag{4.18}$$

Admittedly, this result is a consequence to the rigid-lid approximation. Because the dispersive effect is zero at the waterline to order $O(\alpha\epsilon^4, \alpha^3)$, the moving boundary conditions at the interfacial waterline are the dynamical condition

$$\frac{du_2}{dt} = (\sigma - 1)\zeta_x, \tag{4.19a}$$

with the kinematic condition

$$\frac{dx}{dt} = u_2, \tag{4.19b}$$

and the geometry condition

$$H_2 = h_2 + \zeta = 0. \tag{4.19c}$$

After the central differencing in space and forward differencing in time are taken in Eqs. (4.2) and (4.17), their corresponding difference equations for $h_1 = const$ and $h_2 = h_2(x)$ may be written as

$$\zeta_j^{n+1} = \zeta_j^n + \frac{\Delta t}{2\Delta x}[(H_{1j+1}^n)u_{j+1}^n - (H_{1j-1}^n)u_{j-1}^n], \tag{4.20}$$

$$[A_{3j}^n + \frac{1}{2}A_{2j}^n(\Delta x)]M_{j+1}^{n+1} + [A_{1j}^n(\Delta x)^2 - 2A_{3j}^n]M_j^{n+1} +$$

$$[A_{3j}^n - \frac{1}{2}A_{2j}^n(\Delta x)]M_{j-1}^{n+1} = A_{1j}^n M_j^n(\Delta x)^2 + A_{4j}^n(\Delta x)^2(\Delta t) +$$

$$\frac{1}{2}A_{2j}^n(M_{j+1}^n - M_{j-1}^n)(\Delta x) + A_{3j}^n(M_{j+1}^n - 2M_j^n + M_{j-1}^n), \tag{4.21}$$

where $(\cdot)_j^n = (\cdot)(t = t_n, x = x_j)$. The standard predictor-corrector two-step numerical procedure is used to solve these difference equations (4.20) and (4.21). More specifically,

(i) the first step — the provisional values at the provisional time-level $\overline{n+1}$ are calculated by using the known values at the time-level n;

$$\overline{\zeta_j^{n+1}} = \zeta_j^n + \frac{\Delta t}{2\Delta x}[(H_{1j+1}^n)u_{j+1}^n - (H_{1j-1}^n)u_{j-1}^n], \tag{4.22}$$

$$[A^n_{3j} + \frac{1}{2}A^n_{2j}(\Delta x)]\overline{M^{n+1}_{j+1}} + [A^n_{1j}(\Delta x)^2 - 2A^n_{3j}]\overline{M^{n+1}_j} +$$

$$[A^n_{3j} - \frac{1}{2}A^n_{2j}(\Delta x)]\overline{M^{n+1}_{j-1}} = A^n_{1j}(\Delta x)^2 M^n_j + (\Delta x)^2(\Delta t)A^n_{4j} +$$

$$\frac{1}{2}A^n_{2j}(M^n_{j+1} - M^n_{j-1})(\Delta x) + A^n_{3j}(M^n_{j+1} - 2M^n_j + M^n_{j-1}), \tag{4.23}$$

$$\overline{u^{n+1}_j} = \frac{H^n_{2j} + \overline{H^{n+1}_{2j}}}{(H_1 + \sigma H_2)^n_j + \overline{(H_1 + \sigma H_2)^{n+1}_j}} \frac{(M^n_j + \overline{M^{n+1}_j})}{2}, \tag{4.24}$$

(ii) the second step — the unknown values at the time-level $n+1$ are obtained from the known values at time-levels n and $\overline{n+1}$;

$$\zeta^{n+1}_j = \zeta^n_j + \frac{\Delta t}{4\Delta x}[(H^n_{1j+1})u^n_{j+1} - (H^n_{1j-1})u^n_{j-1}] +$$

$$\frac{\Delta t}{4\Delta x}[(\overline{H^{n+1}_{1j+1}})\overline{u^{n+1}_{j+1}} - (\overline{H^{n+1}_{1j-1}})\overline{u^{n+1}_{j-1}}], \tag{4.25}$$

$$[A^n_{3j} + \frac{1}{2}A^n_{2j}(\Delta x)]M^{n+1}_{j+1} + [A^n_{1j}(\Delta x)^2 - 2A^n_{3j}]M^{n+1}_j +$$

$$[A^n_{3j} - \frac{1}{2}A^n_{2j}(\Delta x)]M^{n+1}_{j-1} = A^n_{1j}(\Delta x)^2 M^n_j + \frac{1}{2}(\Delta x)^2(\Delta t)A^n_{4j} +$$

$$\frac{1}{4}A^n_{2j}(M^n_{j+1} - M^n_{j-1})(\Delta x) + \frac{1}{2}A^n_{3j}(M^n_{j+1} - 2M^n_j + M^n_{j-1}) +$$

$$\frac{1}{2}(\Delta x)^2(\Delta t)\overline{A^{n+1}_{4j}} + \frac{1}{4}\overline{A^{n+1}_{2j}}(\overline{M^{n+1}_{j+1}} - \overline{M^{n+1}_{j-1}})(\Delta x) +$$

$$\frac{1}{2}\overline{A^{n+1}_{3j}}(\overline{M^{n+1}_{j+1}} - 2\overline{M^{n+1}_j} + \overline{M^{n+1}_{j-1}}), \tag{4.26}$$

$$u^{n+1}_j = \frac{H^n_{2j} + H^{n+1}_{2j}}{(H_1 + \sigma H_2)^n_j + (H_1 + \sigma H_2)^{n+1}_j} \frac{(M^n_j + M^{n+1}_j)}{2}. \tag{4.27}$$

Eqs. (4.23)(4.26) are implicit tridiagonal systems which can be solved by the traditional methods. The stability and accuracy of the numerical scheme are

investigated by applying it to compute a free soliton solution (with $s = 0$). The initial data are provided by the standard IW KdV equation with the space interval $\Delta x = 0.1$ and the time step $\Delta t = 0.05$, and the computational trunction error is of $O(\Delta x^2 \Delta t)$. If we continue to reduce the value of $\Delta t < 0.05$, the same results are obtained but with greater CPU times. An adjusted grid is taken for each time step in computations with moving boundary conditions. All computations are done with a Cray Y-MP at UCSD.

4.3.2 Wave Propagation in a Cosine-Shaped Seabed

In this section, a majority of numerical computations are performed to investigate the propagation of ISWs of depression from a subcritical region of constant depth through a gradual cosine-shaped transition to a supercritical region. A sketch of the bottom topography is shown in Figure 4.1. The bottom topography is defined by

$$h_2 = d, \quad x < x_1, \tag{4.28a}$$

$$h_2 = d + \frac{(d - d_1)}{2}[cos\frac{\pi(x - x_1)}{L} - 1], \quad x_1 < x < x_1 + L, \tag{4.28b}$$

$$h_2 = d_1, \quad x > x_1 + L, \tag{4.28c}$$

where the subcritical depth d is greater than the supercritical depth d_1. As for the initial condition, we take an ISW moving to the right with its peak located at $x = x_o$, and with its initial amplitude a_o. The Green's law, which states that the amplitude of every wave is proportional to the $-1/4$-power of the lower-layer depth is well reflected in computations. At least 99% of the initial excess mass moves with waves transmitted, the remainder being reflected back at $x = x_1$.

Figure 4.3(a,b) illustrates an ISW moving from a deep region into the shallow water in the case when $s >> s_w$, with $L = 80, \lambda = 20$. The critical point x_t

is at 73.26. The ISW passes over the whole cosine-shaped shelf with a smooth single-valley profile and starts to oscillate at the tail only when it is close to the flat region of the shallow lower layer. The amplitude and peak location of the ISW of depression during the whole evolution period are shown in Figure 4.4(a,b). The parameters are taken with $a_o = -0.03, x_1 = 40, x_o = 20, \tilde{\rho} = 0.85, h_1 = 0.4, d = 0.6, d_1 = 0.15$.

Figure 4.5 shows the computational results when $s << s_w$, with $L = 600, \lambda = 20$. The critical point x_t is at 289.45. The ISW of depression has an oscillatory tail when it approaches the critical point. There is no reflection as the ISW passes through the trans-critical region. The amplitude and peak location of the ISW of depression are shown in Figure 4.6(a,b). The parameters adopted are $a_o = -0.03, x_1 = 40, x_o = 20, \tilde{\rho} = 0.85, h_1 = 0.4, d = 0.6, d_1 = 0.15$.

Figure 4.7 shows the overtaking interaction of two ISWs with their peaks at x_{1o} and x_{2o}, respectively; it does not exhibit much influence from the presence of the critical point. The parameters adopted in the computation are $x_{1o} = 15, x_{2o} = 45, a_1 = -0.04, a_2 = -0.03, d1 = 0.15, d = 0.6, h1 = 0.4, x_1 = 70, \tilde{\rho} = 0.85, L = 80, s >> s_w$.

Figure 4.8 shows the head-on collision of one ISW of elevation moving to the left with another ISW of depression moving to the right. Figure 4.9(a,b) shows the amplitude and peak position of the ISW of depression changing with time. Its phase shift resulting from the collision is backward, which is about 0.1 in space for time fixed. In parallel, the computation shows the phase shift of the ISW of elevation is about -0.04 (forward) in space for time fixed. The parameters used in the compuation have the following values $x_{1o} = 75, x_{2o} = 190, x_1 = 100, L = 80, \tilde{\rho} = 0.85, h1 = 0.4, h2 = 0.6, d1 = 0.15, a_1 = -0.03, a_2 = 0.01, s >> s_w$.

4.3.3 Results for Evolution of ISWs on a Straight Slope Beach

In this section, the numerical computations performed are similar to that in section 4.3.2 except that the bottom topography adopted here is a uniform sloping seabed in the L section as shown in Figure 4.1. Because the lower-layer depth in the subcritical region is greater than the upper-layer depth, the ISW is supposed to encounter a critical point within the L section. We consider two different slopes and find the numerical results to be similar to those presented in section 4.3.2 before the ISW breaks or reaches the interfacial waterline. The parameters adopted in computations for Figure 4.1 are $x_o = 35, x_1 = 70, \tilde{\rho} = 0.85, h_1 = 1.0, h_2 = 1.5, a_o = -0.1, s_w = 0.002$. At least 99% of the initial excess mass moves with the wave transmitted, the remainder being reflected back at $x = x_1$.

Figure 4.10(a,b) shows a single ISW of depression moving to the right and climbing the seabed with slope $s = 0.01 >> s_w$. The critical point x_t is at 111.53. The ISW wave grows in amplitude with its speed decreasing as it propagates up the slope. The ISW of depression can exist during the time when it passes through the critical point. This case is quite similar to what we observed in our laboratory experiment.

Figure 4.11 shows the propagation of an ISW of depression up a beach of slope $s = 0.001 << s_w$. The ISW developes an oscillatiory tail in the neighbourhood of the critical point x_t at 485.35. The amplitude and peak location of the ISW are shown in Fig. 4.12(a,b).

4.3.4 Comparison with Experiment

Helfrich & Melville (1986) presented an experimental study of propagation of long nonlinear internal waves over a sloping-shelf topography with slope $s = 0.036$

in the L section and an ISW of maximum slope $s_w = 0.024$ (see Fig. 4.1). The density ratio and depth ratio of two layers are $\tilde{\rho} = 0.966$ and $h_1/h_2 = 0.59$. The ratio of d_1 to d is 0.27. The initial amplitude a_o/h_1 is -0.159. In Figure 4.1, we take $\xi = x/L$, and $\xi_o = x_1/L$. The critical point is at $\xi_t = 0.74$. The comparison between their experimental measurement and the computational result based on the ILW model provides a good agreement (see Fig. 4.13). The prediction from the KdV-type equation (4.11) is that the profiles of an ISW in the L section do not change too much relative to the initial condition.

Figures for Chapter 4

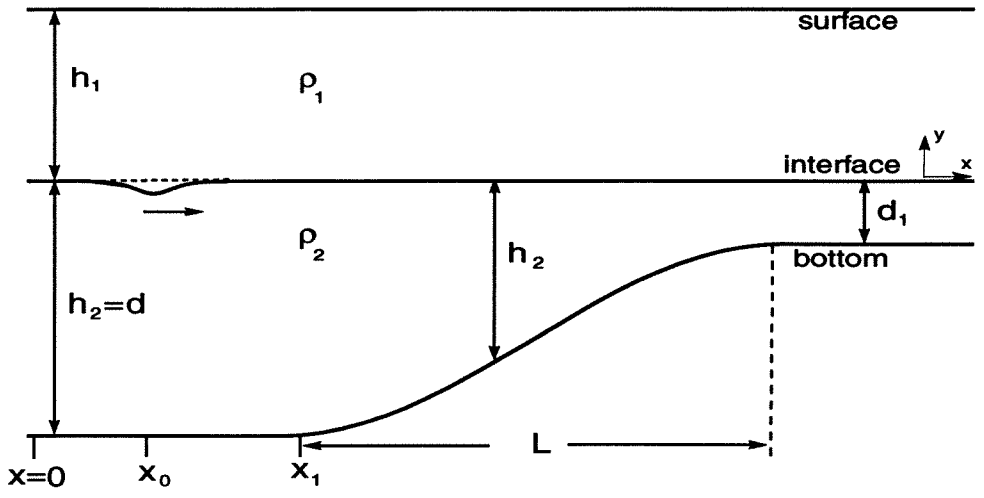

Figure 4.1 The sketch of a cosine-shaped bottom topography in a two-layer system. x_o is the peak position of an initial incident ISW; x_1 is the cosine-shaped transition point; L is the length of the slope.

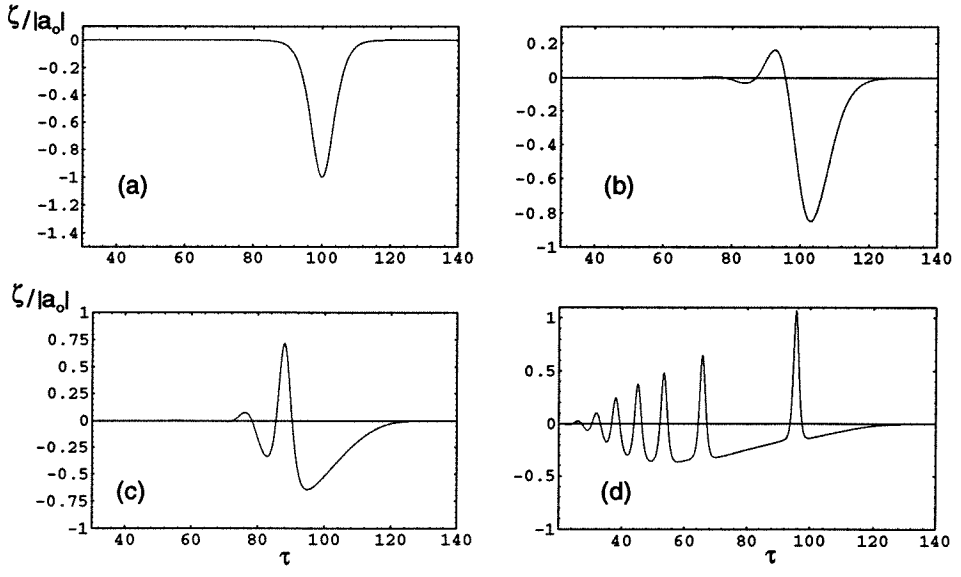

Figure 4.2 Numerical computation of Eq. (4.11) with the initial amplitude of one ISW $a_o = -0.6$. The critical point is at $\eta = 50$. (a)$\eta = 0$; (b)$\eta = 50$;(c)$\eta = 75$;(d)$\eta = 100$.

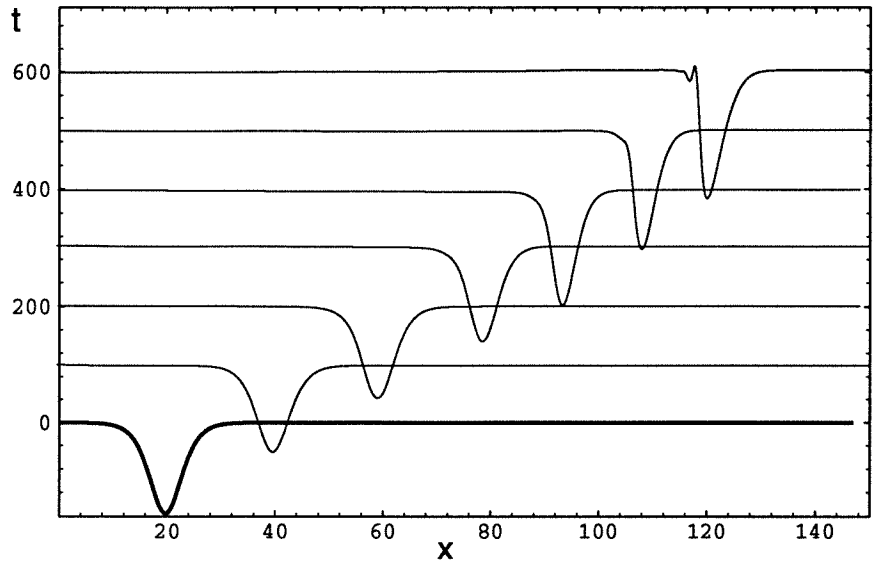

Figure 4.3(a) The wave profiles of an ISW of depression moving on the cosine-shaped bottom as shown in Fig. 4.1 with $s = 0.0056, s_w = 0.0015, a_o = -0.03$, $x_o = 20, x_1 = 40, \tilde{\rho} = 0.85, h_1 = 0.4, d = 0.6, d_1 = 0.15, L = 80$.

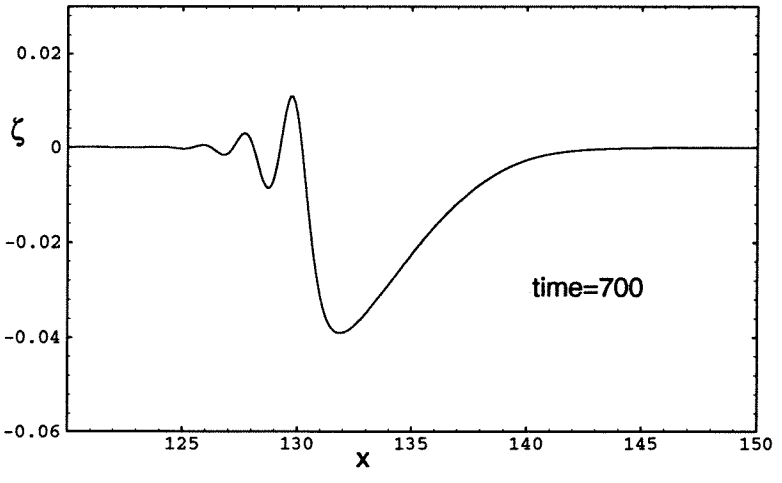

Figure 4.3(b) The wave profile of the ISW of depression in case of Fig. 4.3(a) at $t = 700$.

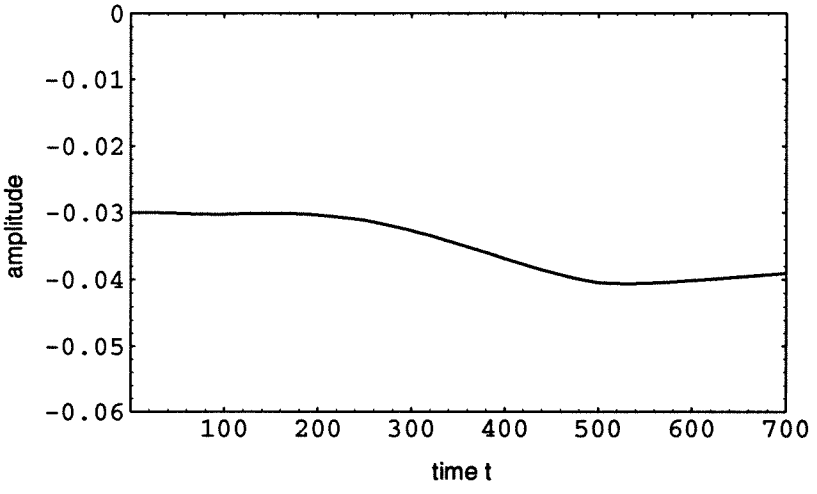

Figure 4.4(a) The time history of the amplitude of the ISW of depression in case of Fig. 4.3(a).

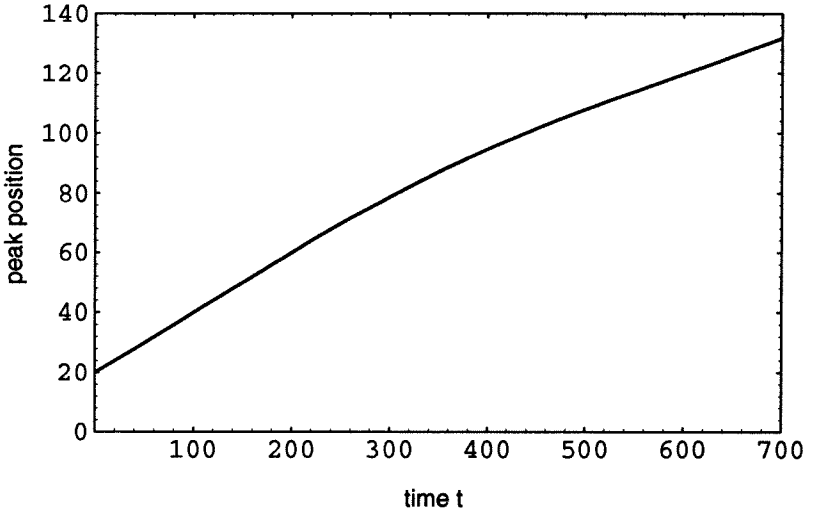

Figure 4.4(b) The time history of the peak position of the ISW of depression in case of Fig. 4.3(a).

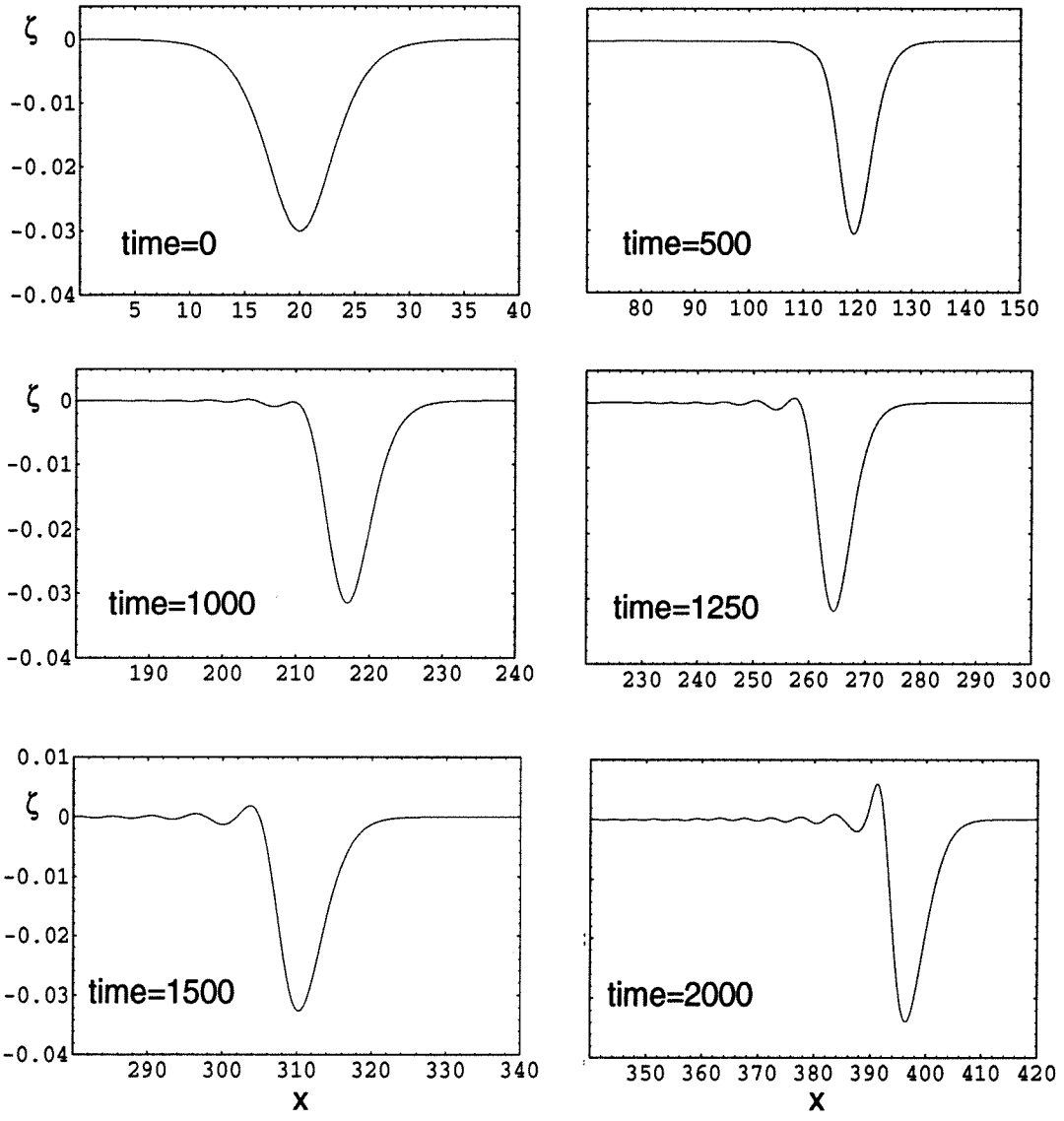

Figure 4.5 The oscillatory tails appear when an ISW of depression moving on the cosine-shaped bottom as shown in Fig. 4.1 with $s = 0.00075, s_w = 0.0015, a_o = -0.03, x_o = 20, x_1 = 40, \tilde{\rho} = 0.85, h_1 = 0.4, d = 0.6, d_1 = 0.15, L = 600$.

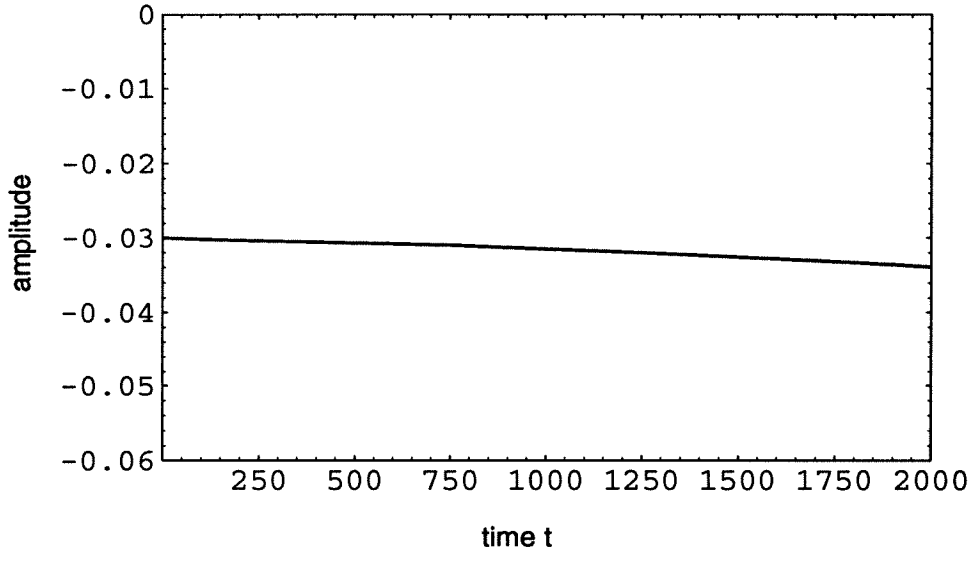

Figure 4.6(a) The time history of the amplitude of the ISW of depression in case of Fig. 4.5.

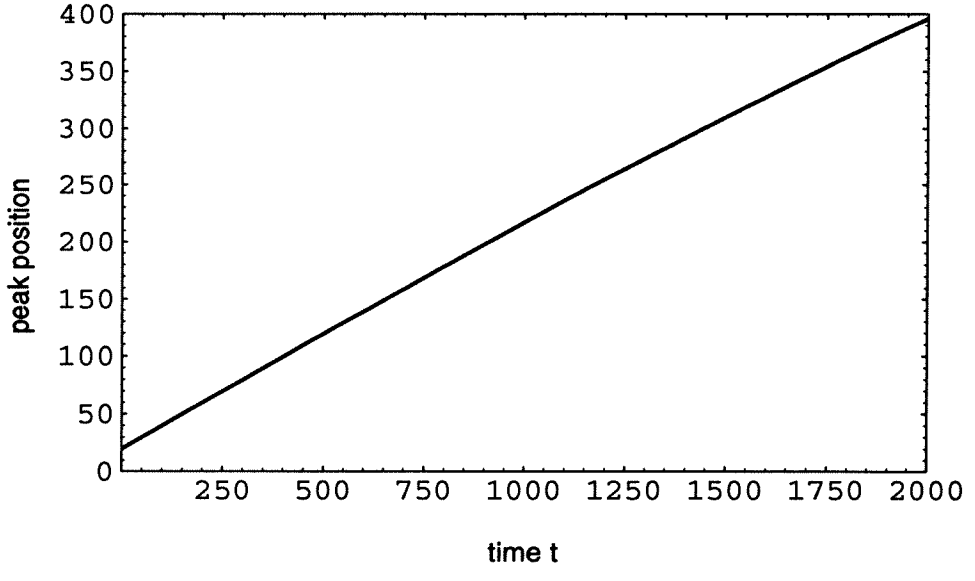

Figure 4.6(b) The time history of peak position of the ISW of depression in case of Fig. 4.5.

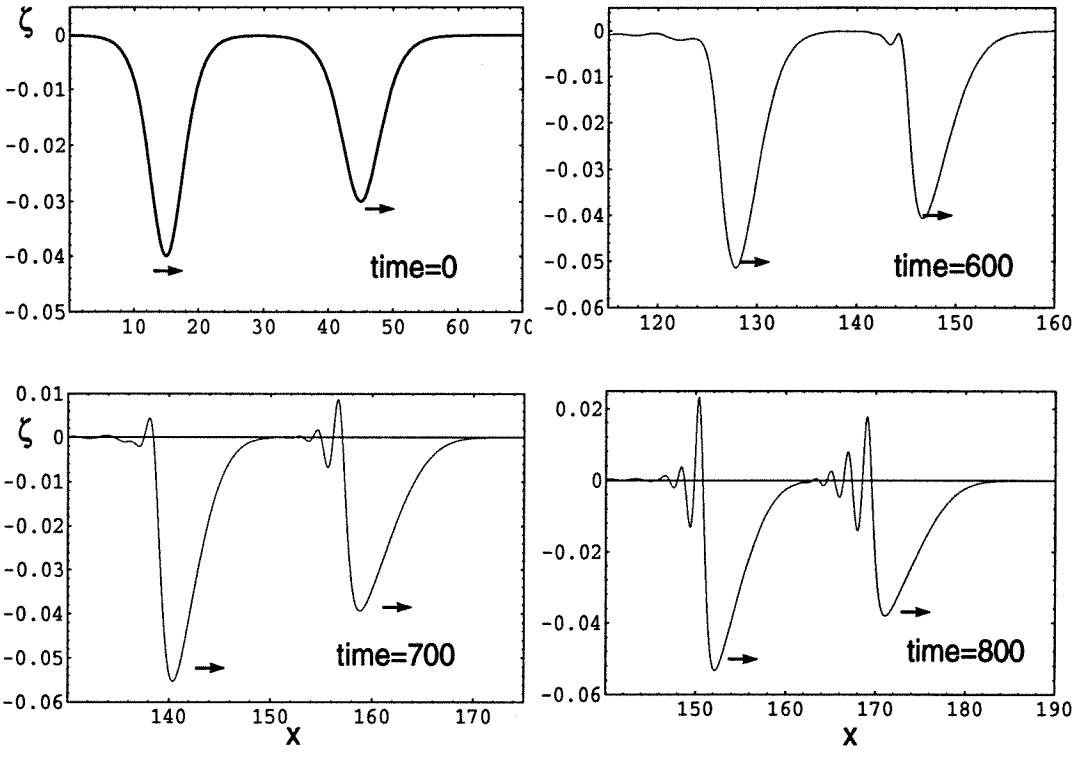

Figure 4.7 The overtaking interaction of two ISWs of depression with their initial peaks at $x_{1o} = 15, x_{2o} = 45$ on the bottom topography as shown in Fig. 4.1 with the parameters $s > s_w, a_1 = -0.04, a_2 = -0.03, x_1 = 70, \tilde{\rho} = 0.85, h_1 = 0.4, d = 0.6, d_1 = 0.15, L = 80$.

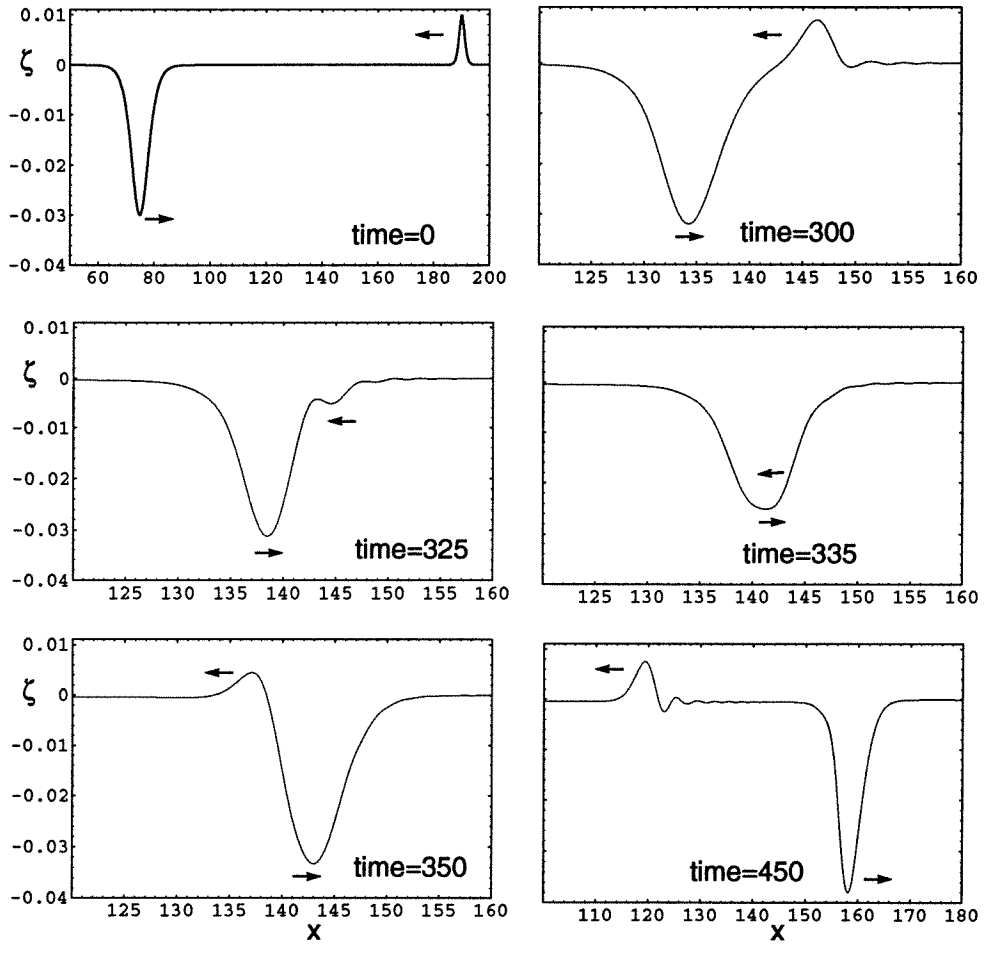

Figure 4.8 The head-on collision of one ISW of depression to the right with another ISW of elevation to the left. Their initial peaks are at $x_{1o} = 75, x_{2o} = 190$, respectively. The parameters adopted in Fig. 4.1 are $s > s_w, a_1 = -0.03, a_2 = 0.01, x_1 = 100, \tilde{\rho} = 0.85, h_1 = 0.4, d = 0.6, d_1 = 0.15, L = 80$.

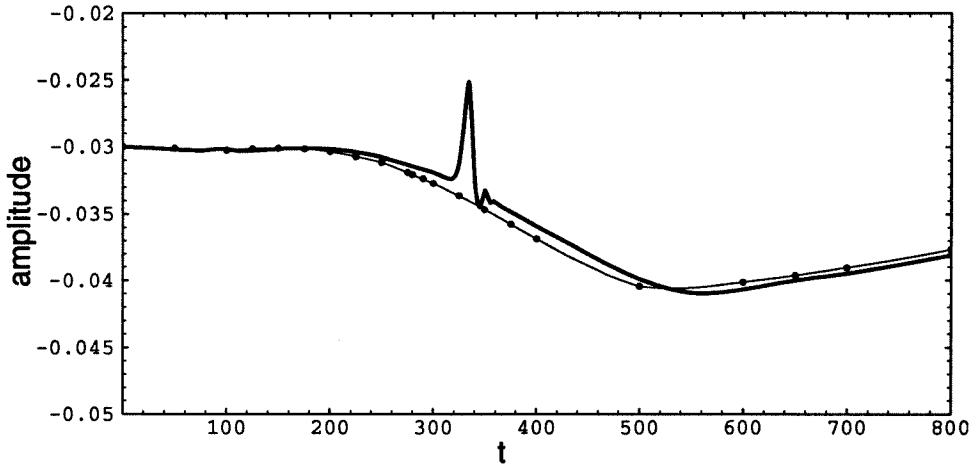

Figure 4.9(a) The comparison of the time histories of the amplitude of the ISW of depression for cases of the collision not involved and involved as shown in Fig. 4.8. —- collision case; -·- no collision case

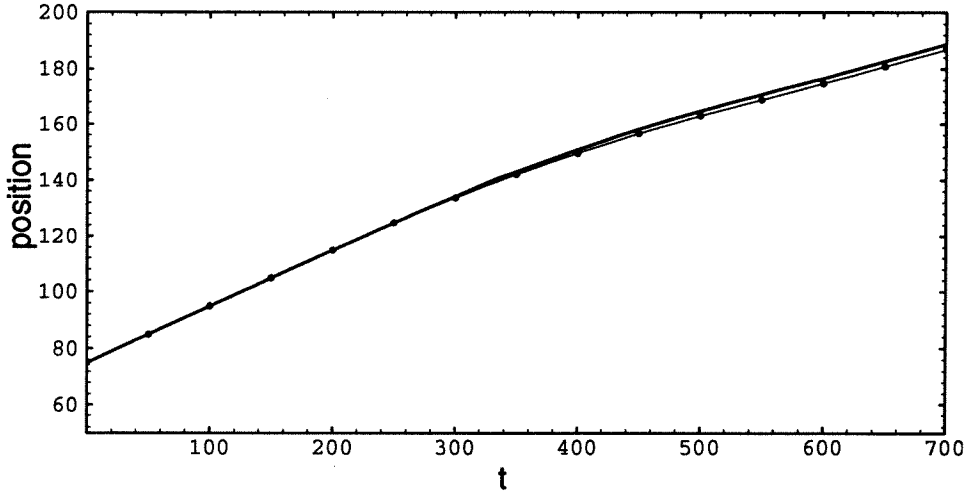

Figure 4.9(b) The comparison of the time histories of the peak position of ISW of depression for cases of the collision not involved and involved as shown in Fig. 4.8. The phase shift is forward in time. —- collision case; -·- no collision case

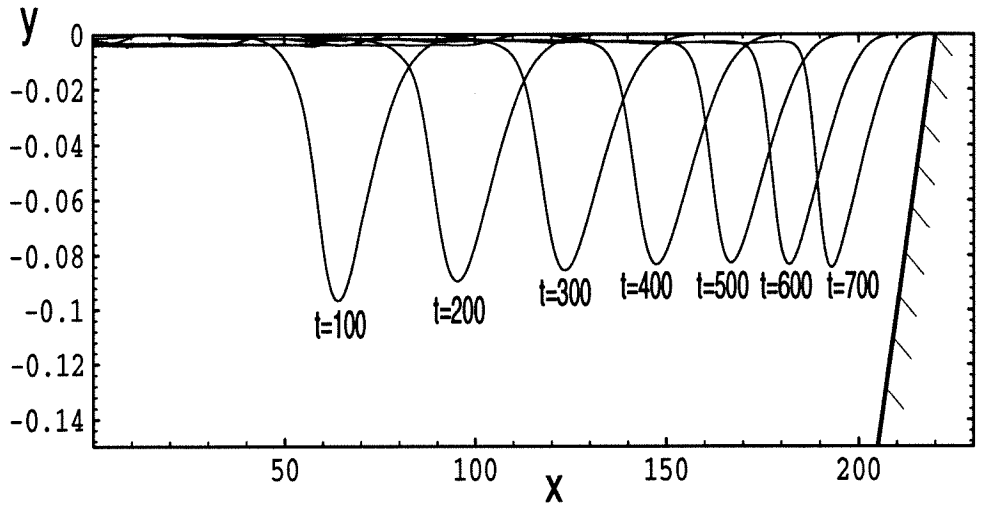

Figure 4.10(a) Wave profiles of an ISW of depression moving on the sloping-shelf bottom as shown in Fig. 3.7 with $s = 0.01, s_w = 0.002, x_o = 35, x_1 = 70, \tilde{\rho} = 0.85, h_1 = 1.0, h_2 = 1.5, a_o = -0.1$.

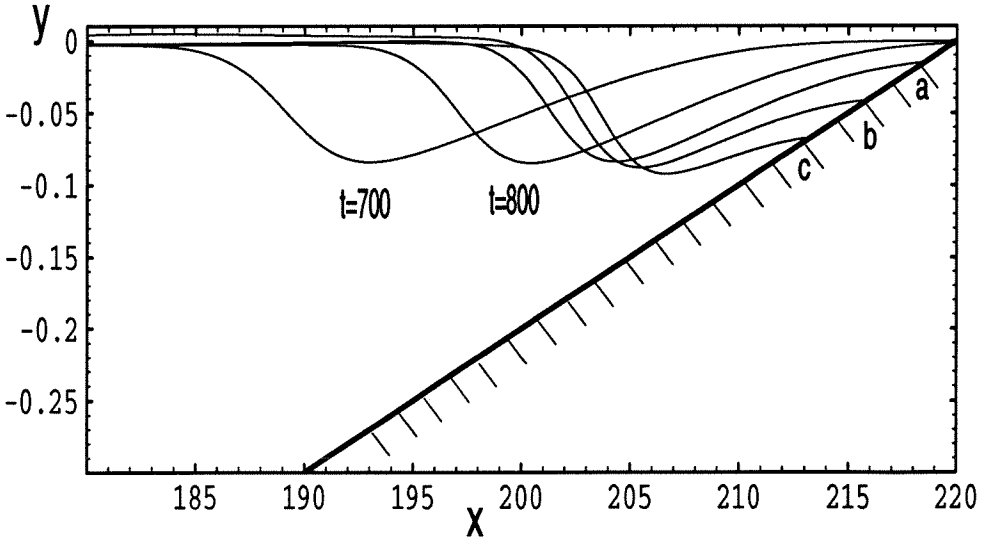

Figure 4.10(b) The wave profile of the ISW of depression near the interfacial waterline in case of Fig. 4.10(a). At point a: $t = 900$; at point b: $t = 1000$; at point c: $t = 1100$.

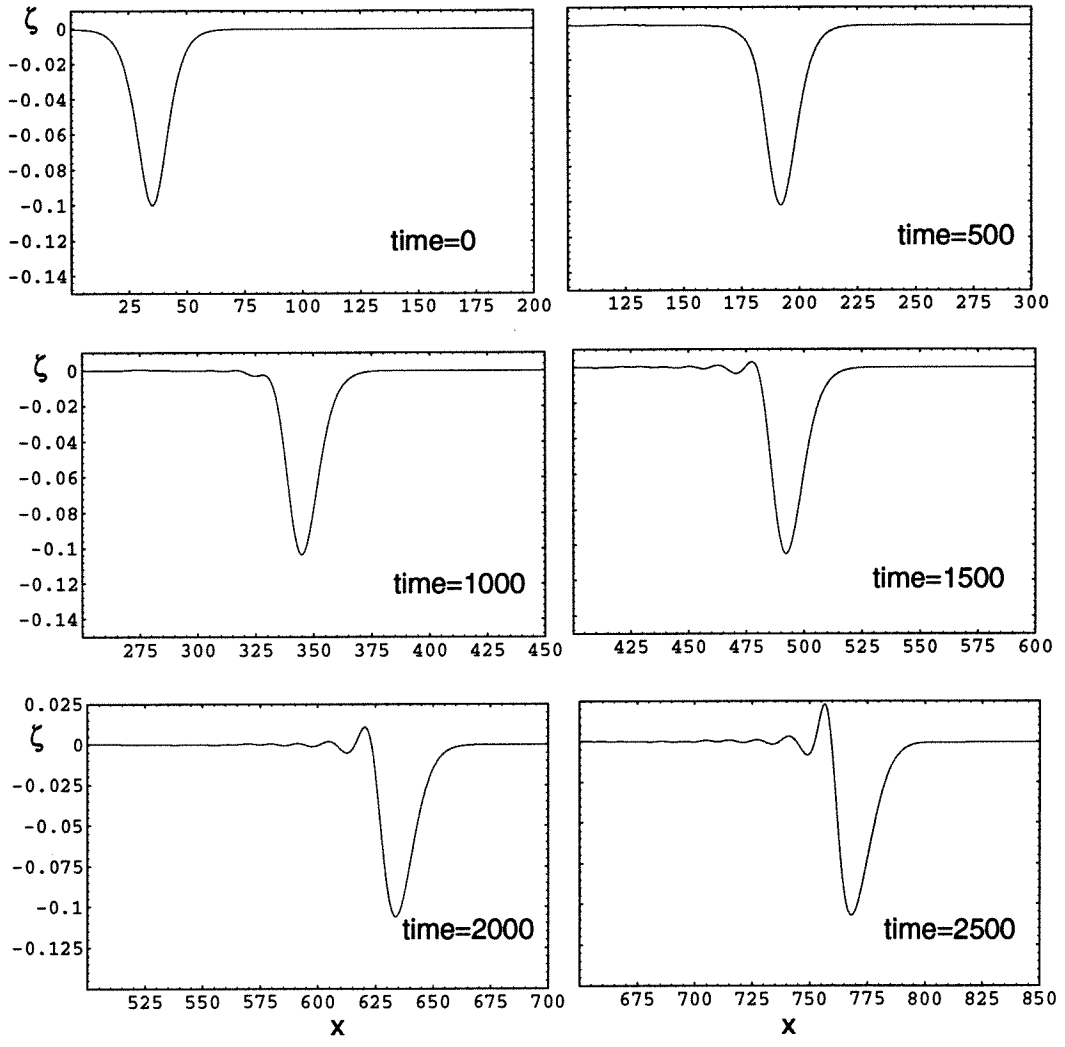

Figure 4.11 The oscillatory tails appear when an ISW moves on the bottom topography as shown in Fig. 3.7 with the parameters $s = 0.001, s_w = 0.002, x_o = 35, x_1 = 70, \tilde{\rho} = 0.85, h_1 = 1.0, h_2 = 1.5, a_o = -0.1$.

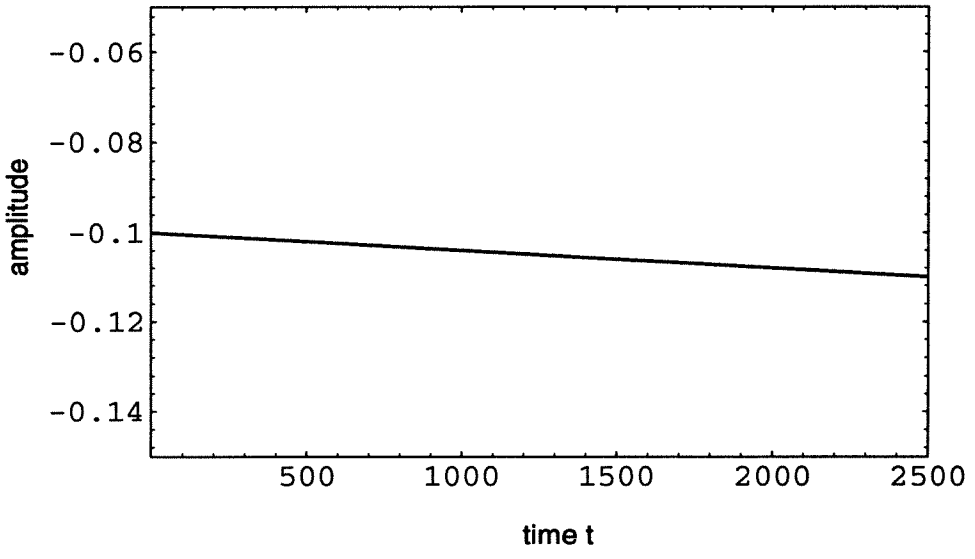

Figure 4.12(a) The time history of the amplitude of the ISW of depression in case of Fig. 4.11.

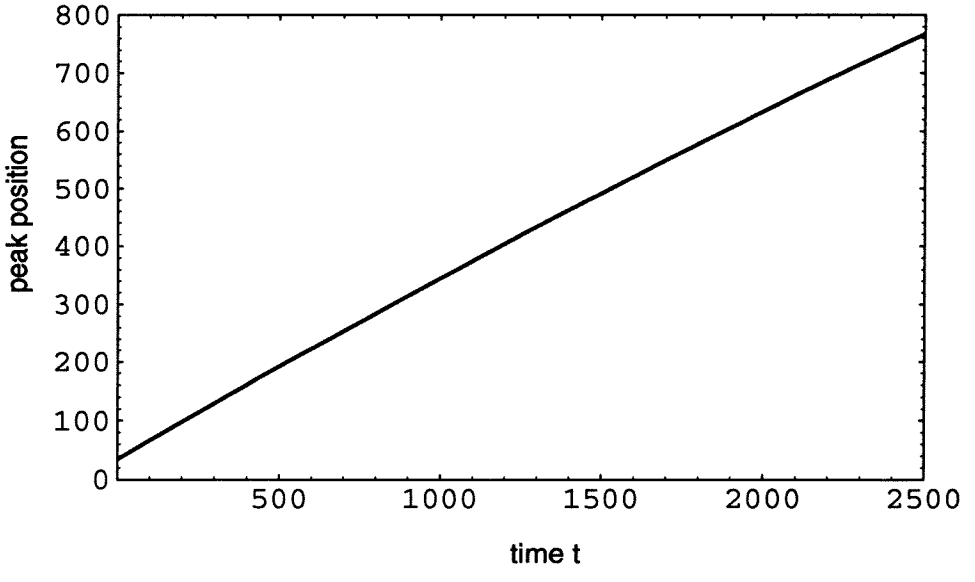

Figure 4.12(b) The time history of the peak position of the ISW of depression in case of Fig. 4.11.

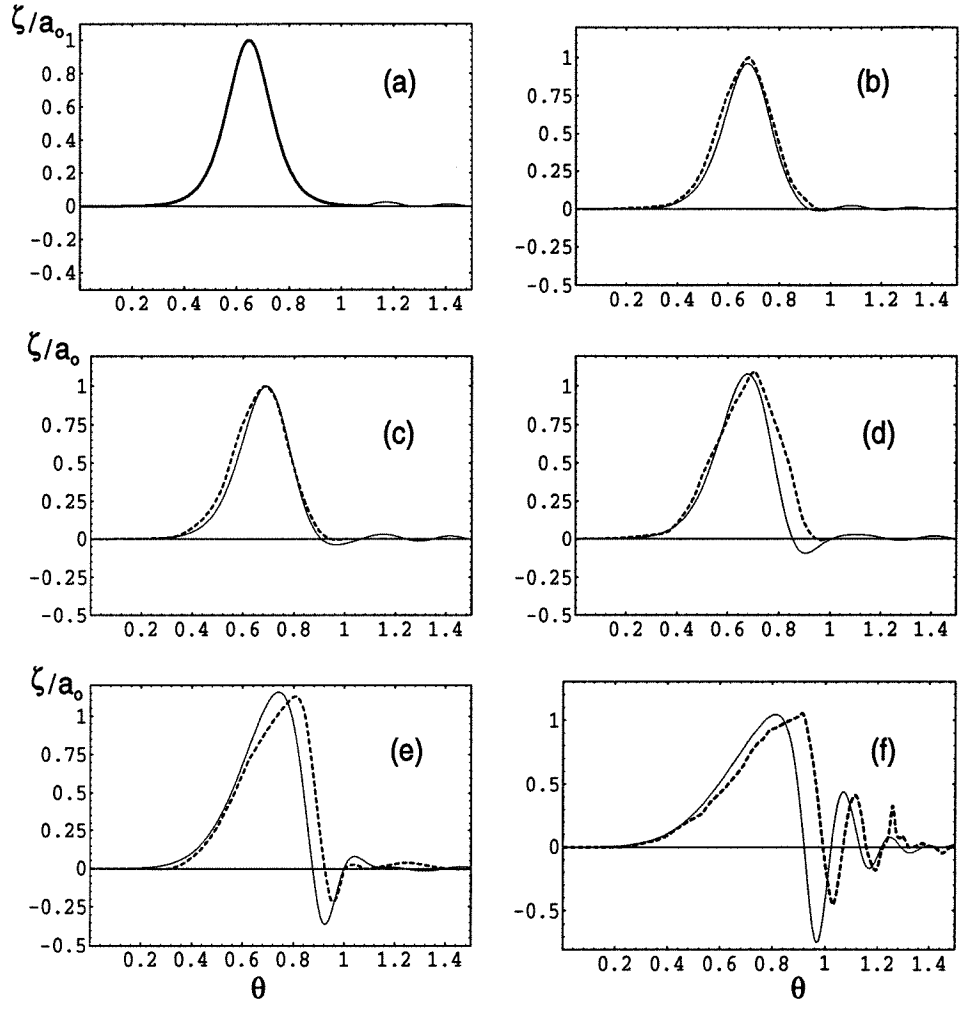

Figure 4.13 The comparison between the experimental measurement and the computational result by the ILW model. Define $\theta = \frac{c_o}{L}(t - \int_o^x \frac{dx}{c(x)})$; $\xi_o = \frac{c_o}{L}\int_o^x \frac{dx}{c(x)}$, $\xi = x/L$. (a)$\xi = 0, \xi_o = 0$; (b)$\xi = 0.39, \xi_o = 0.4$; (c)$\xi = 0.59, \xi_o = 0.62$; (d)$\xi = 0.80, \xi_o = 0.87$; (e)$\xi = 1.0, \xi_o = 1.13$; (f)$\xi = 1.20, \xi_o = 1.41$. —— the ILW model; – – –– the experiment.

Chapter 5

Conclusions

In this chapter, conclusions are presented based on the results obtained in our study. In a system of two-layer fluids with a discontinuity in density, we have developed the ILW model to formulate generation and propagation of oceanic nonlinear internal long waves. For unidirectional waves, the ILW model reduces to the KdV model. For modeling right- and left-going IWs simultaneously, we have derived the bidirectional model systematically from the ILW model. According to this bidirectional model, phase shifts in head-on collision of two ISWs are found for both waves to retard in time, a result which is the same as for head-on collision between two solitons in a single layer of water; this holds whether the two ISWs are both elevated or both depressed in polarity. This kind of phase shift, of course, would never arise in linear theory. With the dispersive effects neglected in the ILW model, we have obtained analytic solutions of the nonlinear equations for run-up of IWs. With such analytic solutions, the matched solution, the solutions of two initial run-up problems and the run-up law for ISWs of small amplitude have been obtained. With the dispersive effects included, we have applied the ILW model with the standard predictor-corrector two-step numerical scheme to

solve the run-up problem of ISWs and find the moving boundary technique very satisfactory. The nonlinear propagation of ISWs of depression across a critical point is investigated numerically and experimentally. Based on the numerical results obtained from the ILW model, we find that when the beach slope is much greater than the ISW wave slope, there is no discernible influence from the presence of critical point. However, when the beach slope is much less than the ISW wave slope, the ISW is seen first to gain its amplitude, to reduce its speed as it passes through the trans-critical region and to develope an oscillatory tail in the neighbourhood of the critical point. In our laboratory experiments, we have not seen any change of ISWs of depression in polarity. We find that the ILW model can give numerical simulations in good agreement with the experiment of Helfrich & Melville (1986). The difference between the numerical results based on the KdV equation and the ILW model shows that the reflected waves play a role in the computations.

	KdV	ILW
Waves Predicted	Unidirectional	Bidirectional
Mass Conserved	No	Yes
Energy Conserved	Yes	Yes
Run-up Problem	Cannot	Can
Polarity Changed	Can	Cannot
Experiment Compared	Not Good	Good

Table 5.1 The comparison between the KdV model and the ILW model

The present study shows that the ILW model is a good theory in predicting generation and propagation of IWs in coastal waters compared to the KdV-type

equation. The comparison between the KdV equation with variable coefficients and the ILW model is presented in Table 5.1.

The KdV-type equation with variable coefficients is a model for only unidirectional waves and does not conserve mass. However, the ILW model is applicable to both unidirectional and bidirectional waves and holds mass conserved. In contrast, both these models conserve energy. The KdV-type equation, being for unidirectional waves, cannot predict interactions between waves and solid walls, but the ILW model can be used to predict wave run-up on sloping seabeds with appropriate boundary conditions and head-on collisions of two ISWs.

So far, we have found the ILW model very satisfatory. Our work highlights some problems to be further studied. More detailed experimental studies of IWs require more work than has been done. Analytical methods for solving the variable-coefficient KdV-type equation are required for further development. More experimental observations are needed to be performed to further study the ILW channel model in 3D cases. Breaking-wave theory and the turbulent mixing in a system of two-layer fluids are still challenging problems.

Appendix A

The Corrected Solution of Eq. (3.38)

The first order solution ψ_o of Eq. (3.38) is

$$\psi_o = \frac{8g_e}{\omega} A J_o(\xi) \cos\vartheta. \tag{A.1}$$

Then, Eq. (3.38) provides for ψ_1 the following equation:

$$\frac{1}{\sigma}(\sigma\psi_{1\sigma})_\sigma - \psi_{1\tau\tau} = K[\frac{1}{4}A_2 \cos 3\vartheta + (A_1 + \frac{3}{4}A_2)\cos\vartheta], \tag{A.2}$$

where

$$A_1 = \frac{A\omega}{4s}\sigma^2 \frac{J_1(\xi)}{\xi}, \quad A_2 = (\frac{2\omega A}{s}\frac{J_1(\xi)}{\xi})^3, \quad K = -\frac{\hat{\rho}}{3m\rho_*}. \tag{A.3}$$

The boundary conditions are

$$\psi_1 \quad \text{is} \quad \text{bounded} \quad \text{at} \quad \xi = 0; \quad \psi_1 = \psi_{1\tau} = 0 \quad \text{at} \quad \vartheta = \frac{\pi}{2}. \tag{A.4}$$

Assume a general solution ψ_1 satisfied by

$$\psi_1 = F(\sigma)\cos\vartheta + G(\sigma)\cos 3\vartheta. \tag{A.5}$$

Then, Eq. (A.2) gives the following equation

$$\frac{1}{\sigma}(\sigma F_\sigma)_\sigma + (\frac{\omega}{2m})^2 F = K(A_1 + \frac{3}{4}A_2). \tag{A.6}$$

For a small σ, we find for ψ_1 the solution

$$\psi_1 = [B_1 J_o(\xi) + F_o + F_1\sigma^2]\cos\vartheta +$$

$$[B_2 J_o(3\xi) + G_o + G_1\sigma^2]\cos 3\vartheta, \tag{A.7}$$

where

$$B_1 = \frac{1}{3}K[1 + \frac{7}{2}(\frac{2mA}{s})^2], \tag{A.8}$$

$$B_2 = -\frac{1}{36}K(\frac{2m}{\omega})^2(\frac{\omega A}{s})^3, \tag{A.9}$$

$$F_o = K(\frac{2m}{\omega})^2(\frac{\omega A}{2s})[\frac{15}{4}(\frac{\omega A}{s})^2 - (\frac{2m}{\omega})^2], \tag{A.10}$$

$$F_1 = K(\frac{2m}{\omega})^2(\frac{\omega A}{8s})[1 - \frac{9}{4}(\frac{\omega A}{s})^2(\frac{\omega}{2m})^2], \tag{A.11}$$

$$G_o = \frac{5}{8}K(\frac{2m}{3\omega})^2(\frac{\omega A}{s})^3, \tag{A.12}$$

$$G_1 = -\frac{1}{96}K(\frac{\omega A}{s})^3. \tag{A.13}$$

Finally, the solution of Eq. (3.38) to the second order is

$$\zeta = -sx + \frac{\sigma^2}{16g_e}(1 + \frac{1}{48}\hat{\rho}\sigma^2)^{-1}, \tag{A.14}$$

$$u_2^2 = (\frac{m\psi_\sigma}{\sigma})^2(1 - \frac{1}{24}\hat{\rho}\sigma^2), \tag{A.15}$$

$$x = x_o(\sigma,\vartheta) + \rho_* x_1(\sigma,\vartheta) + \rho_* x_2(\sigma,\vartheta), \tag{A.16}$$

where

$$x_o = \frac{1}{4}\psi_{o\tau} + (\frac{m}{\sigma})^2(\psi_{o\sigma})^2(1 + \frac{1}{24}\hat{\rho}\sigma^2)^{-1} + \frac{\sigma^2}{16m}(1 + \frac{1}{48}\hat{\rho}\sigma^2)^{-1}, \tag{A.17}$$

$$\begin{aligned} x_1 = &-\frac{\omega}{2m}[(B_1 - 4F_1(\frac{2m}{\omega})^2)J_o(\xi) + F_o + 4F_1(\frac{2m}{\omega})^2]\sin\vartheta \\ &-\frac{3\omega}{2m}[(B_2 - 4G_1(\frac{2m}{3\omega})^2)J_o(3\xi) + G_o + 4G_1(\frac{2m}{3\omega})^2]\sin 3\vartheta, \end{aligned} \tag{A.18}$$

$$\begin{aligned} x_2 = \psi_{1\sigma} = &[-B_1\frac{\omega}{2m}J_1(\xi) + 2F_1(\frac{2m}{\omega})\frac{16}{\xi}(\frac{1}{2} - \frac{J_1(\xi)}{\xi})]\cos\vartheta \\ &+[-3B_2\frac{\omega}{2m}J_1(3\vartheta) + 2G_1(\frac{2m}{3\omega})\frac{16}{3\xi}(\frac{1}{2} - \frac{J_1(3\xi)}{3\xi})]\cos 3\vartheta. \end{aligned} \tag{A.19}$$

References

Benjamin, T. B. 1962 The solitary wave on a stream with an arbitrary distribution of vorticity. J. Fluid Mech., **21**, 97-115

Benjamin, T. B. 1966 Internal waves of finite amplitude and permanent form. J. Fluid Mech., **25**, 241-270

Benjamin, T. B. 1967 Internal waves of permanent form in fluids of great depth. J. Fluid Mech., **25**, 559-592

Carrier, G. F. 1966 Gravity waves on water of variable depth. J. Fluid Mech., **24**, 641-659

Carrier, G. F. & Greenspan, H. P. 1958 Water waves of finite amplitude on a sloping beach. J. Fluid Mech., **4**, 97-110

Djordjevic, V. D. & Redekopp, L.G. 1978 The fission and disintegration of internal solitary waves moving over two-dimensional topography. J. Phys. Oceanogr., **8**, 6, 1016-1024

Dressler, R. F. 1958 Unsteady non-linear waves in sloping channels. Proc. Roy. Soc. A., **247**, 186-198

Fu, L. L. & Holt, B. 1982 Seasat views oceans and sea ice with synthetic-aperture radar. JPL publication 81-120

Garrett, C. & Munk, W. 1975 Space-time scales of internal waves: a progress report. J. Geophys. Res., **80**, 291-298

Garrett, C. & Munk, W. 1979 Internal waves in the ocean. Annu. Rev. Fluid Mech., **11**, 339-369

Glazman, R. E., Spectra of baroclinic intertia-gravity wave turbulence. Submitted

to J. Phys. Oceanogr., Feb. 1995

Grimshaw, R. 1978 Long nonlinear internal waves in channels of arbitrary cross-section. J. Fluid Mech., **86**, 415-431

Hanazaki, H. 1994 On the three-dimensional internal waves excited by topography in the flow of a stratified fluid. J. Fluid Mech., **263**, 293-318

Helfrich, K. R. 1992 Internal solitary wave breaking and run-up on a uniform slope. J. Fluid Mech., **243**, 133-154

Helfrich, K. R. & Melville, W. K. 1986 On long nonlinear internal waves over slope-shelf topography. J. Fluid Mech., **167**, 285-308

Helfrich, K. R., Melville, W. K. & Miles, J. W. 1984 On interfacial solitary waves over slowly varying topography. J. Fluid Mech., **149**, 305-317

Johnson, R. S. 1972 Some Numerical Solutions of a Variable-coefficient Korteweg-de Vries equation (with application to solitary wave development on a shelf). J. Fluid Mech., **54**, 81-91

Joseph, R. I. 1977 Solitary waves in a finite fliud. J. Phys. A: Math. & Gen., **10**, L225

Kubota, T., Ko, D. R. S. & Dobbs, L. D. 1978 Weakly-nonlinear, long internal gravity waves in stratified fluids of finite depth. J. Hydronautics, **12**, 4, 157-165

Kao, T. W., Pan, F. -S. & Renouard, D. 1985 Internal solitons on the pycnocline: generation, propagation, and shoaling and breaking over a slope. J. Fluid Mech., **159**, 19-53

Kaup, D. J. & Newell, A. C. 1978 Solitons as particles, oscillators, and in slowly changing media: a singular perturbation theory. Proc. R. Lond. A., **361**,

413-446

Knickerbocker, C. J. & Newell, A. C. 1980 Internal solitary waves near a turning point. Phys Letters, **75A**, 5, 326-330

Koop, C. G. & Butler, G. 1981 An investigation of internal solitary waves in a two-fluid system. J. Fluid Mech., **112**, 225-251

Lee, S. J., Yates, G. T. & Wu, T. Y. 1989 Experiments and analysis of upstream-advancing solitary waves generated by moving disturbances. J. Fluid Mech., **199**, 569-593

Long, R. R. 1956 Solitary waves in the one- and two-fluid systems. Tellus, **8**, 460-471

Mei, C. C. 1966 On the propagation of periodic water waves over beaches of small slope. Technical Note 12, Hydrodynamics Laboratory, Massachussetts Institute of Technology

Mei, C. C. 1983 The applied dynamics of ocean surface waves. A Wiley- Interscience Publisher, John Wiley & Sons, Inc. USA p526

Muller, P., D'Ascaro, E. & Holloway, G. 1991 Internal gravity waves and mixing, in: Dynamics of oceanic internal gravity waves. eds. P. Muller and D. Henderson (University of Hawaii, Manoa 1991), pp499-508

Ono, H. 1975 Algebraic solitary waves in stratified fluids. J. Phys. Soc. Japan, **39**, 1082-1091

Ostrovsky, L. A. & Pelinovskiy, E. N., 1970 Wave transformation on the surface of a fluid of variable depth. Atmospheric and Oceanic Physics, Academic of Sciences of U.S.S.R., **6**, No. 9, 934-939

Ostrovsky, L. A. & Stepanyants, Yu. A. 1989 Do internal solitons exist in the

ocean? Reviews of Geophysics, **27**, 3, 293-310

Pullin, D. I. & Grimshaw, R. H. J. 1988 Finite-amplitude solitary waves at the interface between two homogeneous fluids. Phys. Fluid, **31**, 12, 3550-3559

Segur, H. & Hammack, J. L. 1982 Soliton models of long internal waves. J. Fluid Mech., **118**, 285-304

Spielvogel, L. Q. 1975 Single-wave run-up on sloping beaches. J. Fluid Mech., **74**, 685-694

Synolakis, C. E. 1986 The run-up of long waves. Ph.D. thesis, California Institute of Technology, Pasadena, CA, U.S.A.

Teng, M. H. 1990 Forced emissions of nonlinear water waves in channels of arbitrary shape. Ph.D. thesis, California Institute of Technology, Pasadena, CA, USA

Teng, M. H. & Wu, T. Y. 1992 Nonlinear water waves in channels of arbitrary shape. J. Fluid Mech., **242**, 211-233

Tuck, E. O. & Hwang, L. -S. 1972 Long wave generation on a sloping beach. J. Fluid Mech., **51**, 449-461

Wang, K. H., Wu, T. Y. & Yates, G. T. 1992 Three-dimensional scattering of solitary waves by vertical cylinder. J. Waterway Port Coastal and Ocean Engineering-ASCE, **118**, 5, 551-566

Watson, G. N. 1952 A treatise on the theory of bessel functions. Cambridge Univerisity Press

Whitham, G. B. 1967 Variational methods and applications to water waves. Proc. R. Soc. A, **299**, 6-25

Wu, T. Y. 1981 Long waves in ocean and coastal waters, J. Engng Mech. Div.,

ASCE, **107**, 501-522

Wu, T. Y. 1994 A bidirectional long-wave model. Methods and Applications of Analysis, **1**, 1, 107-117

Wu, T. Y. 1995 Bidirectional soliton street. ACTA Mech. Sinica, **11**, 4, 289-306

Wu, T. Y. & Lin, D-m. 1994 Oceanic internal waves–their run-up on a sloping seabed. Physica D, **77**, 97-107

Zabusky, N. J. & Kruskal, M. D. 1965 Interaction of solitons in a collisionless plasma and the recurrence of initial states. Phys. Rev. Lett., **15**, 241-243.

Zelt, J. A. 1986 Tsunamis: the response of harbours with sloping boundaries to long wave excitation. Ph.D. thesis, California Institute of Technology, Pasadena, CA, USA

Zelt, J. A. 1991 The run-up of nonbreaking and breaking solitary waves. Coastal Engineering, **15**, 3, 205-246

Zelt, J. A. & Raichlen, F. 1991 Overland flow from solitary waves. J. Waterway Port Coastal and Ocean Engng Div. ASCE., **117**, 247-263

Zhu, J. 1986 Internal solitons generated by moving disturbances. Ph.D. thesis, California Institute of Technology, Pasadena, CA, USA

Zhu, J., Wu, T. Y. & Yates, G. T. 1986 Generation of internal runaway solitons by moving disturbances. In: 16th Symp. on Naval Hydrodynamics. 186-197. Nat. Acad. Sciences Press, Washington, DC.